COMPARING *IN SITU* AND BULK CONSTITUTIVE PROPERTIES OF A STRUCTURAL ADHESIVE

Joshua W. Grohs

Thesis submitted to the Faculty of the
Virginia Polytechnic Institute and State University
in partial fulfillment of the requirements for the degree of
Masters of Science
in
Mechanical Engineering

APPROVED BY:

David A. Dillard, Co-Chairman
Robert L. West, Co-Chairman
Larry D. Mitchell

July 20, 2007
Blacksburg, Virginia

Keywords: bulk adhesive, *in situ* adhesives, constitutive properties, mechanical properties, napkin ring, Iosipescu shear

CONTRASTING *IN SITU* AND BULK CONSTITUTIVE PROPERTIES OF A STRUCTURAL ADHESIVE

Joshua W. Grohs

(Abstract)

In the continuing quest for more efficient designs, structural adhesives are being used in place of, or with, traditional fastening methods; however designing with adhesives is refined as traditional methods. To obtain the adhesive design properties, tests are often performed on bulk tensile and bonded shear specimens. Questions remain about the relationship between properties obtained from *in situ* adhesive joints and bulk adhesive specimens. As a result, an experimental plan was developed which characterized both the linear and nonlinear region of bulk and *in situ* adhesive performance of a two-part acrylic adhesive from Dow Chemical Company. A standard uniaxial tensile test was used for the bulk normal, while an Iosipescu shear test was used to characterize the bulk shear performance. *In situ* testing was performed on a napkin-ring specimen loaded in both tension and torsion. Stress-strain relationships in both shear and normal were developed and bulk and *in situ* adhesive performance was compared. Observations from testing were:

1. Bulk shear and *in situ* shear tests showed similar performance in both the linear and nonlinear regions.
2. Modulus of elasticity in bulk adhesive tests was similar to the effective modulus of elasticity in *in situ* tests.
3. Prediction of normal yield strengths of the *in situ* adhesive through simple failure theory models proved to be inaccurate. Stress singularities, loading imperfections, and potentially a hydrostatic sensitivity were considered possible explanations.
4. Adhesive showed sensitivity to voiding and surface flaws when loaded in a tensile configuration, refinement of specimen fabrication minimized these effects.

ACKNOWLEDGMENTS

"I can do everything through Him who gives me strength." – Philippians 4:13 (NIV)

First and foremost, I thank God for his desire to have a relationship with me in this life and all His wonderful blessings that I so often take for granted. He has given me the energy to finish both my undergraduate and graduate degrees, as well as helping me be patient and understanding when my research has not gone as planned. He has provided the many helpful people who have made my years at Virginia Tech both productive and entertaining. Of these people, most important to me is my wife, Mandie, who has put up with me and my late nights at work as well as provided a haven at home where I can relax. She and the other key members of my fan club, Brad, Caleb, Anna, & Zach, help me to realize that the most important things in life are not related to work and school, but rather the foundation of our family. I would also like to thank my parents, immediate family and extended family who have supported me through everything. Without you guys I honestly would not be where I am today.

Now onto all the people at work who have been a tremendous help. At the top of that list is my advisor, Dr. Dillard, who has always been accessible and helpful (especially when I could not figure out those back of the envelope simple calculations). I know that God has blessed him with longsuffering patience and understanding to mentor me. I also want to thank Dr. Dillard for always finding ways, and most importantly funding, for me to put food on my family's table. The Mechanical Engineering Department's Dr. West and Dr. Mitchell have been very helpful in encouraging me to not be hesitant about giving my own interpretations of test results before asking for their insight. I also want to thank Dr. Ohanehi who helped me get my feet under me when I was just an undergraduate lost in this wild world of adhesives. The guys in the Engineering Science and Mechanics machine shop, Darrell Link and Dave Simmons, always answered all my machining questions, and have given me the freedom to work on my own. I have honestly learned as much from you guys in the shop as in most of my academic classes. Another person in the Engineering Science and Mechanics department, Bob Simonds, has also been a huge help in letting me use his test machines when ours were acting up, and in also serving as my electronics/signal conditioning go-to guy for quite some time. And last but not

least, I would like to thank Shelia Collins who has always been the sweetest and most helpful person when I am calling to try and fit in a meeting into Dr. Dillard's hectic day.

Well, that about sums up all the Faculty and staff at Virginia Tech who have helped me through … now on to my fellow students! I would like to thank everyone in the Adhesion Lab in 217 Norris for being around to help me when I was learning the equipment. I would specifically like to thank John Hennage, Jeremy Garret, Chris Cassino, Brian Painter, and Vinay Goyal for their help making/cleaning/etching specimens for me when things got busy. I hope I have covered everyone… if I forgot someone, I am sorry and, "Thanks!"

Table of Contents

ABSTRACT……ii
ACKNOWLEDGEMENTS……iii
LIST OF FIGURES……vii
LIST OF TABLES……ix
CHAPTER 1: INTRODUCTION……1
1.1 BACKGROUND INFORMATION……1
1.2 OBJECTIVES AND SIGNIFICANCE……3
1.3 ORGANIZATION OF THIS THESIS……4
1.4 REFERENCES……5
CHAPTER 2: BACKGROUND AND LITERATURE REVIEW……8
2.1 INTRODUCTION……8
2.2 SPECIFIC STUDIES OF BULK AND *IN SITU* PERFORMANCE……9
2.3 RECORDED ADHESIVE PERFORMANCE DIFFERENCES……16
2.4 POSSIBLE EXPLANATIONS……20
2.5 SUMMARY AND CLOSING REMARKS……27
2.6 REFERENCES……27
CHAPTER 3: BULK ADHESIVE TESTS……31
3.1 INTRODUCTION……31
3.2 SPECIMEN PREPARATION……32
3.3 ASTM D-638 TENSILE TESTS……32
3.4 ASTM D-5379 SHEAR TESTS……40
3.5 COMPARISON OF BULK NORMAL AND SHEAR TESTS……48
3.6 CONCLUSIONS……50
3.7 REFERENCES……51
CHAPTER 4: *IN SITU* ADHESIVE TESTS……53
4.1 INTRODUCTION……53
4.2 SPECIMEN PREPARATION……53
4.3 ASTM E-229 NAPKIN RING TESTS……55
4.4 COMPARISON OF *IN SITU* NORMAL AND SHEAR TESTS……67
4.5 CONCLUSIONS……74

4.6 REFERENCES.....75
CHAPTER 5: BULK & *IN SITU* ADHESIVE COMPARISON.....77
5.1 INTRODUCTION.....77
5.2 EXPERIMENTAL DETAILS..... 78
5.3 RESULTS AND DISCUSSION.....82
5.4 CONCLUSIONS.....86
5.5 REFERENCES.....87
CHAPTER 6: SUMMARY AND CONCLUSIONS.....91
6.1 ACCOMPLISHMENTS AND OBSERVATIONS.....91
6.2 AREAS FOR IMPROVEMENT.....92
6.3 FUTURE WORK..... 93
APPENDIX A: BULK ADHESIVE SPECIMEN REFINEMENT ……. 95
APPENDIX B: YIELD DEFINITION ……... 98
APPENDIX C: “UNCRACKED” CRACKED LAP SHEAR ……..103
VITA……108

LIST OF FIGURES

Figure 1.1. Initial stress-strain plots obtained from manufacturer for normal (bulk dogbone) and shear (*in situ* thick adherend) behavior.....3
Figure 2.1 Correlation between bulk and *in situ* fracture energy's for various Elastomer concentrations, Bascom et. al..... 10
Figure 2.2 Schematic of the symmetric lap shear specimens used by Brinson and Sancaktar.....11
Figure 2.3 Comparison between bulk tensile results and an optimized thick adherend shear test, Lilleheden..... 15
Figure 2.4 Shear modulus and strength trends as a function of bond thickness for three different adhesives, Tanner.....17
Figure 2.5 The amount of plastic strain significantly increases as the bondline thickness decreases, Stringer..... 18
Figure 2.6 Bond strength prediction and experimental data based on critical interface Corner fracture toughness, Reedy and Guess..... 20
Figure 2.7 Tensile strengths and failure inducing flaw size for varying volumes of adhesive, Odom and Adams..... 21
Figure 2.8 Micrographs showing the two transitional adhesive layers, note a difference in scales 100 nm (top) and 1 μm (bottom), Crompton.....23
Figure 2.9 Different specimens and locations of the indentations for nanoindentation study, Safavi-Ardebili.....24
Figure 2.10 Beveled specimen used in acoustic microscope tests, Safavi-Ardebili et. al.... 25
Figure 3.1 Schematic of ASTM D-638 Type I tensile specimen.....33
Figure 3.2 Stress-strain regions in typical results from a tensile dogbone specimen..... 35
Figure 3.3 Initial stress-strain plots from tensile dogbone tests at crosshead rate of 1 mm/min.....36
Figure 3.4 Initial linear region of the lateral versus axial strain from tensile dogbone tests. 37
Figure 3.5 LESA adhesive characterization plotted with manufacturer's preliminary data..39
Figure 3.6 Specimen quality differences between machined and cast surfaces..... 40
Figure 3.7 Iosipescu shear specimen..... 41
Figure 3.8 Iosipescu shear specimen instrumented with Iosipescu strain gage.....41
Figure 3.9 Iosipescu test fixture and loading description..... 44
Figure 3.10 Initial shear stress-strain plots..... 45
Figure 3.11 Failed Iosipescu shear specimen..... 45
Figure 3.12 Initial shear stress-strain plots with linear curve fits for determining the modulus of rigidity.....46
Figure 3.13 Initial shear stress-strain plots..... 47
Figure 4.1 Schematic and picture of half of a napkin.....56
Figure 4.2 The alignment blocks and spacers controlled adhesive thickness and alignment.....57
Figure 4.3 Picture of half of a napkin ring specimen ready for adhesive to be dispensed.... 58
Figure 4.4 Schematic of specimen halves during cure showing where the spew was directed..... 58
Figure 4.5 Fully cured specimen ready to be tested.....59

Figure 4.6 A Capacitec model HPB-75 was used to measure axial deformations..... 60
Figure 4.7 A MTS extensometer was used to measure the shear deformations..... 60
Figure 4.8 Stress-strain plots from the napkin ring tension tests.....63
Figure 4.9 Initial linear portion of the stress-strain plots from the napkin ring tension tests.....63
Figure 4.10 Stress-strain plots from the napkin ring torsion tests..... 66
Figure 4.11 Initial linear portion of the stress-strain plots from the napkin ring torsion tests..... 66
Figure 4.12 Picture of a failed napkin-ring specimen with voids…….....68
Figure 4.13 Representation of the different points where the stress state estimated ….....69
Figure 5.1 Schematic of ASTM D-638 Type I tensile specimen..... 79
Figure 5.2 Schematic of ASTM D-5379 Iosipescu shear specimen.....80
Figure 5.3 Schematic and picture of one napkin-ring adherend….....81
Figure 5.4 Bonded napkin-ring specimen ready for testing.....82
Figure 5.5 Comparison of bulk and *in situ* stress-strain curves..... 84
Figure 5.6 Comparison of bulk and *in situ* shear stress-strain curves..... 84
Figure A.1 Aging Time Effects in Tensile Test Specimens..... 96
Figure A.2 Aging Time Effects and Post-Curing Heating in Tensile Test Specimens.....96
Figure A.3 Tensile Test Results from Different Fabrication Methods.....97
Figure B.1 Loading and Unloading of a Tensile Dogbone Specimen.....99
Figure B.2 Yield Point Comparison for the Bulk Adhesive – Normal Configuration..... 100
Figure B.3 Yield Point Comparison for the Bulk Adhesive – Shear Configuration.....101
Figure B.4 Yield Point Comparison for the *In Situ* Adhesive – Normal Configuration.....101
Figure B.5 Yield Point Comparison for the *In Situ* Adhesive – Shear Configuration.....102
Figure C.1 Schematic of an “Uncracked” Crack Lap Shear Specimen..... 103
Figure C.2 Finished “Uncracked” Crack Lap Shear Specimen..... 104
Figure C.3 “Uncracked” Crack Lap Shear Specimens with Interfacial Failure……..... 105
Figure C.4 “Uncracked” Crack Lap Shear Specimens with Cohesive Failure..... 106
Figure C.5 “Uncracked” Crack Lap Shear Specimens with a Void..... 106

List of Tables

Table 2.1 Modulus, yield strength, and failure strains of bulk shear specimens compared with Bonded shear tests, Brinson and Sancaktar..... 11
Table 2.2 Reproduction of Gali and Ishai's comparison of properties and yield strengths from tensile and napkin ring geometries.....13
Table 2.3 Shear moduli from tensile, torsional pendulum, and thick adherend tests from Jeandrau..... 14
Table 2.4 Shear moduli for the Lord 320 and 3M 563 adhesives, Spigel and Roy..... 16
Table 2.5 Comparison of average properties between two interfacial regions for the HYSOL EA-9346 adhesive, Safavi-Ardebili et. al.....27
Table 3.1 Tensile Test LESA Properties.....38
Table 3.2 Iosipescu Shear Test LESA Properties..... 47
Table 3.3 Combined Tensile and Shear Test Results..... 51
Table 4.1 Napkin Ring Tensile LESA Properties.....64
Table 4.2 Napkin Ring Torsion LESA Properties..... 67
Table 4.3 Predicted Axial Stress at Failure @ Point 1……..... 72
Table 4.4 Predicted Axial Stress at Failure @ Point 2……..... 74
Table 4.5 *In Situ* Adhesive Properties.....75
Table 5.1 Bulk and *In Situ* Adhesive Properties From Testing..... 83
Table 5.2 Comparison of Bulk and *In Situ* Adhesive Performance..... 85
Table B.1 Comparison of Yield Properties from the Offset & Slope Change Methods.....102

Chapter 1: Introduction

1.1 BACKGROUND INFORMATION

Structural adhesives have many desirable design advantages over traditional fasteners and fastening methodologies such as welding and brazing, however the design methodology for utilizing structural adhesives is not as advanced as for traditional fasteners such as bolts and rivets. For adhesives to be included in structural and semi-structural applications, the ability to predict adhesive joint failure and durability is of utmost importance. Predicting joint failure often requires an accurate determination of the adhesive performance, which in turn requires the determination of the specific adhesive's constitutive properties under various loading conditions. Adhesive strength-based characterization and mathematical material modeling for finite element analysis have the capabilities to predict adhesive bond performance. These analyses require adhesive characterization through a variety of standardized tests. Due to the difficulty of measuring bulk shear properties, one of the preferred methods is combining bulk tensile properties with bonded shear joint results [1,2]. Inferring material properties from such a combination of bulk normal properties with *in situ* shear properties is convenient, however some researchers have noted significant mechanical property differences of bulk and *in situ* adhesives for quite some time [3,4,5]. As a result, many specific studies have been performed to examine these differences and determine the mechanisms responsible for differences in bulk versus *in situ* adhesive performance. This will be discussed in detail in later chapters [6,7,8,9,10,11,12,13,14 ,15]. Most of the studies performed concluded that there is substantial agreement between measured linear elastic mechanical properties and Young's and shear moduli. However, some researchers showed nonlinear design properties such as tensile and shear strengths as well as tensile and shear ultimate strains had substantial deviation from the bulk adhesive properties. Two different explanations have arisen from these differences. Some researchers believe that experimental problems have created fictitious differences [14], while other researchers believe there are actual differences in nonlinear adhesive performance between the bulk and *in situ* adhesive [10]. Those believing that experimental problems caused the differences commonly cite poor bonded specimen quality (voiding and/or incomplete curing), inaccuracies of measuring the very small bondline deformations, and non-uniform stresses induced during testing. The

purpose of this thesis is to present a comprehensive study of the bulk and *in situ* properties of a structural adhesive while attempting to correct for any of the cited experimental problems. By minimizing these experimental issues, a more accurate understanding of the bulk and *in situ* adhesive behavior is possible.

This thesis describes work that has been part of a larger research project to develop design methodologies on a specific acrylic adhesive for Dow Chemical Company of Auburn Hills, Michigan. The adhesive chosen for this study, designated low energy substrate adhesive (LESA), is a two-part acrylic with a 1:1 mix ratio. The motivation for this portion of the larger research project stemmed out of some preliminary stress-strain data received from the adhesive manufacturer, as shown in Figure 1.1. In this plot, the curve represented by solid squares displays the test results from a standard dogbone tensile test of the bulk adhesive, while the other curve, represented by open squares, shows the results from a thick-adherend shear test of the adhesive bonding two aluminum adherends. As shown in this plot, there is a significant difference seen between the bulk normal and *in situ* shear test results. The neat tensile performance suggests the adhesive is fairly brittle and incapable of good energy dissipation, while the shear test suggests just the opposite, with a large amount of plasticity and energy dissipation. The brittle dogbone and ductile shear differences are fairly typical for structural adhesive systems [16]. This smaller research project was given the task of exploring the brittle tensile and ductile shear adhesive performance in depth to determine the mechanisms that could cause such a difference. In the process of investigating this aspect, useful constitutive properties were obtained for use in finite element analysis and selection of appropriate material models.

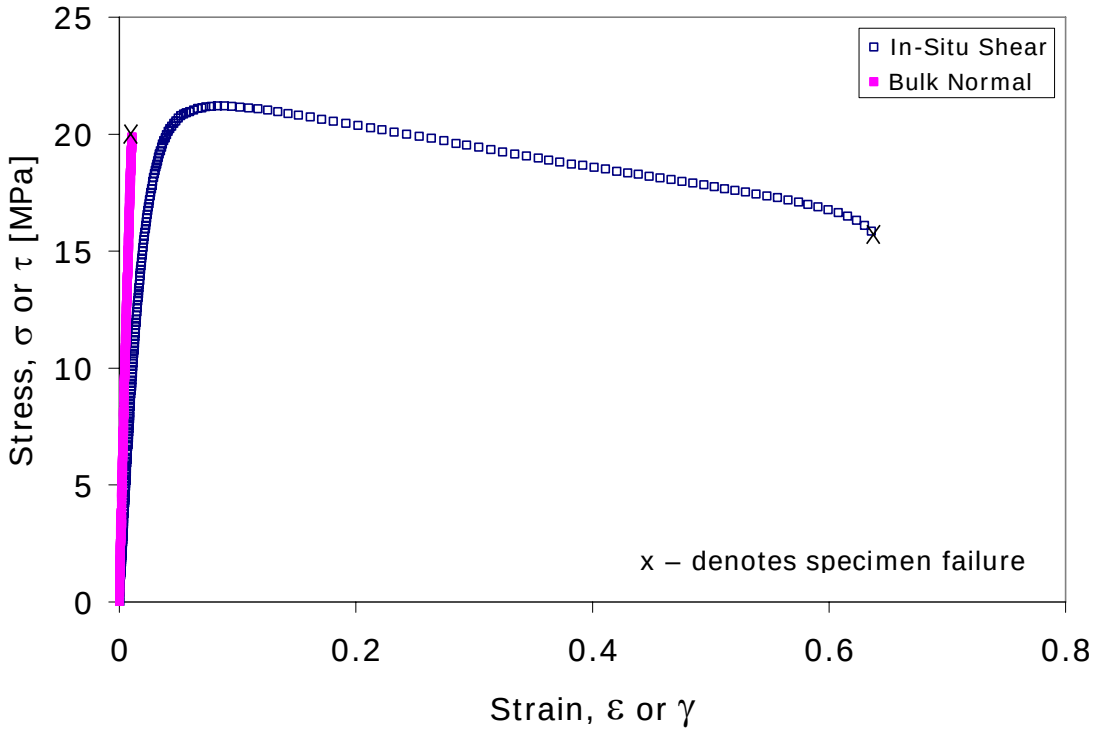

Figure 1.1 Initial stress-strain plots obtained from manufacturer for normal (bulk dogbone) and shear (*in situ* thick adherend) behavior.

1.2 OBJECTIVES AND SIGNIFICANCE

The purpose of this thesis is to gain a better understanding of structural adhesive performance in both bulk and *in situ* forms. The following aspects of this thesis are detailed in the paragraphs below.

1. Develop an experimental test plan and instrumented test geometries which address concerns raised in previous research.
2. Obtain the linear and nonlinear stress-strain behavior of bulk and bonded adhesive samples in both shear and normal loading.
3. Compare the bulk and bonded adhesive responses and make conclusions based on the adhesive performance under these conditions.

The first objective in this study was to carefully develop an experimental plan that could explore many of the issues blamed for creating differences in bulk and *in situ* performance. As

mentioned above, the four main concerns were voiding and improper curing of the adhesive, inaccuracies resulting from insufficient measurement systems, and non-uniform stress states induced in bonded specimens during testing. The test geometries chosen to evaluate the bulk adhesive performance were a tensile dogbone geometry and an Iosipescu shear test. Testing of the *in situ* performance was performed on a napkin-ring geometry loaded independently in either tension and torsion. Working with another graduate student (John Hennage), custom-made high-resolution displacement transducers were manufactured to capture the adhesive bondline deformations. By utilizing these geometries, one could characterize the bulk and *in situ* adhesive response.

With the test geometries selected, the second objective of this study was to execute the experimental plan and obtain the adhesive's bulk and *in situ* constitutive performance in both the linear and nonlinear region. An iterative process of specimen fabrication and testing was performed to perfect both the specimen fabrication and experimental methods. Following this optimization, high quality specimens could be constructed and tested easily and efficiently. In order to ensure complete curing of the adhesive in both the bulk and bonded tests, an elevated temperature postcure was performed. With the specimen fabrication procedure finalized, it was possible to complete the experimental plan and obtain both the linear and nonlinear stress-strain relationship of the adhesive.

The third objective of this study addressed a comparison of the obtained stress-strain responses of both the bulk and *in situ* adhesive. The direct comparison of the bulk and *in situ* adhesive responses enabled conclusions to be drawn on potential mechanisms responsible for adhesive property differences. These conclusions were based on an understanding of adhesive mechanics, analyzing stress-based failure theories, and reviewing current scientific literature of structural adhesives. While the end goal of this comparison was to gain insight into the differences between the bulk and *in situ* constitutive properties, the test results suggested that the adhesive performance in shear was very similar for both the bulk and *in situ* adhesive.

1.3 ORGANIZATION OF THIS THESIS

This study is divided into six chapters and each chapter is described briefly below:

Chapter 1 gives a brief description of background information related to this research and presents the objectives and motivation for this study.

Chapter 2 gives a comprehensive discussion of previous research that explores differences between bulk and *in situ* properties and suggests mechanisms that could have accounted for the differences. This chapter was written as a review paper in journal article form for the *Journal of Adhesion* and could be submitted for publication as a two-part publication along with Chapter 5.

Chapter 3 covers the bulk adhesive tests performed for this research. This description includes both the experimental setup as well as the results from both the normal and shear geometries.

Chapter 4 covers the *in situ* adhesive tests performed for this research. Again this chapter provides both the experimental setup as well as the results from napkin-ring specimens loaded in both tension and torsion.

Chapter 5 is entitled "Bulk and *in situ* comparison of a two-part acrylic structural adhesive." This was written for submission to the *Journal of Adhesion* and could be the second part of the two-part publication. As a result of being an independent document, some of the information may be shared with the previous chapters. This paper will discuss the results of this research, highlight the observed differences between the bulk and *in situ* adhesive. In addition to a discussion of the differences and similarities, possible explanations for these physical differences will be suggested.

Chapter 6 provides a summary of the important observations and findings of this research work while commenting on some areas for improvement. Lastly this chapter suggests some future work which could be performed to provide further insight into the bulk and *in situ* adhesive.

Finally, Appendix A will briefly presents tests results gathered during specimen quality refinement. Appendix B presents some preliminary testing and the methodology using a modified "uncracked" cracked lap shear specimen.

1.4 REFERENCES

[1] Dean, G., Crocker, L., Read. B, and L. Wright., "Prediction of deformation and failure of rubber-toughened adhesive joints." *Int. J. Adhesion Adhesives.* **24**, 295-306 (2004).

[2] Zgoul, M. and A. D. Crocombe. "Numerical modeling of lap joints bonded with a rate-dependent adhesive." *Int. J. Adhesion Adhesives.* **24**, 355-366 (2004).

[3] Gardon, J., "Variables and Interpretation of Some Destructive Cohesion and Adhesion Tests," in *Treatise on Adhesion and Adhesives*, Vol. 1, (Dekker, New York, 1966), Chap 8, pp. 269-324.

[4] Tanner, W., "Manufacturing Processes with Adhesive Bonding." *Appl. Polymer Symposia.* **19**, 1-21 (1972).

[5] Miller, G., "Adhesion and the Glassy State," in *Treatise on Adhesion and Adhesives*, Vol. 3, (Dekker, New York, 1973), Chap 3, pp. 123-159.

[6] Bascom, W. D., Cottington, R. L., Jones, R. L., and Peyser, P. J., "The Fracture of Epoxy- and Elastomer-Modified Epoxy Polymers in Bulk and as Adhesives." *Appl Polym Sci*,**19**, 2545-2562 (1975).

[7] Adams, R. and Coppendale, J., "The Elastic Moduli of Structural Adhesives," in *Adhesion*, Vol. 1, (Applied Science Publishers, London, UK, 1977), pp. 1-17.

[8] Sancaktar, E. and Brinson, H., "The Viscoelastic Shear Behavior of a Structural Adhesive," in *Adhesion and Adsorption of Polymers*, Vol. 12A, (Plenum Press, New York, 1980), pp. 279-299.

[9] Dwight, D., Sancaktar, E. and Brinson, H., "Failure Characterization of a Structural Adhesive," in *Adhesion and Adsorption of Polymers*, Vol. 12A (Plenum Press, New York, 1980), pp. 141-163.

[10] Brinson, H. F., "The Viscoelastic Constitutive Modeling of Adhesives." *Composites*, **13**, 377-382 (1982).

[11] Gali, S., Dolev, G., and Ishai, O., "An Effective Stress/Strain Concept in the Mechanical Characterization of Structural Adhesive Bonding." *Int. J. Adhesion and Adhesives*, **1**, 135-140 (1981).

[12] Dolev, G., and Ishai, O., "Mechanical Characterization of Adhesive Layer in-situ and as bulk material." *J. Adhesion*, **12**, 283-294 (1982).

[13] Jeandrau, J. P., “Intrinsic Mechanical Characterization of Structural Adhesives.” *Int. J. Adhesion and Adhesives*, **6**, 229-231 (1986).
[14] Lilleheden, L., “Mechanical Properties of Adhesives in situ and in bulk.” *Int. J. Adhesion and Adhesives*, **14**, 31-37 (1994).
[15] Spigel, B. and Roy, S., “Comparison of the Adhesive Shear Modulus in Bulk and Bonded States.” *J. Adhesion*, **47**, 151-163 (1994).
[16] A.J. Kinloch, *Adhesion and Adhesives: Science and Technology*, Chapman and Hall, 1987.

Chapter 2: Background and Literature Review

This chapter is written in a format for publication in the *Journal of Adhesion* with the title "A review: Comparing bulk and *in situ* behavior of structural adhesives."

2.1 INTRODUCTION

For many structural and semi-structural adhesive applications, the prediction of adhesive bond failure is of utmost importance. The accurate prediction of these failures requires extensive characterization of the structural adhesives used in the design. Adhesive strength-based characterization is accomplished through a variety of standardized tests and currently one of the preferred methods is combining bulk tensile properties with bonded shear joint results[1,2]. Such a combination of bulk normal properties with *in situ* shear properties is convenient; however, this application of bulk material properties to bonded joints must be validated. Researchers[3,4,5] have noted potential mechanical property differences of bulk and *in situ* adhesive test specimens for quite some time and as a result, several specific studies have been performed to examine these differences. The purpose of this paper is to review the existing literature and then highlight some fundamental principles, specifically moduli and both yield and failure stresses and strains, behind adhesive behavior in both bulk and *in situ* situations.

The complexities of bonded joints, over bulk adhesive samples present numerous possibilities for differences in adhesive behavior. The concept of an interphase was introduced by Sharpe[6] to denote the possibility of fundamental differences in the nature and properties of the material in the vicinity of an interface between an adhesive and a substrate. This is due to the interactions of the adhesive with the surface of a substrate. This paper will explore the effects of this interphase, additional geometric constraints, and critical flaws on the overall adhesive performance.

This review will first present the specific studies of bulk and *in situ* performance and discuss the resulting trends. Following these specific studies are some of the literature suggesting different bulk and *in situ* performance at the macroscopic level. Immediately following the recorded differences in adhesive performance, several possible explanations for such differences are discussed along with some of the literature that supports these explanations.

2.2 SPECIFIC STUDIES OF BULK AND *IN SITU* PERFORMANCE

One of the first studies that began to look into the possible mechanical property differences between bulk and *in situ* performance of adhesives was published in 1975 by Bascom, et. al.[8]. This study focused on examining the opening mode fracture energy using tapered double cantilever beam (TDCB) tests of a high strength, high modulus epoxy, Dow Chemical Company's (Midland, Michigan) DER-332 (σ_{yield}=73 MPa, E =3.4 GPa). The authors also explored the addition of an elastomer to the epoxy to increase the toughness. The two specimen configurations used were a bulk TDCB specimen cast in a silicone rubber mold and bonded 6061 aluminum adherends treated with an acid-chromate etch. Using a linear elastic fracture mechanics approach, they showed similar crack initiation fracture energies for both the bulk and bonded specimens. A comparison of the arrest adhesive energies was not possible since the bulk specimen crack propagated catastrophically and never arrested. The authors varied the adhesive bondline thickness, noting an increase in adhesive fracture energy as bond thickness increased, and a reduction of adhesive fracture energy for bondlines thicker than 1 mm (as shown in Figure 2.1a). In Figure 2.1a the upper curve represents test results for the modified epoxy, whereas the lower curve represents the same epoxy without an elastomer additive. Additionally in this Figure, the solid data points represent sTable crack growth, while the open data points represent unsTable crack growth. Since structural applications typically utilize bond thicknesses between 0.15 mm and 2 mm, the bond thickness effect observed by Bascom, et. al. could be expected in typical structural applications. However, the authors concluded from their study, as shown in Figure 2.1b, that there was little or no difference between the fracture energy of the bulk adhesive (represented by solid data points) and the bonded joints (represented by the open data points). However, the bond thickness of the bonded joints used for this comparison, Figure 1b, was not specified.

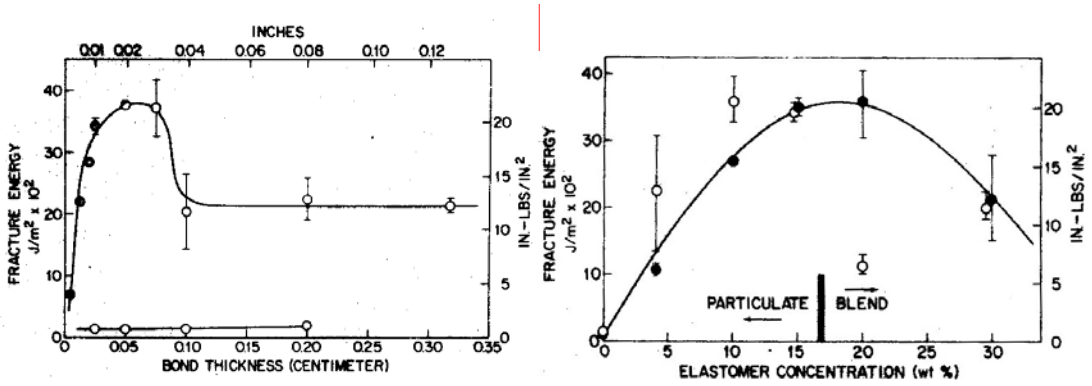

a) b)

Figure 2.1 Correlation between bulk and *in situ* fracture energy's for various elastomer concentrations, Bascom et. al.[8].

A few years later Adams and Coppendale set out to determine appropriate methods for measuring the elastic modulus of various structural adhesives[9]. This research sought to explore the difference between the true bulk modulus and an effective modulus created by the lateral constraint applied by the stiffer metal substrates. Three different epoxy adhesives, containing varying amounts of plasticizers, were tested in several different geometries. The Young's moduli were measured using static tension, static flexure, low frequency dynamic flexure, and resonant bar specimens, while shear moduli were determined using static torsion, low frequency torsional pendulum, and resonant bar specimens. The resonant bar specimens were two aluminum bars bonded with varying bondline thicknesses, with a maximum bondline thickness of 1.3 mm. These resonant bars were then excited either axially or torsionally and the resonant natural frequencies were measured and compared to the other results. The authors found good correlation, moduli values within a couple of percent, between the static and dynamic tests for the brittle epoxies with little damping capacities, Ciba-Geigy Ltd's (Basel, Switzerland) MY750 and BSL308A, (E =3.5 GPa and 3 GPa, respectively). The more plasticized epoxy, Ciba-Geigy Ltd's AY103 (E =2.5 GPa), showed significant viscoelastic effects, and both the Young's and shear moduli were higher for the dynamic tests than the static tests. The higher frequency resonant bar specimens had higher moduli values than the lower frequency dynamic flexure and torsion pendulum tests, as predicted by viscoelasticity principles. In conclusion, the authors

[4] Copyright 1975 From *Journal of Applied Polymer Science*. Reproduced by permission of John Wiley & Sons.

found little or no performance differences other than the slight difference between the high and low frequency tests between the moduli of bulk and bonded geometries for these tests.

Although the main goal of the research performed by Brinson, Sancaktar, and Dwight was not a direct comparison of bulk and *in situ* properties, their research did provide some interesting insights into the matter[10,11]. In their research, the authors were attempting to measure bulk stress-strain, strain rate, creep, relaxation, yield and/or failure properties of two structural epoxies, Narmco's (Costa Mesa, California) Metlbond 1113 and Metlbond 1113-2, (E =2.3 GPa) using tensile dogbone and symmetric rail shear tests. The information from tensile dogbone tests was then used to predict symmetric lap shear performance. The authors chose to measure the shear strains in the rail shear test with resistance strain gages bonded on the specimens and a crack opening displacement gage for the lap shear tests. Aluminum adherends, etched in a sulfuric acid and sodium dichromate solution, were used for the symmetric lap shear specimens, which resemble a thick adherend shear test geometry, only with thin adherends and is shown schematically in Figure 2.2. The symmetric lap shear geometry, with a 0.15 mm bondline thickness, was used to reduce bending and introduce a more uniform shear stress than the traditional lap shear geometry by minimizing the load eccentricity. The results from these studies gave an accurate prediction of the stress-strain relationship of bonded shear joints in the initial linear elastic region, however the prediction quickly broke down as viscoelastic and plastic deformation began to occur. The symmetric rail shear joints had higher yield strengths and slightly larger failure strains than seen in the bulk adhesive tests, while the symmetric lap shear test had a slightly higher yield strength and much larger failure strains. The results from Brinson and Sancaktar's work are summarized in Table 2.1, however the lack of error analysis complicates the comparison shown.

Figure 2.2 Schematic of the symmetric lap shear specimens used by Brinson and Sancaktar[10].

Table 2.1 Modulus, yield strength, and failure strains of bulk shear specimens compared with bonded shear tests, Brinson and Sancaktar[10].

	Elastic Modulus [MPa]	Yield Stress [MPa]	Failure Strains
Tensile Prediction	818	26	5.50%
Symmetric Rail Shear	839	34.5	6.80%
Symmetric Lap Shear	937	26.5	36.40%

Brinson continued the work, and looked more deeply into the viscoelastic modeling and compared the creep strains of both bulk tensile and symmetric lap shear specimens[12]. In keeping with his previous study, he found larger failure strains in bonded joints than in bulk specimens, however this time the difference was observed in creep tests. He measured the creep failure strains between the bulk tensile and bonded symmetric lap shear specimens to be 6-8% normal strain and 40% shear strain, respectively. Brinson attributed this significant difference to the effects of the interface between the adhesive and the aluminum adherends, specifically the constraint added by the aluminum adherends.

Shortly after Brinson's research, Gali, Dolev, and Ishai published two articles describing the application of a modified von Mises function to the mechanical characterization as well as a direct comparison of bulk and *in situ* performance of a ductile structural adhesive, American Cyanamid Company's (Havre de Grace, Maryland) FM73 epoxy (E=2.25 GPa)[13,14]. This research focused on the results from bulk tension and compression specimens, a torsional bulk shear specimen, and a bonded shear specimen. Aluminum adherends were used for the bonded shear tests with bondline thicknesses ranging from 0.15 to 0.2 mm. Using the data collected from the tensile tests and the elastic relationship for isotropic materials, a shear modulus was computed. This shear modulus was then compared to the bulk and bonded shear specimens, and found be essentially the same, shown in Table 2.2. Additionally, using a modified von Mises criterion the authors predicted the yield strengths of the bonded shear joints using the bulk tension and compression properties. A summary of the results from their research is shown in Table 2.2.

Table 2.2 Gali and Ishai's comparison of properties and yield strengths from tensile and napkin ring geometries[14].

Test Temperature	Tensile Test Results			Shear Test Results	
	Young's Modulus	Poisson's ratio	Predicted Shear Modulus	Bulk Tests	*In Situ* Tests
°C	E [kg/mm^2]		G [kg/mm^2]	G [kg/mm^2]	G [kg/mm^2]
23	225	0.43	78.7	80	75
60	145	0.4	51.8	60	55

Test Temperature	Tensile Yielding Results		Shear Yielding Results		
	Compressive Yield	Tensile Yield	Bulk Tests	In Situ Tests	Predicted Shear Yield
°C	σ_y [kg/mm^2]	σ_y [kg/mm^2]	τ_y [kg/mm^2]	τ_y [kg/mm^2]	τ_y [kg/mm^2]
23	-6.6	4.7	3	3.15	3.16
60	-3.5	2.8	1.65	1.7	1.8

Jeandrau also performed a study of the characterization of two structural epoxies, Hexcel Composites' (Stamford, Connecticut) Redux 322 and Emerson and Cuming's (Canton, Massachusetts) Eccobond 45 LV[15]. Jeandrau chose to collect bulk adhesive data using tensile dogbone specimens and torsional pendulum specimens. He chose to compare the bulk results to thick adherend shear specimen results. Excellent agreement was found between the elastic properties of both epoxies when comparing the shear modulus calculated from the elastic relationship for isotropic materials, the shear modulus measured from the bulk torsion specimens, and the thick adherend shear test specimens. The results of these experiments are summarized in Table 2.3. The adhesive bondline thickness used was not specifically mentioned, however a finite element analysis was performed on the thick adherend shear test specimen to analyze the shear stress state with adhesive bondline thicknesses ranging from 0.2 to 0.4 mm. Therefore, one can assume the thick adherend shear test specimens utilized bond thicknesses in this range. The comparison presented in his article only included a comparison in the linear elastic region.

Table 2.3 Shear moduli from tensile, torsional pendulum, and thick adherend tests from Jeandrau[15].

Adhesive	Young's Modulus, E_c [MPa]	Shear Modulus, G_c [MPa]	Poisson's Ratio, ν_c
Redux 322 epoxy film (cure: 1 h at 175°C)	4570[a]	1650[b]	0.38[a]
		1630[c]	
		1660[d]	
Eccobon 45 LV two-part epoxy paste (cure: 30 min at 70°C)	4570[a]	1800[b]	0.324[a]
		1760[c]	
		1800[d]	

[a] Tensile test on bulk specimens (NFT 51034)

[b] Torsion pendulum (NFT 51104) on bulk specimens

[c] Shear test on thick adherend specimen according to DIN 54451

[d] Derived from the relationship $G_c = E_c/2\,(1+\nu_c)$

Lilleheden performed a careful review of the previous literature on the issue of different performance of adhesives both bulk and *in situ*[16]. His conclusions indicated that many of the previous performed experiments, specifically some of the work by Brinson and Pertez, were plagued with flaws. Specifically, these flaws include not utilizing sufficiently accurate measurement systems, working with specimens having complex stress states, or having variations in curing conditions between an actual joint and the bulk adhesive. Addressing these issues, Lilleheden conducted a study where bulk tensile properties were compared to the results from an optimized thick adherend shear test using American Cyanamid (Havre de Grace, Maryland) FM73 epoxy. The optimization was performed to further refine the shear stress state and reduce peel stresses. Moiré interferometry was utilized to determine the strain in both the bulk and in-situ geometries, which allowed determination of the displacement field with a resolution of 0.0417 μm. Several different bondline thicknesses, ranging from 0.16 mm to 0.50 mm, were used for the optimized thick adherend tests. As shown conclusively in Figure 2.3, there were no differences between the in-situ and bulk properties in the linear elastic region when the normal stress was scaled by $2(1+\nu)$ to convert to shear moduli.

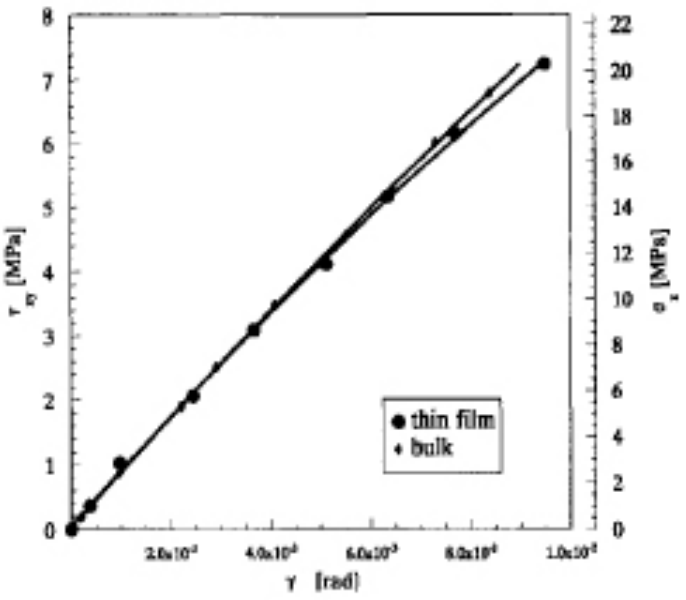

Figure 2.3 Comparison between bulk tensile results and an optimized thick adherend shear test, Lilleheden[16].

Spigel and Roy approached the situation differently. They performed a comparison of the shear modulus of the bulk adhesive, bonded joints using a sandwich beam under three-point bend, and a bonded napkin ring geometry[17]. They chose to use two adhesives, Lord's (Cary, North Carolina) Fusor 320 (E=3.5 GPa) and 3M's (St. Pauls, Minnesota) AF-563 (E=1.68 GPa), on 1018 steel substrates that had been gritblasted and cleaned with acetone prior to bonding. All of the bonded joints, sandwich beams, and napkin-ring specimens, had a bondline thickness of 1.3 mm. The results from the tests indicated that the shear modulus calculated from the tensile tests was an order of magnitude greater than obtained for the two bonded geometries. To examine the reason for the large discrepancy, micrographs at several different magnifications were performed, examining the bondlines of the joints. From these micrographs the authors were able to determine that there were large areas where the adhesive had not adhered to the steel substrates. The authors did perform an experimental computation analysis which suggested that an error as large as 50% could be realized if the shear modulus of an adhesive used to model a bonded joint was determined from tensile tests as opposed to an *in situ* shear test. The results from these tests are shown in Table 2.4, however since the bonded specimen quality was poor, the validity of these results is questionable.

[16] Copyright 1994 From *International Journal of Adhesion and Adhesives.* Reproduced by permission of Elsevier.

Table 2.4 Shear moduli for the Lord 320 and 3M 563 adhesives, Spigel and Roy[17].

Adhesive	Tensile Modulus [ksi]	Poisson's Ratio	Shear Modulus [ksi] (average ± standard deviation)	
			Tensile Test (computed)	3-pt Bend Test
Lord 320	505	0.38	183 ± 41	12.1 ± 1.6
3M 563	243	0.3	93 ± 5	11.3 ± 0.2

Surveying these specific studies of the bulk and *in situ* adhesive performance, several trends in the literature are evident. With high quality bonds that effectively wet the substrate, the mechanical constitutive properties up to yield seem to be similar regardless of whether the adhesive is in bulk form or in a bonded joint. When the bondline thicknesses are sufficiently large in comparison to the interphase region, which may have both different properties as well as effected zones, this conclusion seems to hold merit. Although the elastic modulus is useful in performing a stress analysis of many bonded joints, frequently design applications require the use of properties such as yield stress or strain, and ultimate stress or strain. Unfortunately many of these yield and post-yield properties seem to show some significant differences when comparing bulk and *in situ* geometries. Therefore, the next section will begin to look at experimental studies which have recorded these yield and post-yield property differences.

2.3 RECORDED ADHESIVE PERFORMACE DIFFERENCES

Many studies over the past 30 years have shown differences between strengths and toughness of *in situ* and bulk adhesives, whereas a few studies have shown slight differences between linear elastic mechanical properties. Tanner performed a survey of several different modulus adhesives, characterized as high, intermediate, and low modulus (specific ranges were not given in his article)[4]. The relationships between shear strength and shear modulus as a function of adhesive bondline thickness, Figure 2.4, agree with a majority of the research presented in the section above. The author, however, does not specify the specimen geometry and strain measurement technique. As shown, there was very little difference in modulus for both the low and intermediate modulus adhesives when the bondline thicknesses approached the typical thickness for structural adhesives (greater than 0.15 mm). Another study, performed by Peretz, yielded similar results. Pertez bonded napkin-ring specimens with an epoxy consisting of a 2:1 ratio of Shell Chemical Company's (Houston, Texas) Resin 828 and General Mills (believed to be manufactured by Cognis Corporation of Cinncinatti, Ohio) Versamid V-140.

These specimens were instrumented with extensometers to measure the shear deformation[18]. Peretz's results suggested a similar trend to that in the Tanner article, decreasing shear moduli as the bondline thickness decreased for an intermediate modulus adhesive.

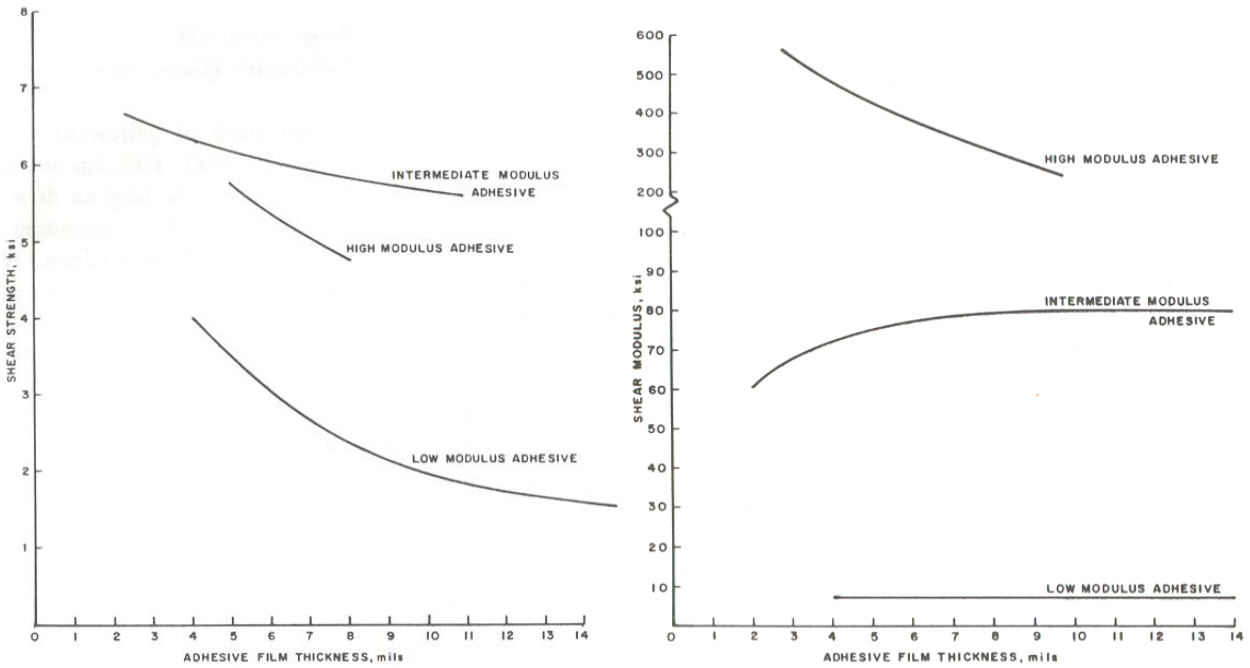

Figure 2.4 Shear modulus and strength trends as a function of bond thickness for three different adhesives, Tanner[4].

In addition to the modulus observations, Tanner also claimed to observe increased ductility in the bonded napkin ring adherends but did not quantitatively report this increase in the article[4]. For all three adhesives tested, the thinner adhesive bondlines exhibited higher shear strain capabilities. These strains were sufficient to exceed the maximum shear strain measurement capability of the instrumentation. Unfortunately, further evaluation of these results is difficult since there was not a description of how these strains were measured. Research presented by Chai showed that the increased shear strain capabilities of a bonded joint were more dramatic for brittle adhesives than for more ductile adhesives[19]. In his study, Chai performed tests using a napkin-ring geometry, with an extensometer to measure relative shear displacement across the bondline, on a brittle (Whittaker Narmco (Costa Mesa, California) 5208) and ductile

[4] Copyright 1972 From *Journal of Applied Polymer Symposia*. Reproduced by permission of John Wiley & Sons.

epoxy (American Cyanamid (Havre de Grace, Maryland) BP-907). He recorded increases in ultimate shear strain and ultimate shear stress when the bondline thickness was decreased. Differences were noted for bonds with adhesive thicknesses greater than 0.15 mm. However, for extremely thin bondlines (micrometers), the ultimate shear strain is drastically increased by as much as 3000%. Chai presented both experimental evidence and analytical considerations suggesting that such a large difference in the ultimate shear strain was a result of premature bond failure due to tensile microcracks or voids formed during loading on the geometries with larger bondline thicknesses. He performed a careful analysis of the deformations and corrected for the substrate deformations to verify these results.

Stringer studied the shear stress-strain behavior of seven (six epoxies and one acrylic) different structural adhesives[20]. Stringer also used a napkin-ring geometry to determine the shear stress-strain properties while varying bondline thickness. As in previous studies, there was a significant increase (approximately 30%) in shear strength and an even more drastic increase in failure strain as the bondline thickness decreased, as shown in Figure 2.5.

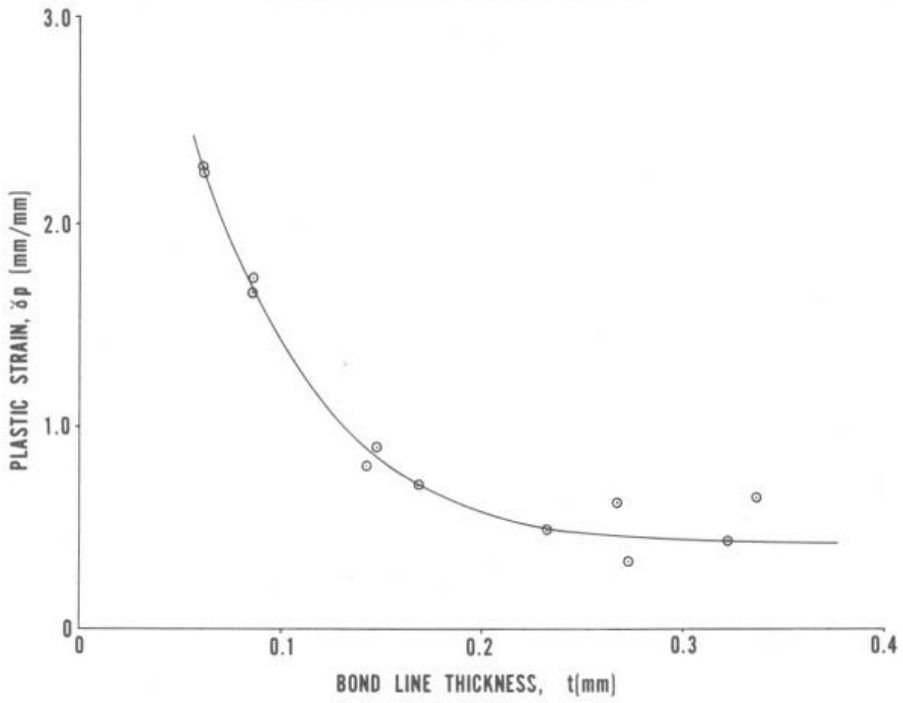

Figure 2.5 The amount of plastic strain significantly increases as the bondline thickness decreases, Stringer[20].

[20] Copyright 1985 From *Journal of Adhesion* by Stringer. Reproduced by permission of Taylor & Francis., http://www.routledge-ny.com

The increase of strength with decreasing bond thickness was not only observed in shear loading but also under tensile loading for some other structural adhesives. Ikegami, et. al. also performed napkin-ring tests loaded in tension on Showa Kobunshi's (company location unknown) R-820 epoxy[21]. These authors showed a significant increase (as large as 200%) of tensile strength as the bondline was decreased. Meissner and Merill similarly tested steel butt joints bonded with a poly(methyl methacrylate) and also found very large increases in tensile failure stress as the bondline thickness decreased. From the data presented in their article, Meissner and Merill showed over a 500% increase in failure stress when adhesive bondline thicknesses decreased from slightly larger then 4 mm down to approximately .25 mm[22].

Upon review of the presented articles, several trends can be identified. As the adhesive bondline thickness decreases, there are significant increases in strengths and strains of the bonded joints. An unaddressed question at this point is whether the actual adhesive properties have changed or is it simply that the driving mechanism has changed? To explore this, Reedy and Guess have performed careful work on the effect of bondline thickness of brittle adhesive systems. They have performed extensive research on stainless steel and aluminum tensile butt joints bonded with Epon (Sylmar, California) 828/T-403 epoxy (E =3.5 GPa)[23,24,25,26]. These authors observed similar strength trends for the bondline thicknesses surveyed (ranging from 0.254 to 2 mm), however they concluded that a material property, the critical interface corner fracture toughness, remained constant and was the controlling mechanism. Their work applied a generalized stress intensity factor, without assuming an initial flaw, but rather examined the stress singularity of an adhesive-adherend interface. The interface corner stress intensity factor accounts for the constraint of the stiff adherends on the Poisson contraction of the adhesive, as well as incorporating the Dundur's elastic mismatch parameters[27]. The result of this analysis is the prediction of bond strength at various bond thicknesses as long as the system is brittle and linear to failure in a tensile test. All of Reedy and Guess's work is validated by experimental results, with statistical analyses that strengthen their claims. This could help explain possible differences between the bulk and *in situ* properties without a physical change in the adhesive. There are many other possible mechanisms that have been proposed by the scientific community to account for these differences, and the next section will discuss some of these ideas.

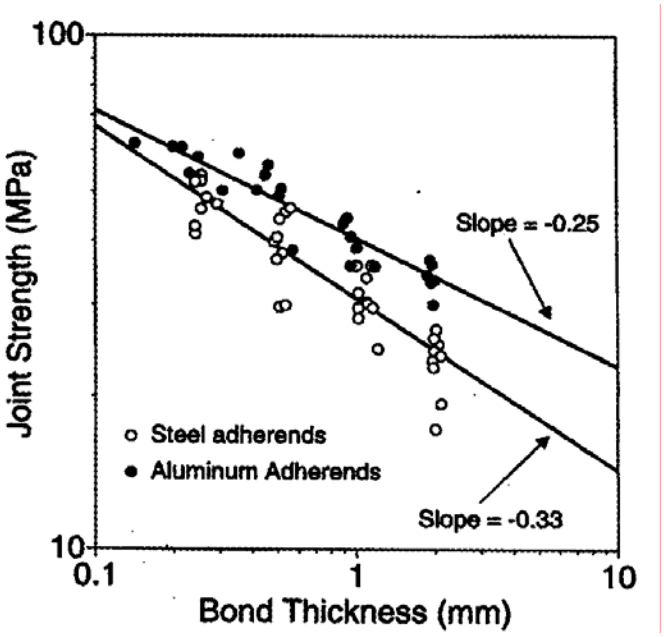

Figure 2.6 Bond strength prediction and experimental data based on critical interface corner fracture toughness, Reedy and Guess[26].

2.4 POSSIBLE EXPLANATIONS

Many different mechanisms have been proposed to explain the differences between bulk and *in situ* adhesive performance, ranging from possibilities of critical flaw size, adhesive constraint, and interfacial effects stemming from the adhesive interphase region. Due to the complexities of adhesives, some or all of these proposed mechanisms could contribute to the observed differences in performance. This section will provide some insight into each of these concepts and present some of the work performed in these areas.

Increased Probability of Critical Flaw

With increasing bondline thickness, the probability of the presence of a critical-sized flaw is also increased. This was suggested by Lund and Byrne[28] as one of the possible interpretations of Leonardo da Vinci's famous iron wire strength experiment[7]. This phenomenon and the importance of imperfections has been discussed by Timoshenko[30] and Weibull[31] and seen experimentally in areas ranging from high phosphorus steel imperfections[32] to the more recent materials of composite matrices and adhesives[33,34,35,36]. In two relevant adhesive studies, Towse

[26] Copyright 1997 From *International Journal of Fracture* by Reedy and Guess. Reproduced with kind permission of Kluwer Academic Publishers.

et. al. using a ductile epoxy[36], 3M's (St. Pauls, Minnesota) EC3448, and Odom and Adams using a brittle epoxy[35], Hercules (New York, New York) 3501-6, used standard tensile dogbones with varying cross-sectional areas to explore this size effect. All of these studies have shown that the bonds with the smaller adhesive volumes were stronger and failed at smaller internal flaws, as represented in Figure 2.7. The left side of Figure 2.7 displays the correlation between the adhesive tensile strength decreasing as the cross-sectional area, and thus the volume of adhesive increases. The plot on the right displays the critical flaw size, determined from micrographs of failed surfaces, that initiated failure of the specimens in the plot on the left. As the adhesive volume increases, the size of the critical flaw also increases. Therefore the proposed mechanism is simply that the possibility exists that the increase in strength and toughness of a thinner adhesive bond is simply a direct result of the lower probability of a critical defect.

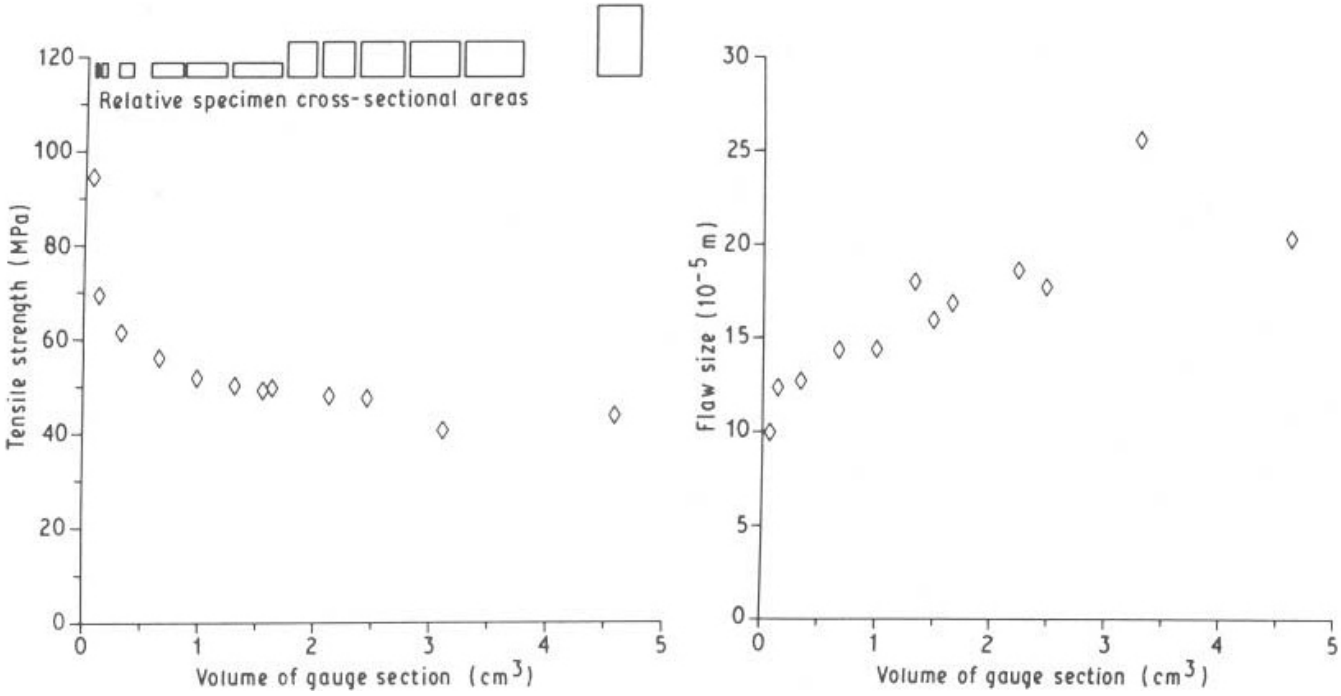

Figure 2.7 Tensile strengths and failure inducing flaw size for varying volumes of adhesive, Odom and Adams[35].

Adherend Induced Constraint

Both Gardon and Miller provided their interpretations and attempted to provide insight on the increased tensile strength of butt joints as the adhesive thickness decreased[3,5]. When metal

[35] Copyright 1992 From *Journal of Material Science* by Odom and Adams. Reproduced with kind permission of Kluwer Academic Publishers.

adherends are bonded together by an adhesive, the stiff adherends inhibit Poisson's contraction of the adhesive. Suppression of the Poisson effect results in a triaxial tension stress state, which could expand the free volume, making the polymer more mobile and hence more ductile. Several other researchers support and have further discussed this issue[19,37,40].

The increased strength and toughness is also present in shear, and one of the explanations is strain hardening. Chai determined that irrespective of the bondline thickness, strain hardening occurred once the nonlinear shear strain exceeded 77%, while softening takes place when the nonlinear shear strain exceeds 52%.[19]. Strain hardening is not seen in the thicker bondlines due to the early failure caused by void growth, but the thinner bondlines are able to enter the strain hardening region, thus allowing for further plastic deformation. He also suggested that for more ductile adhesives with thin bondlines, a significant amount of straining occurs, but cracks and void growth cannot form due to adherend constraints. This results in a large amount of plastic deformation in shear.

Interphase Effects

As mentioned in the introduction of this article, the interface between the adhesive and the substrate is inherently different from a bulk adhesive portion. After Sharpe's introduction[6], the interphase and its effect on adhesive performance has been an area of significant interest, with studies ranging from mechanical properties to material modeling for finite element analysis[38,39]. These differences arise from factors such as the increased constraint placed on the polymer by removing half of the space the molecule would have occupied in its equilibrium conformation. Other factors include the possibility of different stoichiometry near the interface during curing. Yet another factor would be the effect of different surface roughness and porous oxide layers that might extend a distance into the polymer. The area that exhibits the modified behavior is termed the interphase, and several articles have explored the size and properties of the interphase on epoxy-aluminum interfaces and the properties in this interphase.

A study performed by Crompton carefully examined the localized region of an epoxy-aluminum interphase[38]. This study utilized transmission electron microscopy (TEM) and scanning electron microscopy (SEM) to examine the bondlines at a microscopic level. The author found visually that there seemed to be two different transitional layers, one within the first

10 nm and the other extending as far as 1 μm into the adhesive. Micrographs of these regions are shown in Figure 2.8, where the two different transitional regions are easily visible.

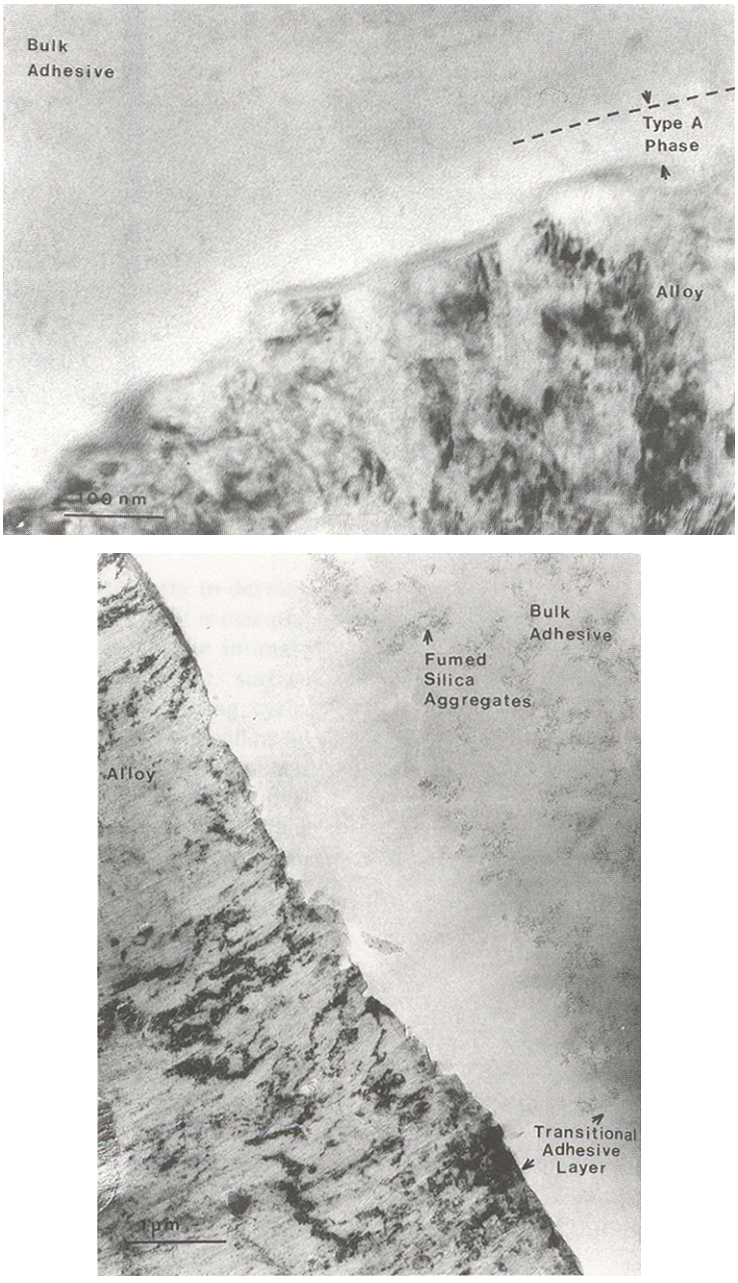

Figure 2.8 Micrographs showing the two transitional adhesive layers, note a difference in scales 100 nm (top) and 1 μm (bottom), Crompton[38].

[38] Copyright 1989 From *Journal of Material Sciencee* by Crompton. Reproduced with kind permission of Kluwer Academic Publishers.

Two studies performed by Safavi-Ardebili, Sinclair, and Spelt examined the effect of these interphases and determined the mechanical properties in these regions. The first utilized nanoindentation and SEM to study an aluminum-epoxy interface[42]. The authors used several bonded 1100 aluminum specimens, treated with a Forest Products Laboratory (FPL) etch[41], to examine differing areas of interest, as shown in Figure 2.9. The adhesive used in this study was Hysol Aerospace (owned by Loctite/Henkel based in Hartford, Connecticut) HYSOL EA-9346 (E =2.1 GPa). Upon examination of the micrographs, this adhesive system was found to have a morphological difference of the interphase within the first 5 μm of adhesive thickness. Additionally, the authors found that the effective modulus of the adhesive was 13% greater and adhesive itself was 4% harder than the bulk adhesive far from the interface.

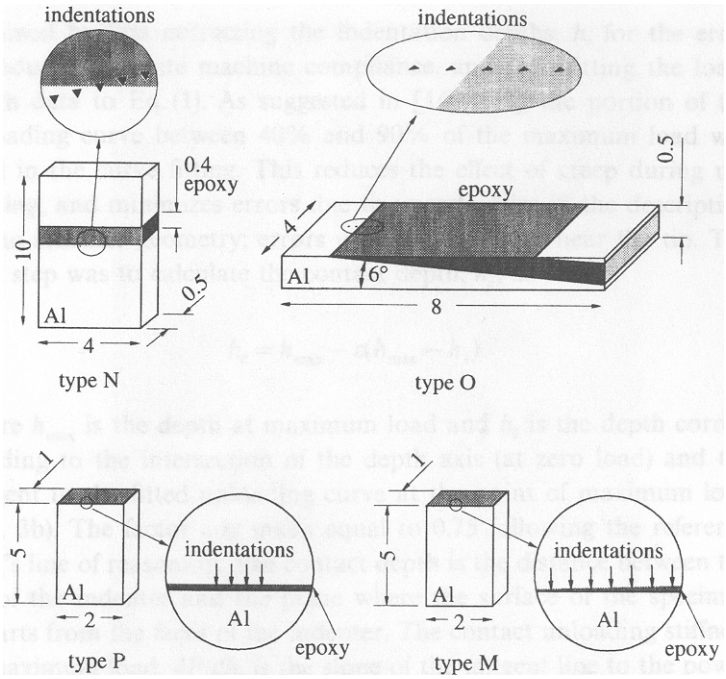

Figure 2.9 Different specimens and locations of the indentations for the nanoindentation study, Safavi-Ardebili et. al.[42].

The authors continued their study to include an acoustic microscope that was able to further quantify the size and properties of the epoxy-aluminum interphase[43]. The same adhesive

[42] Copyright 1997 From *Journal of Adhesion* by Safavi-Ardebili et. al. Reproduced by permission of Taylor & Francis., http://www.routledge-ny.com

system was used, 1100 aluminum treated with an FPL etch and the HYSOL EA-9346, for this study. Specimens were bonded and then portions machined off to provide a taper where sections of adhesive of the desired bondline thickness could be tested, as displayed in Figure 2.10. Since a morphological difference was found within the first 5 μm, a comparison between bondline thicknesses of 0-5 μm and 20-40 μm was performed, however the properties seemed to flatten out after a bondline thickness of 10 μm. A significant difference was found between the two regions, summarized in Table 2.5. The authors believe that reduction in density in the interphase is indicative of differences in the polymeric structure of the adhesive between the bulk and interphase regions. The bulk (20-40 μm deep in the adhesive) modulus values measured by the acoustic probe were more than twice as large as recorded by the manufacturer. The authors attribute this effect to the high speed loading induced by the sound wave, when compared to the quasistatic tensile test. The authors believe that while the values do not correspond with other bulk tests, the trends of significant difference of properties and densities that extend as far in a 10 μm into a bondline are significantly more important than previously thought, but agreed with their previous research using the nanoindentation.

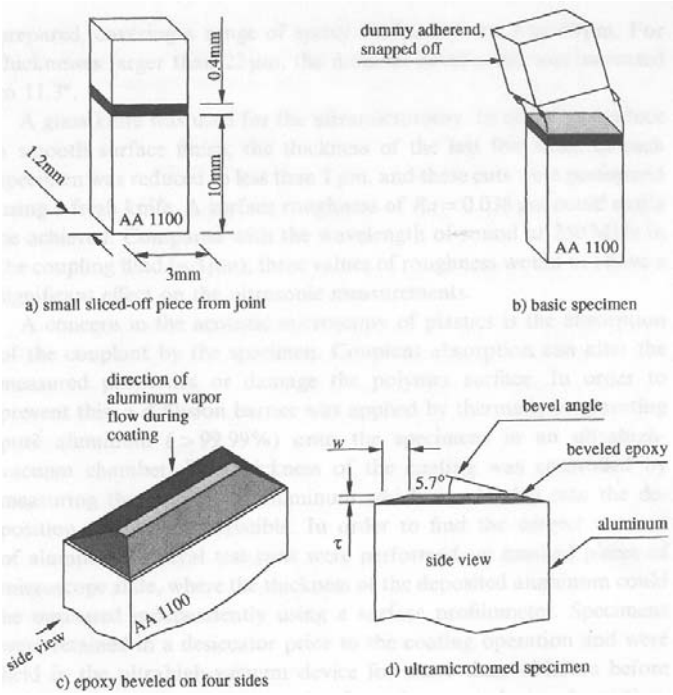

Figure 2.10 Beveled specimen used in acoustic microscope tests, Safavi-Ardebili et. al.[43].

[43] Copyright 2000 From *Journal of Adhesion* by Safavi-Ardebili et. al. Reproduced by permission of Taylor & Francis., http://www.routledge-ny.com

Table 2.5 Comparison of average properties between two interfacial regions for the HYSOL EA-9346 adhesive, Safavi-Ardebili et. al. [43].

Property	v_l [m/s]	v_s [m/s]	ρ [kg/m^3]	E [GPa]	G [GPa]	E_r [GPa]
Average 0 < t < 5 μm	3086	1309	1140	5.52	2.01	6.4
Average 20 < t < 40 μm	2778	1150	1207	4.46	1.6	5.29
% Difference	11.1%	13.8%	-5.5%	23.8%	25.8%	21.7%

The observations in these studies show that possible substrate interactions as deep as 10 μm into the bond were seen and although these interactions may have little effect on the overall average modulus of a joint with a bondline thickness in excess of 0.15 mm, they could greatly affect the overall strength of a bonded joint. Considering this, the possibility exists that these interactions contribute to the mechanisms that cause increased strength and plasticity of the *in situ* geometry over the bulk adhesive.

2.5 SUMMARY AND CLOSING REMARKS

Overall this paper attempted to survey the literature on the performance similarities and differences of *in situ* and bulk adhesive properties. There have been several studies that specifically compared various structural adhesives in bulk and bonded joint tests to directly contrast the performances. The conclusions from these tests indicate that there is substantial agreement between measured linear elastic mechanical properties such as Young's and shear moduli. However, nonlinear design properties such as tensile and shear strengths and tensile and shear ultimate strains showed deviation from the bulk adhesive. As supported by the majority of the research, strength and ductility increased as the adhesive bondline thickness decreased – when the bondline thickness increased the strength and toughness approached the values of the bulk adhesive. Although this article presented several possible mechanisms that could possibly explain these trends, a conclusion about the exact change in mechanisms was not possible. Currently, the authors of this paper are performing a specific study of bulk and *in situ* properties on a two-part acrylic adhesive that will hopefully help answer some of these questions.

Acknowledgements

The author would like to thank the Dow Automotive Corporation and the Center for Adhesive and Sealant Science (CASS) for supporting this research.

2.6 REFERENCES

[1] Dean, G., Crocker, L., Read. B, and L. Wright., "Prediction of deformation and failure of rubber-toughened adhesive joints." *Int. J. Adhesion Adhesives.* **24**, 295-306 (2004).

[2] Zgoul, M. and A. D. Crocombe. "Numerical modeling of lap joints bonded with a rate-dependent adhesive." *Int. J. Adhesion Adhesives.* **24**, 355-366 (2004).

[3] Gardon, J., "Variables and Interpretation of Some Destructive Cohesion and Adhesion Tests," in *Treatise on Adhesion and Adhesives*, Vol. 1, (Dekker, New York, 1966), Chap 8, pp. 269-324.

[4] Tanner, W., "Manufacturing Processes with Adhesive Bonding." *Appl. Polymer Symposia.* **19**, 1-21 (1972).

[5] Miller, G., "Adhesion and the Glassy State," in *Treatise on Adhesion and Adhesives*, Vol. 3, (Dekker, New York, 1973), Chap 3, pp. 123-159.

[6] Sharpe, L, "The Interphase in Adhesion," *J. Adhesion*, **4**, 51-64 (1971).

[7] Leonardo Da Vinci (1972) *I Libri Di Meccanica*, reconstructed from the original notes by Arturo Uccelli, Kraus Reprint, Nendeln, Liechtenstein.

[8] Bascom, W. D., Cottington, R. L., Jones, R. L., and Peyser, P. J., "The Fracture of Epoxy- and Elastomer-Modified Epoxy Polymers in Bulk and as Adhesives." *Appl Polym Sci*,**19**, 2545-2562 (1975).

[9] Adams, R. and Coppendale, J., "The Elastic Moduli of Structural Adhesives," in *Adhesion*, Vol. 1, (Applied Science Publishers, London, UK, 1977), pp. 1-17.

[10] Sancaktar, E. and Brinson, H., "The Viscoelastic Shear Behavior of a Structural Adhesive," in *Adhesion and Adsorption of Polymers*, Vol. 12A, (Plenum Press, New York, 1980), pp. 279-299.

[11] Dwight, D., Sancaktar, E. and Brinson, H., "Failure Characterization of a Structural Adhesive," in *Adhesion and Adsorption of Polymers*, Vol. 12A (Plenum Press, New York, 1980), pp. 141-163.

[12] Brinson, H. F., "The Viscoelastic Constitutive Modeling of Adhesives." *Composites*, **13**, 377-382 (1982).
[13] Gali, S., Dolev, G., and Ishai, O., "An Effective Stress/Strain Concept in the Mechanical Characterization of Structural Adhesive Bonding." *Int. J. Adhesion and Adhesives*, **1**, 135-140 (1981).
[14] Dolev, G., and Ishai, O., "Mechanical Characterization of Adhesive Layer in-situ and as bulk material." *J. Adhesion*, **12**, 283-294 (1982).
[15] Jeandrau, J. P., "Intrinsic Mechanical Characterization of Structural Adhesives." *Int. J. Adhesion and Adhesives*, **6**, 229-231 (1986).
[16] Lilleheden, L., "Mechanical Properties of Adhesives in situ and in bulk." *Int. J. Adhesion and Adhesives*, **14**, 31-37 (1994).
[17] Spigel, B. and Roy, S., "Comparison of the Adhesive Shear Modulus in Bulk and Bonded States." *J. Adhesion*, **47**, 151-163 (1994).
[18] Peretz, D., "Shear Stress – Strain Characteristics of Adhesive Layers." *J. Adhesion*, **9**, 115-122 (1978).
[19] Chai, H., "Deformation and Failure of Adhesive Bonds Under Shear Loading." *J. Mater. Sci.*, **28**, 4944-4956 (1993).
[20] Stringer, L., "Comparison of the Shear Stress-strain Behaviour of Some Structural Adhesives." *J. Adhesion*, **18**, 185-196 (1985).
[21] Ikegami, K., Kajiyama, M., Kamiko, S., and Shiratori, E., "Experimental Studies of the Strength of an Adhesive Joint in a State of Combined Stress." *J. Adhesion*, **10**, 25-38 (1979).
[22] Meissner, H. P. and Merrill, E. W., *ASTM Bull.*, **151**, 80 (1948), in: Kinloch, A. J., *Adhesion and Adhesives Science and Technology*, Chapman and Hill, London, pp. 211.
[23] Reedy, E. D. and Guess, T. R., "Asymptotic Interface Corner Solutions for Butt Tensile Joints," *Int. J. Solids Structures*, **30**, 767-777 (1993).
[24] Reedy, E. D. and Guess, T. R., "Comparison of Butt Tensile Strength Data with Interface Corner Stress Prediction," *Int. J. Solids Structures*, **30**, 2929-2936 (1993).
[25] Reedy, E. D. and Guess, T. R., "Butt Joint Strength: Effect of Residual Stress and Stress Relaxation," *J. Adhesion Sci. Tech.*, **9**, 237-251 (1995).
[26] Reedy, E. D. and Guess, T. R., "Interface Corner Failure Analysis of Joint Strength: Effect of Adherend Stiffness," *Int. J. Fracture.* **88**, 305-314 (1997).

[27] Dundur, J., "Edge Bonded Dissimilar Orthogonal Elastic Wedges Under Normal and Shear Loading." *Transactions of the ASME.* 650-652 (1969).
[28] Lund, J.R. and J.P. Byrne, "Leonardo Da Vinci's Tensile Strength Tests: Implications for the Discovery of Engineering Mechanics," *Civil. Eng. And Env. Syst.*, **18**, 243-250 (2001).
[29] Bikerman, J. J., *J. Soc. Chem. Ind.*, **60T**, 23 (1941).
[30] Timoshenko, S., *Strength of Materials Part II: Advanced Theory and Problems* (D. Van Nostrand Co., Inc., New York, 1956), 3rd ed, pp. 394-400.
[31] Weibull, W., *A Statistical Theory of the Strength of Materials* (Royal Swedish Institute for Engineering Research, 1939), no. 151, pp. 5-10.
[32] Davidenkov, N., Shevandin, E. and Wittmann, F., "Influence of
Size on the Brittle Strength of Steel," *J. Applied Mechanics*, **14**, 63-67 (1947).
[33] Rezaifard, A., Bader, M. G., and Smith, P. A. "Investigation of the Transverse Properties of a Unidirectional Carbon/Epoxy Laminiate: Part 1 – Matrix Properties," *Comp. Sci. Tech..*, **52**, 275-285 (1994).
[34] Wisnom, M. R. and Jones, M. I., "Size Effects in Interlaminar Tensile and Shear Strength of Unidirectional Glass Fibre/Epoxy," *J. Reinf. Plas. Comp.*, **15**, 2-15 (1996)
[35] Odom, E. M. and Adam, D. F., "Specimen Size Effect during Tensile Testing of an Unreinforced Polymer," *J. Mater. Sci.*, **27**, 1767-1771 (1992).
[36] Towse, A., Potter, K., Wisnom, M. R., and Adams, R. D., *J. Mater. Sci.*, **33**, 4307-4314 (1998).
[37] Orowan, E., "Notch Brittleness and the Strength of Metals," *Trans. Inst. Engrs. Shipbuilders Scotland*, **89**, 165-215 (1945).
[38] Crompton, J., "Interfacial Properties and Stability in Bonded Aluminum." *J. Mater. Sci.*, **24**, 1575-158 (1989).
[39] Yan, C., Mai, Y. W., Yuan, Q., and Sun, J., "Effects of Substrate Materials on Fracture Toughness Measurement in Adhesive Joints" *Int. J. Mech. Sci.* **43,** 2091-2102 (2001).
[40] Chai, H., "On the Correlation Between the Mode I Failure of Adhesive Joints and Laminated Composites," *Engng. Fract. Mech.*, **24**, 413-431 (1986).
[41] Russell, W.J., and Garnis, E.A., "A Chromate-Free Low Toxicity Method of Preparing Aluminum Surfaces for Adhesive Bonding," *SAMPE J*, **17**, 19-23 (1981).

[42] Safavi-Ardebili, V., Sinclair, A., and Spelt, J., “Experimental Investigation of the Interphase in an Epoxy-Aluminum System.” *J. Adhesion*, **62**, 93-111 (1997).
[43] Safavi-Ardebili, V., Sinclair, A., and Spelt, J., “Elastic Properties of an Epoxy-Aluminum Interphase Measured Using an Acoustic Microscopes.” *J. Adhesion*, **73**, 385-416 (2000).

Chapter 3: Bulk Adhesive Tests

3.1 INTRODUCTION

As introduced in Chapter One, for this research two bulk adhesive tests, tensile dogbone and Iosipescu shear tests, were performed on the LESA adhesive. The standard tensile test has long been used for characterization of polymers and has been standardized by the American Society for Testing and Materials [1], while the Iosipescu shear specimen, first introduced in the 1960s [2], has been used with much success in the composites field [3,4]. These tests provide some of the necessary data required for modeling the adhesive using finite element analysis. Finite element analysis has proven to be a very powerful method of predicting adhesive joint strength, however these models rely on accurate adhesive characterization obtained from experiments such as these bulk tests. The end goal of finite element analysis with adhesives is to utilize simple experimental tests and the resulting characterization to make predictions of the adhesive performance in complex joints. Zgou and Crocombe have recently published an article on modeling adhesives with a focus on complex models that closely represent adhesive performance in both the linear and nonlinear regions [5]. Others, including Crocombe, have attempted to greatly simplify the modeling of adhesive joints into hybrid models representing various joint configurations [6]. Additionally, other researchers, such as Yan and Mai, have examined not only the adhesive but also the effect of the mechanical properties of the nearby substrate [7]. With significant research efforts being focused on modeling adhesives, corresponding research on the performance differences between bulk and *in situ* scenarios becomes even more important for accurately predicting joint performance. The tests and results presented in this chapter could be used to help develop material models for finite element analyses of the LESA adhesive in a similar manner as the researchers mentioned above. For both bulk adhesive test geometries, specimens were cast, machined, and then instrumented for testing in order to collect the required data for modeling. This chapter discusses the details of the fabrication, instrumentation and testing procedure, as well as the results obtained from these two test geometries. After both the tensile and shear results are discussed, a comparison of the normal and shear properties is presented.

3.2 SPECIMEN PREPARATION

In order to mix the LESA adhesive, a two-part acrylic system, a pneumatic adhesive dispenser, model PPA-300A from Cox North America of Haslett, Michigan, was used with a static mixer tube to mix and dispense the adhesive. The static mixer tubes were model MC-08-24 (24 elements in an 8 inch tube) from MIXPAC Systems AG of Switzerland. This combination is an effective and widely accepted method of dispensing two-part adhesive systems. Initially, specimens were cast in individual molds as suggested by the manufacturer. However this resulted in poor specimen quality due to adhesive shrinkage as the polymer crosslinked and as the density increased. The effect of shrinkage was only observed at the outside edges of the original specimens. Consequently, for this research large patties were cast and many specimens were machined out of this large casting. These patties were originally created by sandwiching the liquid adhesive between two 6.35 mm thick aluminum plates. In order to aid in separation of the aluminum plates, a PTFE-based mold release agent was used. The patty thickness was set by 2.85 mm thick spacers. Approximately 300 mL of adhesive was dispensed onto these aluminum plates to create an oval shaped patty with approximate major and minor diameters of 380 mm and 250 mm, respectively. This apparatus was then clamped and allowed to cure overnight, then disassembled. This procedure worked fairly well, however disassembly was problematic, since the adhesive was still able to bond to the coated aluminum plates. In order to further simplify the fabrication technique, 0.051 mm thick stainless steel foil was placed between the adhesive and aluminum plates. The aluminum plates provided the rigid backing required to maintain uniform adhesive thickness during the curing process, and the compliant stainless steel foil was easily peeled off the adhesive patty, as the LESA adhesive did not bond well to stainless steel. This technique easily provided high quality patties. Even though the LESA adhesive was a room temperature cure adhesive, an elevated temperature postcure at 40°C for four days was used to ensure complete curing, as recommended by the adhesive manufacturer. After the postcure process, the patties were machined into tensile and Iosipescu shear specimens. In order to randomize the test matrix, both Iosipescu shear and tensile specimens were machined out of each patty.

3.3 ASTM D-638 TENSILE TESTS

After fabricating these patties, tensile dogbone specimen machining was very simple. The patties were first cut into 165 mm x 19 mm rectangular strips with a nominal thickness of

2.85 mm and then machined into ASTM D-638 Type 1 specimens using a Tensilkut® machine (Maryville, Tennessee). The Tensilkut® machine utilized a stainless steel jig and a high speed router to create the necked area of the specimen, as shown in the schematic in Figure 3.1. The specimens were then ready to be tested.

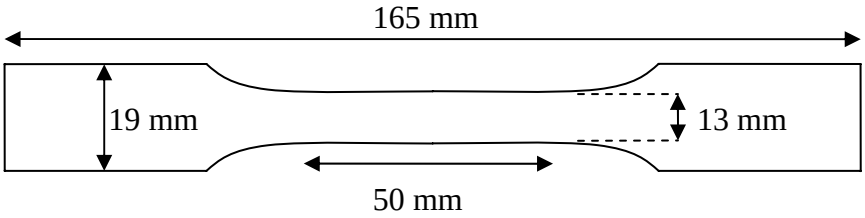

Figure 3.1: Schematic of ASTM D-638 Type I tensile specimen

Testing was performed at room temperature in an Instron 4505 (Canton, Massachusetts) load frame running under displacement control at a crosshead displacement rate at 1 mm/min. A pair of MTS extensometers (Eden Prairie, Minnesota) were used to measure the specimen strains. For some of the tests a biaxial extensometer, MTS model 632.85B-05, was used to measure both axial and lateral strain, however, this extensometer lacked sufficient axial travel to capture the extent of plastic strain seen in some samples. Therefore, a single-axis extensometer, MTS model 632.11B-20, was used to also capture the larger axial strains following yielding. The maximum extensions of the MTS model 632.85B-05 and 632.11B-20 were 1.25 and 2.54 mm respectively. The load was measured with an Instron 5-kN load cell. All of these data values were sampled and collected by the Instron's computer and then transferred to a desktop computer, running National Instruments (Austin, Texas) LabVIEW Software, through a GPIB interface. The following standard equations were used to convert the data into engineering stress and strain:

$$\sigma_{axial} = \frac{P}{A} \tag{3.1}$$

$$\varepsilon_{axial} = \frac{\delta_{axial}}{l} \tag{3.2}$$

$$\varepsilon_{lateral} = \frac{\delta_{lateral}}{w} \tag{3.3}$$

where P is the load, A is the cross-sectional area, δ_{axial} is the axial extension, $\delta_{lateral}$ is the lateral extension, l is the extensometer gage length, and w is the specimen width. After determining the

stress and strain values, the first step in the data analysis was to create stress-strain curves as shown in Figure 3.2. There are three different regions of the stress-strain curve, a quasi-linear portion of the stress-strain curve with the adhesive response showing only slight nonlinearity below yield, a second containing the yielding portion where adhesive response becomes more nonlinear, and a third region involving post-yield plastic flow behavior of the adhesive. For this testing a new method for determining yield stress was developed and is discussed in detail later. From the linear region, necessary design properties such as modulus of elasticity and Poisson's ratio can be determined. From simple mechanics of linear elastic, homogeneous, isotropic materials under uniaxial loading, the modulus of elasticity, E, and Poisson's ratio, ν, are defined by the following equations for an axially loaded specimen:

$$E = \frac{\sigma_{axial}}{\varepsilon_{axial}} \tag{3.4}$$

$$\nu = -\frac{\varepsilon_{lateral}}{\varepsilon_{axial}} \tag{3.5}$$

The modulus of elasticity was determined, according to ASTM D-638, by applying a linear regression to the initial linear region of the stress-strain curves, which translated into utilizing the data between 5 and 50% of the yield stress. The slope of the linear regression of this data subset was taken as the modulus of elasticity. For tests that included measurement of the lateral strain, the Poisson's ratio of the adhesive was also determined. At first this was troublesome to measure since the biaxial extensometer utilized sharp points and had a strong clamping force, resulting in a large amount of lateral creep as the points deformed the specimen. In order to only capture the Poisson contraction during testing, the extensometer was mounted and then allowed to creep into the specimen for several minutes, typically on the order of 10-20 minutes, until the rate of deformation into the specimen was no longer measurable by the extensometer. With the Poisson contraction isolated, the lateral strain and axial strain were plotted with the same initial linear region and data subset, 5 to 50% of the yield stress. Again a linear regression was applied to the data and the slope of this regression was the Poisson's ratio of the adhesive. Additionally the yield region also had important design properties, the yield stress and yield strain. There was also an important property in the last region, which is termed post-yield, the strain at break. Determination of all of these properties completed the normal characterization of the adhesive under ideal uniaxial loading. However, the constitutive properties determined by the tensile

dogbone test did not give direct insight into yield or plastic flow of an adhesive under multiaxial loading.

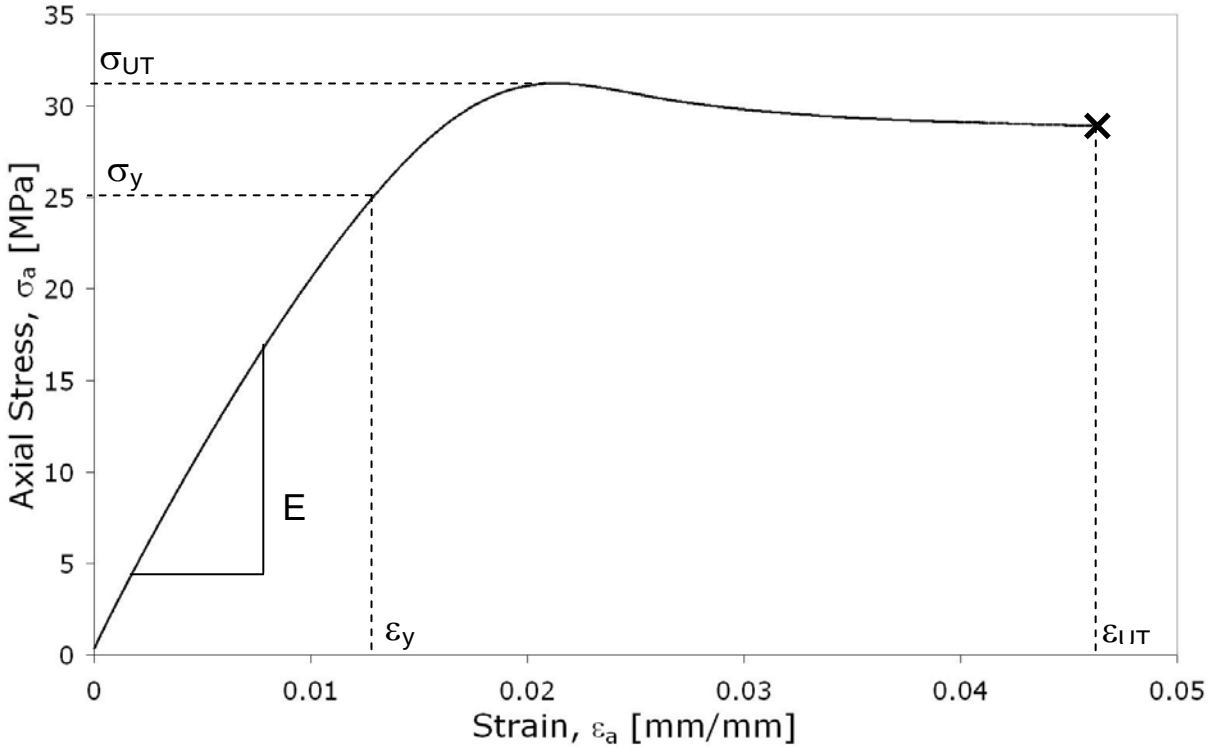

Figure 3.2: Stress-strain regions in typical results from a tensile dogbone specimen.

With the analysis explained, one can move on to the actual test results. As mentioned, all of the data collected from the 10 replicate tests was converted from loads and displacements into stresses and strains. This converted data is plotted in Figure 3.3, which clearly shows the three different regions mentioned above. From these curves the necessary design properties being discussed were determined. According to the ASTM standard, a yield point was determined as the first instance where the strain increased without a corresponding increase in stress for materials that exhibit a zero slope region. However, such a yield criterion did not seem appropriate, this was more of the ultimate stress and would not be a conservative design value. An alternative method for determining yield is the offset method that has been used in metals with great success. An attempt was made to use the offset method, however, applying this method to all of the different test geometries, both bulk and *in situ*, proved to be overly conservative at times and non-conservative at others. Without an applicable previous standard, a new method of consistently determining yield in all test geometries was formed and is briefly

described below; details can be found in Appendix B: Yield Definition. The new yield criterion monitored the slope changes of the stress-strain curve using a several point average to accommodate for scatter in the data. The yield point was determined when the slope of the multipoint average dropped below 50% of the modulus of elasticity determined from the initial linear portion. This criterion allowed for uniformity for all various test geometries and helped determine conservative yield values. In addition to the yield data, the ultimate stress and strain as well as the breaking stress were determined. Using these criteria, the yield stress and strain were determined to be 29.6 MPa with a standard deviation of 1.8 MPa and 1.64% with a standard deviation of 0.16%, respectively. The ultimate stress and strain were determined to be 32.6 MPa with a standard deviation of 1.8 MPa and 4.94% with a standard deviation of 0.553%, respectively. The breaking stress was determined to be 30.8 MPa with a standard deviation of 2.1 MPa. The yield stress and strains were not as prone to scatter as the ultimate values, due to the dependence of ultimate values on critical sized flaws. The amount of scatter shown in Figure 3.3 is typical of results presented in the ASTM standard.

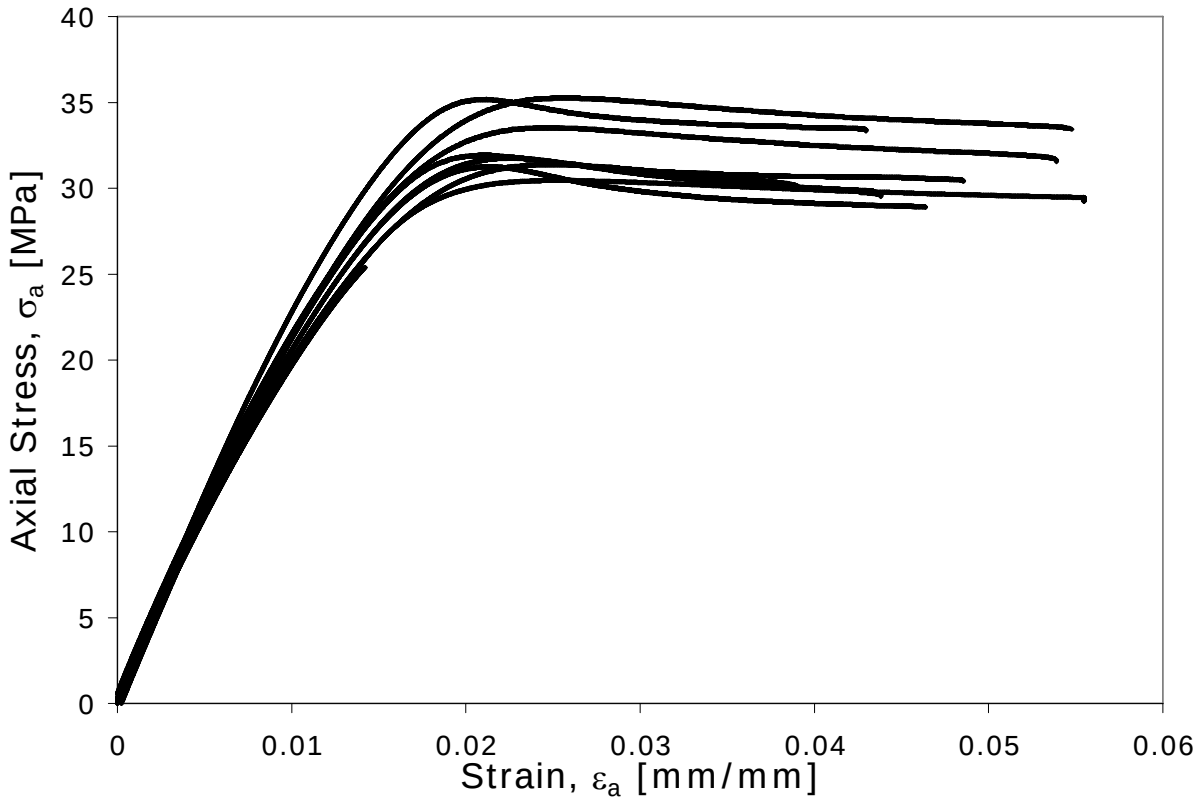

Figure 3.3: Stress-strain plots from tensile dogbone tests at crosshead rate of 1 mm/min.

Using the initial linear portion, from the 5-50% of yield method, of the stress-strain curve plotted in Figure 3.3, the modulus of elasticity could be determined. Similarly, when the lateral strain was plotted against the axial strain, as shown in Figure 3.4, Poisson's ratio was obtained. For both of these properties, a least squares linear regression was used to determine the slope of the line fitting the data. The modulus of elasticity was determined to be 2.29 GPa with a standard deviation of 110 MPa, while Poisson's ratio was determined to be 0.387 with a standard deviation of 0.003. As evident by both of these properties' standard deviations, there was significantly less scatter in this linear region than the subsequent response. Again the amount of scatter was typical of the results shown in the ASTM standard.

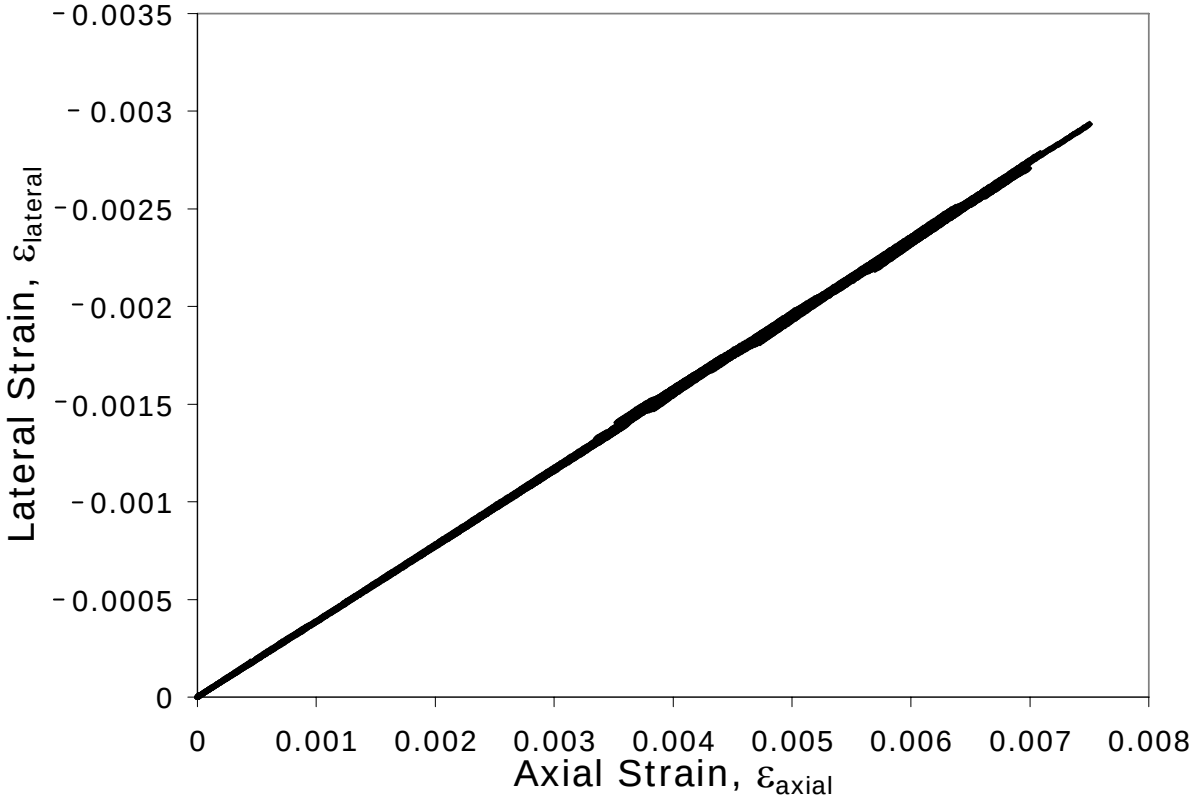

Figure 3.4: Initial linear region of the lateral versus axial strain from tensile dogbone tests.

After performing these analyses, the bulk normal characterization could now be compared to the manufacturer's preliminary data, as shown in Figure 3.5. The tests performed in this research project are represented by the black solid diamonds, while the manufacturer's preliminary data are represented by gray open diamonds. Since the original motivation of this project focused on gaining insight into why a structural adhesive would be brittle in tension, and

ductile in shear, a comparison of the manufacturer's data and the data collected in this study proved very important. There was a large difference in performance between the specimens made from the cast patties and the original individual cast specimens. This finding was attributed to the improvement in specimen quality. Figure 3.6 shows the difference in specimen quality under magnification (magnification unknown), where the piece on the left was a specimen that was machined out of a large patty, while the specimen on the right was an individually cast specimen as originally made by the manufacturer. In this figure, the surface flaws from the individually cast specimens are obvious, and when the failure surfaces were examined, these surface flaws were clearly initiating the specimen failure. By changing fabrication methods and reducing the surface flaws, the adhesive performance changed from a very brittle failure to a more ductile failure. Elimination of the surface flaws did not completely solve the specimen quality problems, and occasional voids proved to be troublesome causing premature failure in specimens, which required the data to be eliminated from averages. In order to eliminate a specimen from the analysis, a tested specimen must have a visible void in the area of failure. Flaw sensitivity became a key observation over the scope of this research project, and will be examined in each test configuration for the effect of flaws on adhesive performance. The overall bulk adhesive performance as measured by these tensile tests is summarized in Table 3.1. Next, the discussion will shift to the bulk adhesive performance in shear, using the Iosipescu shear test geometry.

Table 3.1: Tensile Test LESA Properties

LESA Bulk Adhesive Properties		
	Average	Standard Deviation
Young's Modulus [MPa]	2290	110
Poisson's Ratio	0.387	0.003
Yield Stress [MPa]	29.6	1.8
Yield Strain [%]	1.64	0.16
Ultimate Stress [MPa]	32.6	1.8
Breaking Stress [MPa]	30.8	2.1
Strain at Break [%]	4.94	0.53

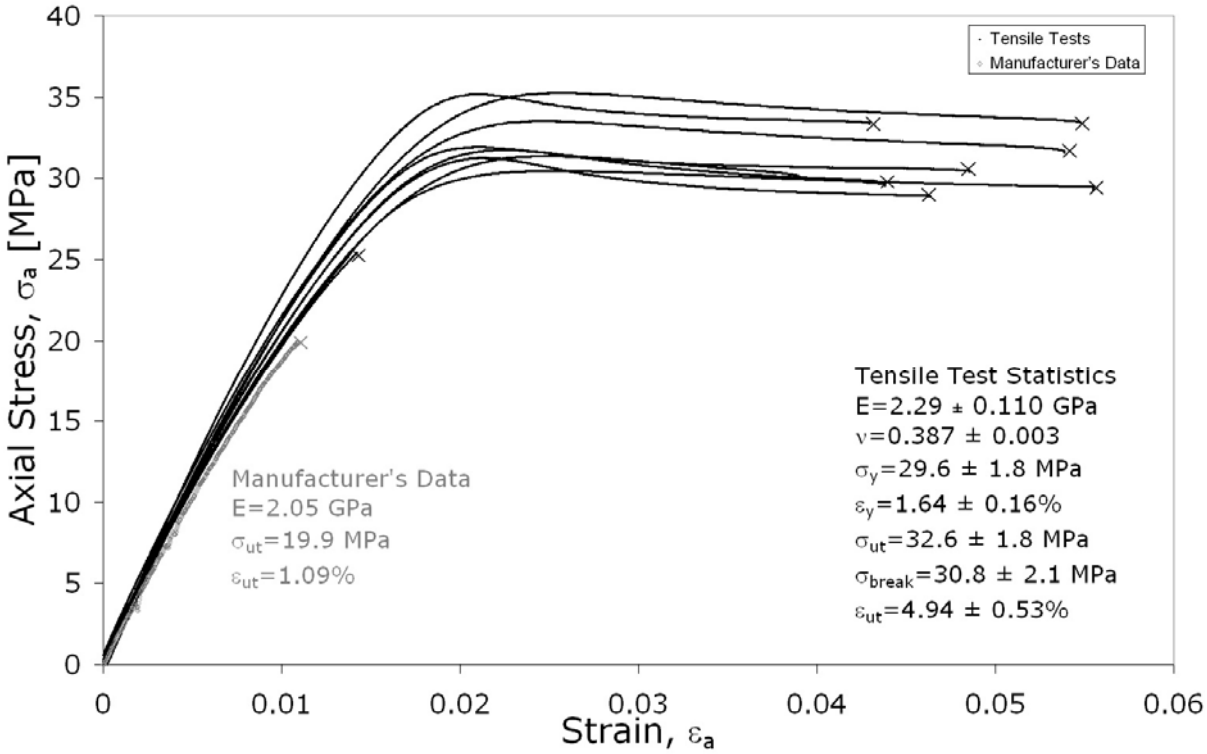

Figure 3.5: LESA adhesive characterization plotted with the manufacturer's preliminary data.

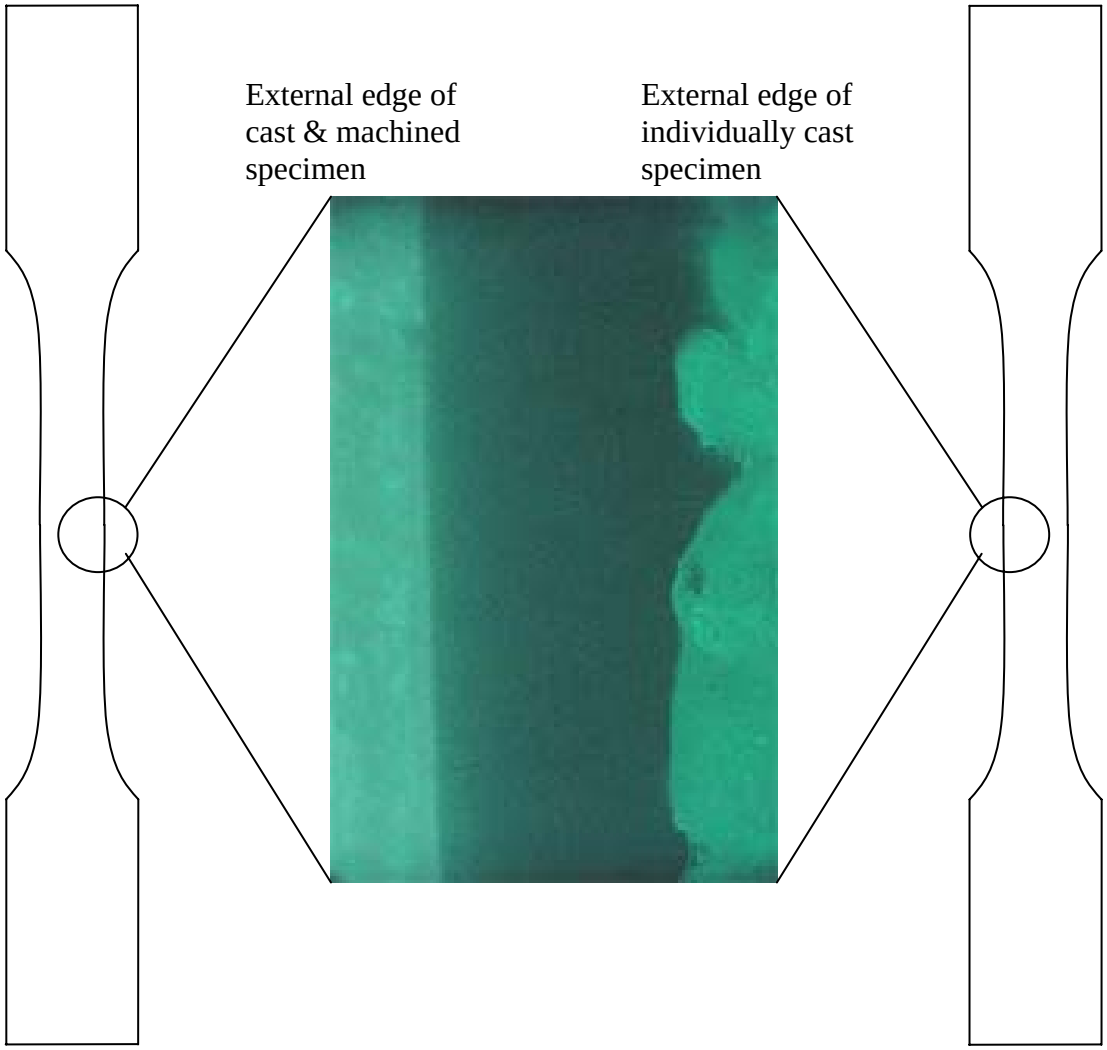

Figure 3.6: Specimen quality differences between machined and cast surfaces.

3.4 ASTM D-5379 SHEAR TESTS

To determine the adhesive performance under shear loading, the Iosipescu shear test was used. The Iosipescu shear test utilizes a double notched specimen tested under an asymmetric four-point-bend loading mode to create a fairly uniform shear stress within the notched region of the test specimens [10,12]. The loading and analysis is described below following the details of the specimen geometry.

The Iosipescu shear specimens were also cut from the cast patties used in fabrication of the tensile test specimens. The same patties used for the tensile tests, with a 2.85 mm nominal

thickness, were cut into 76 mm by 20 mm strips, and then notches were machined into the specimens using a double-angle cutter with a custom tip radius of 1.3 mm. After machining, these specimens conformed to ASTM D 5379 composite specimens and Figure 3.7 shows a schematic of the finished Iosipescu specimen [8]. Several researchers have explored the effect of notch depth, notch angle, and notch radius however most specimens used for isotropic materials used the ASTM suggested geometries [9,10,11]. Special shear modulus gages (Gage Number: N2P-08-C032A-500/SP61), manufactured by Micro-Measurements Group (Raleigh, North Carolina) were used for this test, with the gage layout shown in Figure 3.8. These Iosipescu gage specifications suggested capabilities of measuring up to 20% shear strain; however, a few gages in the actual tests continued to provide strain readings above the maximum specification. With the specimens machined and instrumented, they could then to be tested.

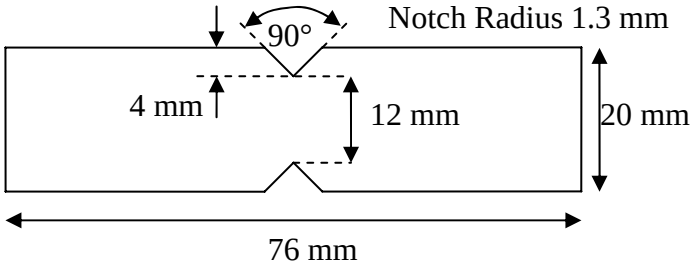

Figure 3.7: Iosipescu shear specimen

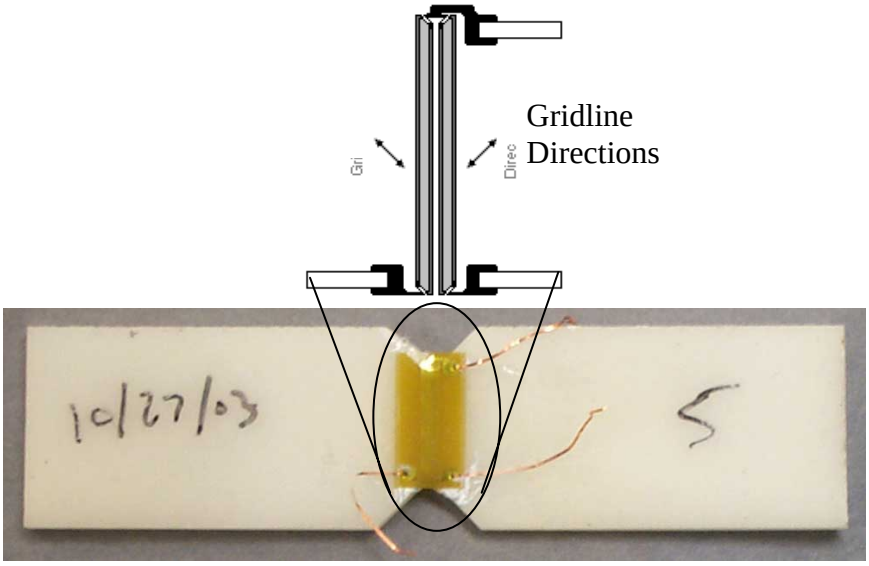

Figure 3.8: Iosipescu shear specimen instrumented with Iosipescu strain gage.

Again an Instron 4505 load frame, running under displacement control at a crosshead displacement rate of 1 mm/min, was used with a Wyoming Test Fixtures (Larame, Wyoming) Modified Iosipescu shear fixture for these bulk adhesive tests. This test fixture is described in further detail below. The load was again measured by an Instron 5-kN load cell, however, the data was read through a 12-bit analog-to-digital converter. The strain gages located in the V-notched area of the specimen were connected to a Micro-Measurements Group 2310 Signal Conditioning Amplifier in a half bridge configuration. Bridge excitation, which was set at 10 V, and bridge completion as well as signal output scaling and gain, was performed in the 2310 Signal Conditioning Amplifier.

The test fixture, shown in Figure 3.9, was used to introduce asymmetric four-point bending that ideally eliminate bending stresses within the V-notch portion of the specimen. This loading, coupled with the specimen's notched geometry, resulted in a fairly uniform shear stress distribution within the gage section. A shear and moment diagram is also shown in Figure 3.9, and this shows that the notched area is nominally in a state of simple shear. When loaded in the Wyoming Test Fixture's Modified Iosipescu shear fixture, the Iosipescu shear specimen is actually a close approximation of a "pure shear" stress state. This modified Iosipescu shear fixture was the product from a large amount of research performed by various scientists. In this modified fixture, unsymmetric shear stress distributions resulting from concentrated load effects were eliminated by moving the contact points away from the notch area.[10,12]. Utilizing the modified fixture, researchers using a true asymmetric four-point bend have published values ranging from 4.5% to 9.8% percent error from the theoretical values of isotropic materials [10,12]. Using the following equations the shear stress, τ_{ave}, was determined for this test geometry:

$$\tau_{ave} = \frac{P}{A} \tag{3.6}$$

where P was the applied load and A was the cross-sectional area, corresponding to the smallest area of the double notched section of the specimen, measured prior to loading. Due to the orientation of the biaxial strain gage, two grids, and the gage factor of these particular gages, the data collected by the computer coincided directly to shear strain. After determining the shear stresses, they were combined with the measured shear strains to create the shear constitutive behavior of the adhesive. The same three regions discussed in the tensile section were present in

shear loading. In the linear region, linear elastic mechanics of materials were used to correlate the shear stresses and strains as shown in the following equation:

$$\tau = G\gamma \tag{3.7}$$

where G is the modulus of rigidity and γ is shear strain. As in the tensile tests, the modulus of rigidity was measured by applying a linear regression to the data in linear loading region that was between 5-50% of the yield stress. The modulus of rigidity was taken as the slope of this curve fit line. Again, the yield region also had important design properties, the yield stress and strain. Since the Iosipescu shear tests has often been used for composite systems, where yield points are not typically seen, the new yield criterion described above was used for these bulk shear tests. Again, the yield point was defined when the slope of the stress strain curve determined from a multiple point average dropped below 50% of the modulus of rigidity. In these tests the adhesive never exhibited an ultimate point of catastrophic failure in the test region. The test specimens continued to plastically deform until cracks originated near the notch points and began to slowly propagate. Therefore, this study was not able to determine a breaking stress and strain for this adhesive, and only reports the maximum stress as the ultimate shear stress.

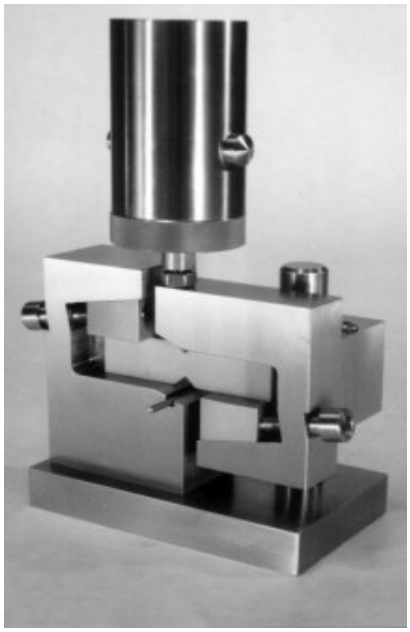

Picture from Wyoming Test Fixtures [13]

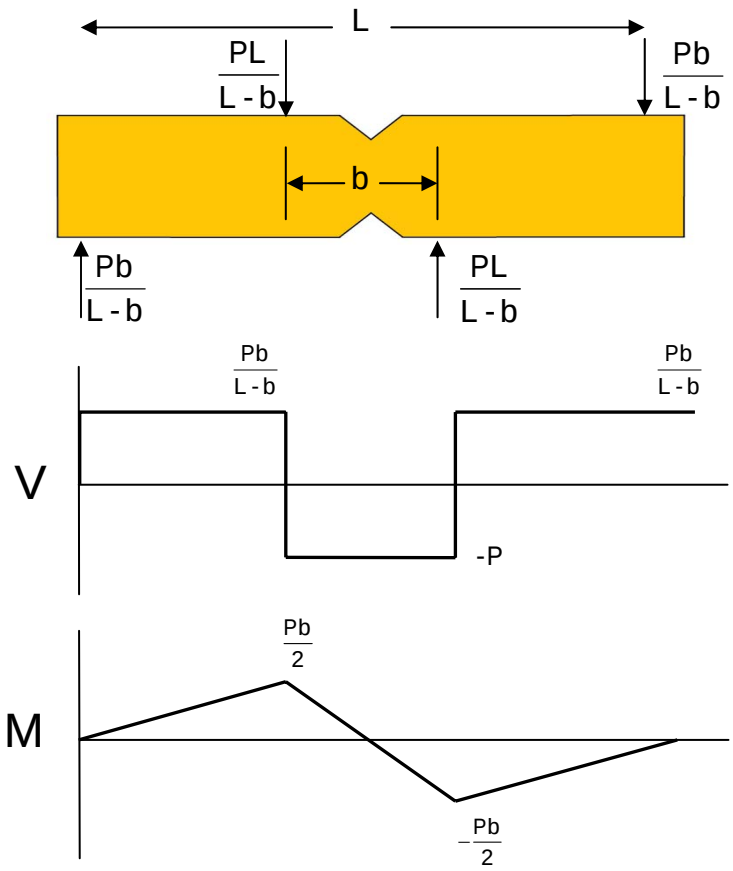

Figure 3.9: Iosipescu test fixture and loading description.

The test results from the Iosipescu shear testing were analyzed using the methods and techniques described above. As in the tensile tests, the stresses and strains were plotted for the analysis of the shear constitutive behavior of the test adhesive and this response is shown in Figure 3.10. Several of the tests experienced strain gage delamination or data acquisition system saturation. The test runs which have an arrow indicate continued deformation; however, the instrumentation was not able to continue to collect meaningful data. The tests which broke while the instrumentation was functioning properly (i.e. no visual delamination or anomalies in strain curve to suggest potential problems) are designated with an "x" to indicate specimen failure. The different regions are once again clearly seen, however the post-yield region was not completely determined since the strain gages delaminated late in the tests. A key aspect to note is that significant plastic deformation continued to occur after the strain gages delaminated or the data acquisition system saturated. Visual estimates of this plastic deformation suggest approximately 100% shear strain permanent deformation and Figure 3.11 shows such a specimen

after testing. The cracks in the adhesive shown in this figure introduce another interesting event that occurred towards the end of the tests. As mentioned, these cracks began to open and propagate slowly near the end of the tests. As with the tensile tests, voids in several specimens resulted in the exclusion of these results in averaging during the data analysis.

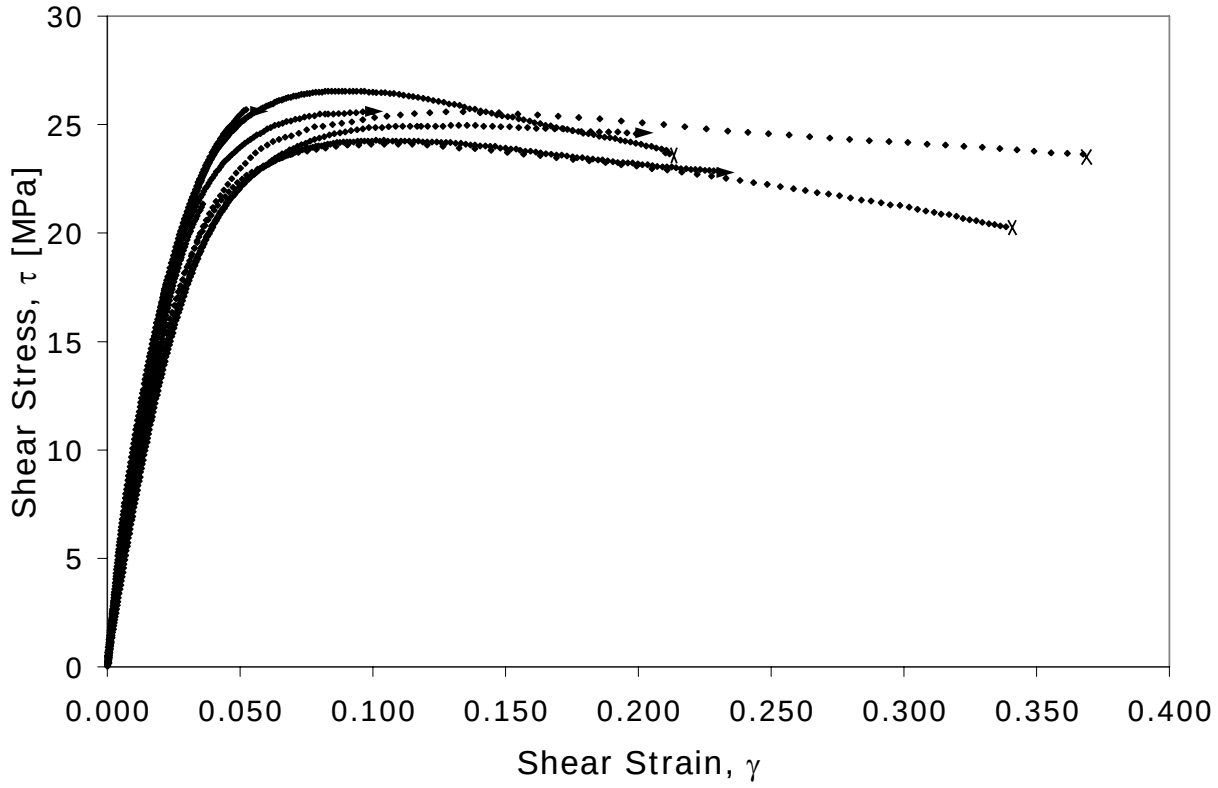

Figure 3.10: Initial shear stress-strain plots.

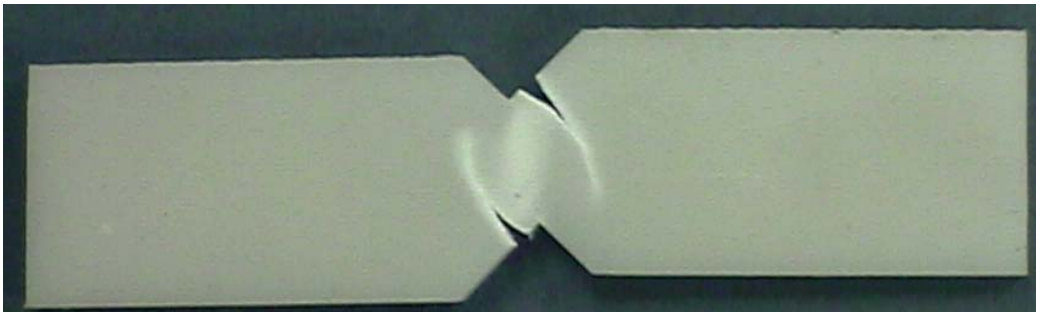

Figure 3.11: Failed Iosipescu shear specimen

Focusing attention on the linear region, the linear elastic properties were determined. Figure 3.12 shows the plot used to determine the modulus of rigidity as described by the curve fitting

procedures above. Due to the more complex nature of the test and approximate "pure shear" loading, more scatter in the data was seen than with the tensile test results. The modulus of rigidity was determined to be 773 MPa with a standard deviation of 86 MPa. Additionally, using the criterion specified above, the yield stress and strains were measured and determined to be 19.1 MPa with a standard deviation of 1.5 MPa, and 2.9% with a standard deviation of 0.2%, respectively. The ultimate shear stress was determined to be 25.2 MPa with a standard deviation of 1.6 MPa.

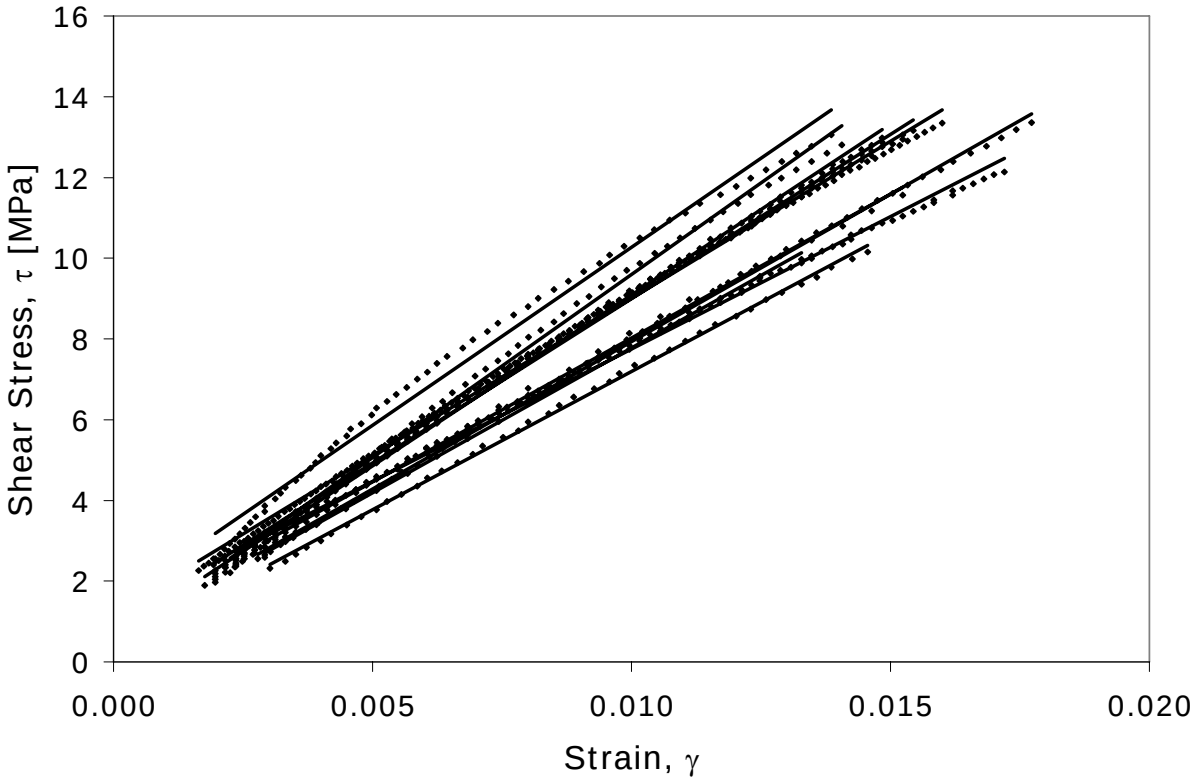

Figure 3.12: Initial portion of the shear stress-strain plots with linear curve fits used for determining the modulus of rigidity.

As with the tensile testing, the shear data was compared to the manufacturer's preliminary *in situ* shear data, and this is shown in Figure 3.13. As a reminder, the manufacturer performed the shear tests on a thick adherend test specimen and, therefore, the plot actually is comparing a bonded joint to a bulk shear specimen. The modulus of rigidity found in the bulk shear tests was approximately 12% lower, while the plastic strains seen in the manufacturer's

data were much higher than the strain gages were capable of measuring. The larger shear strains measured in the manufacturer's thick adherend test are consistent with the visual estimates of approximately 100% shear strain in the Iosipescu shear testing. The similarity between these two very different tests was a very interesting observation. There was a very large amount of ductility shown in shear, upwards of 40% captured by the gages and even higher visual estimates as suggested. Flaws also played an important role in this testing; however they did not appear as dominating as in tensile tests, and as a result, less test data was eliminated from data averaging.

Table 3.2: Iosipescu Shear Test LESA Properties

LESA Bulk Adhesive Properties		
	Average	Standard Deviation
Shear Modulus [MPa]	773	86
Yield Shear Stress [MPa]	19.1	1.5
Yield Shear Strain [%]	2.9	0.2
Ultimate Shear Stress [MPa]	25.2	1.6

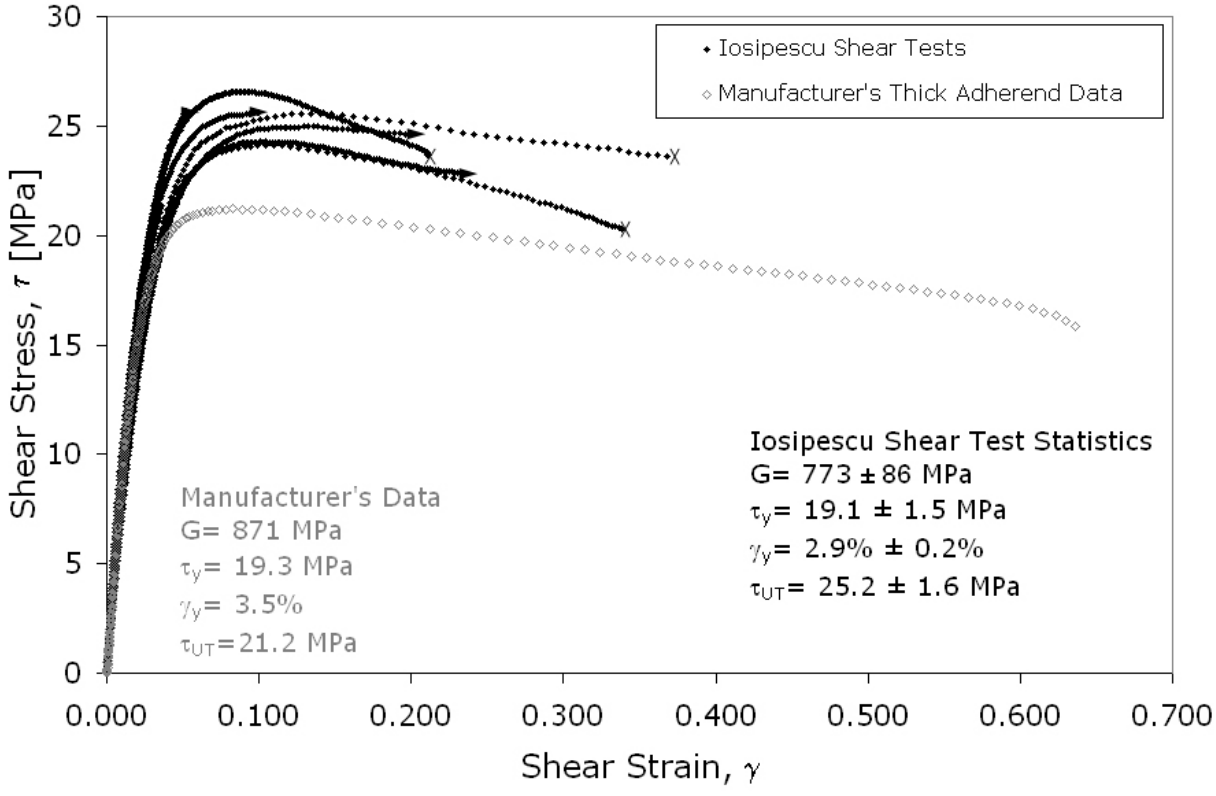

Figure 3.13: Initial shear stress-strain plots.

3.5 COMPARISON OF BULK NORMAL AND SHEAR TESTS

Some important conclusions were made by examining the bulk adhesive performance in normal and shear loading. There are a few different ways to derive the relationship between normal and shear elastic properties; however, this analysis will begin from the more complete constitutive properties. The three-dimensional form of Hooke's law was used to determine the relationship between the moduli of elasticity and rigidity [14]. This law states that for a linear elastic material, the stress components are linear functions of the strain tensor, which is shown by this system of equations relating the stresses and strains,

$$\begin{Bmatrix} \sigma_{xx} \\ \sigma_{yy} \\ \sigma_{zz} \\ \sigma_{xy} \\ \sigma_{xz} \\ \sigma_{yz} \end{Bmatrix} = \begin{bmatrix} C_{11} & C_{12} & C_{13} & C_{14} & C_{15} & C_{16} \\ C_{21} & C_{22} & C_{23} & C_{24} & C_{25} & C_{26} \\ C_{31} & C_{32} & C_{33} & C_{34} & C_{35} & C_{36} \\ C_{41} & C_{42} & C_{43} & C_{44} & C_{45} & C_{46} \\ C_{51} & C_{52} & C_{53} & C_{54} & C_{55} & C_{56} \\ C_{61} & C_{62} & C_{63} & C_{64} & C_{65} & C_{66} \end{bmatrix} \begin{Bmatrix} \varepsilon_{xx} \\ \varepsilon_{yy} \\ \varepsilon_{zz} \\ \gamma_{xy} \\ \gamma_{xz} \\ \gamma_{yz} \end{Bmatrix} \tag{3.8}$$

where C_{11} through C_{66} are elastic coefficients that make up the constitutive matrix, C. Another useful relationship required for such a modulus comparison was the strain-energy density, U_0, and the stresses, which was found to be the following,

$$\begin{aligned} \sigma_{xx} &= \frac{\partial U_0}{\partial \varepsilon_{xx}},\ \sigma_{yy} = \frac{\partial U_0}{\partial \varepsilon_{yy}},\ \sigma_{zz} = \frac{\partial U_0}{\partial \varepsilon_{zz}} \\ \sigma_{xy} &= \frac{\partial U_0}{\partial \gamma_{xy}},\ \sigma_{xz} = \frac{\partial U_0}{\partial \gamma_{xz}},\ \sigma_{yz} = \frac{\partial U_0}{\partial \gamma_{yz}} \end{aligned} \tag{3.9}$$

Using some appropriate differentiations and Equations 3.8 and 3.9, one can show that of the original 36 elastic coefficients, only 21 coefficients are distinct since the stiffness matrix is symmetric (i.e. C_{12}=C_{21}). Assumptions that the material is both isotropic and homogenous further simplify the stiffness matrix from 26 to only two distinct coefficients. For a linear elastic isotropic homogenous material the strain-energy density can be shown to be,

$$U_0 = \frac{1}{2}\lambda\left(\varepsilon_{xx} + \varepsilon_{yy} + \varepsilon_{zz}\right)^2 + G\left(\varepsilon_{xx}^{\ 2} + \varepsilon_{yy}^{\ 2} + \varepsilon_{zz}^{\ 2} + 2\varepsilon_{xy}^{\ 2} + 2\varepsilon_{xz}^{\ 2} + 2\varepsilon_{yz}^{\ 2}\right) \tag{3.10}$$

where λ and G are called the Lamé elastic constants. Converting this relationship back from the strain-energy density back to the stresses using Equation 3.9 yields the following,

$$\begin{aligned} &\sigma_{xx} = \lambda e + 2G\varepsilon_{xx}, \sigma_{yy} = \lambda e + 2G\varepsilon_{yy}, \sigma_{zz} = \lambda e + 2G\varepsilon_{zz} \\ &\sigma_{xy} = G\gamma_{xy}, \sigma_{xz} = G\gamma_{xz}, \sigma_{yz} = G\gamma_{yz} \end{aligned} \tag{3.11}$$

where $e \approx \varepsilon_{xx} + \varepsilon_{yy} + \varepsilon_{zz}$. After inverting Equation 3.11 and introducing two new terms, the well known three dimensional Hooke's law takes the form:

$$\varepsilon_{xx} = \frac{1}{E}\left(\sigma_{xx} - \nu\sigma_{yy} - \nu\sigma_{zz}\right),\ \varepsilon_{yy} = \frac{1}{E}\left(\sigma_{yy} - \nu\sigma_{xx} - \nu\sigma_{zz}\right),\ \varepsilon_{zz} = \frac{1}{E}\left(\sigma_{zz} - \nu\sigma_{xx} - \nu\sigma_{yy}\right)$$
$$\gamma_{xy} = \frac{1}{G}\sigma_{xy} = \frac{2\left(1+\nu\right)}{E}\sigma_{xy},\ \gamma_{xz} = \frac{1}{G}\sigma_{xz} = \frac{2\left(1+\nu\right)}{E}\sigma_{xz},\ \gamma_{yz} = \frac{1}{G}\sigma_{yz} = \frac{2\left(1+\nu\right)}{E}\sigma_{yz} \tag{3.12}$$

where *E* is the modulus of elasticity and ν is Poisson's ratio. After this manipulation the relationship between *G*, the modulus of rigidity, and *E*, the modulus of elasticity, can be shown to be,

$$G = \frac{E}{2\left(1+\nu\right)} \tag{3.13}$$

In order to perform a comparison of these two test results, Equation 3.13 was used with the modulus of elasticity and Poisson's ratio determined from the bulk tensile tests to calculate a predicted modulus of rigidity that was then compared to the shear test results. Uncertainty and error propagation were used in this calculation and the predicted modulus of rigidity was 825 ± 40 MPa. The Iosipescu shear tests measured the modulus of rigidity to be 773 ± 86 MPa. While these values are not identical, the results are encouraging since they are very similar and have overlapping standard deviation ranges, thus giving confidence to the assumption that these test geometries provide uniform uniaxial and pure shear stress states.

Another useful comparison between the tensile and shear tests was the examination of the amount of plastic strain observed. The manufacturer's data suggested that the adhesive performed in a brittle manner in tensile tests. However, by eliminating flaws, ductile behavior was also observed. Typically in the tensile tests, yield occurred at a tensile nominal strain of approximately 1.6% strain and the adhesive was capable of plastically deforming to a nominal failure strain about 4.9% strain at fracture. Conversely in shear, the specimens typically yielded around a nominal shear strain of 2.9% and, as mentioned, possibly strained as much as 100%. All of these strains are reported as engineering, or nominal, strains. The adhesive showed a much larger capability for dissipating energy when loaded in shear.

Comparing the yield stress was also interesting. Under uniaxial tension the adhesive yielded at 29.6 MPa while under shear the adhesive yielded at 19.1 MPa, 64.5% of the normal yield strength, these yield strengths were analyzed using typical failure criteria [15]. Under a

maximum shear stress criterion the yield strength in shear should be 50% of the normal yield stress. Alternatively, the two yield stresses were converted to von Mises effective stresses, σ', using the following equation in order to perform a comparison using the distortion-energy hypothesis:

$$\sigma' = \frac{1}{\sqrt{2}}\left[\left(\sigma_x - \sigma_y\right)^2 + \left(\sigma_y - \sigma_z\right)^2 + \left(\sigma_z - \sigma_x\right)^2 + 6\left(\tau_{xy}^2 + \tau_{yz}^2 + \tau_{xz}^2\right)\right]^{1/2} \qquad (3.14)$$

The effective stress in the tensile tests was equal to the applied stress, while the effective stress in the bulk shear tests was approximately 1.118 times the applied shear stress. When compared to the tensile results using the introduced yield method, the adhesive was 29.1% and 11.8% stronger in shear than predicted by the Tresca and von Mises criterions, respectively. These comparisons helped to understand and provide insight into possible differences between normal and shear loading. Similar comparisons of the *in situ* properties will better help to understand adhesive performance.

3.6 CONCLUSIONS

In conclusion, the results from the bulk testing provide some very interesting details on the fundamental differences and similarities between bulk properties when the LESA adhesive is tested in shear and normal tests. A crucial observation from these tests was the necessity for high quality specimens where the flaw sizes were reduced and then the failure was not dominated by these flaws. In the tensile dogbone tests, the adhesive performance went from a very brittle system to a system that showed significant ductility and energy dissipation when small surface flaws were minimized. In both the tensile and shear tests, small voids proved to be a nuisance, and many specimens' data was eliminated from data averaging because the specimens failed at these voids. After the specimen manufacturing process was optimized, approximately 75% of specimens were void-free. Regardless of specimen problems, the adhesive bulk normal and shear constitutive properties were determined and Table 3.3 summarizes the bulk adhesive properties. From this table, one can see that the LESA adhesive was stronger in shear, τ_y = 19.1 MPa, than predicted from the normal test results by 11.8% (von Mises failure criteria) and 29.1% (Tresca failure criteria). Additionally the LESA adhesive had large amounts of elastic and plastic flow in shear with yield strains in shear almost double that of the normal and gross plastic deformation in shear failures The moduli of elasticity and rigidity compared well between the two different tests and showed good correlation with only a 6.5%

difference. Overall these tests provided many useful concepts that were carried over into the characterization of the *in situ* properties of the adhesive which is described in Chapter 4.

Table 3.3: Combined Tensile and Shear Test Results

LESA Bulk Adhesive Properties		
	Average	Standard Deviation
Young's Modulus [MPa]	2290	110
Poisson's Ratio	0.387	0.003
Yield Stress [MPa]	29.6	1.8
Yield Strain [%]	1.64	0.16
Ultimate Stress [MPa]	32.6	1.8
Breaking Stress [MPa]	30.8	2.1
Ultimate Strain [%]	4.94	0.53
Shear Modulus [MPa]	773	86
Yield Shear Stress [MPa]	19.1	1.5
Yield Shear Strain [%]	2.9	0.2
Ultimate Shear Stress [MPa]	25.2	1.6

3.7 REFERENCES

[1] "Standard Test Method for Tensile Properties of Plastics" *ASTM Standard D 638-01, Amer. Soc. Test. and Mat.,* Philadelphia (2001).

[2] Iosipescu, N., "New Accurate Method for Single Shear Testing of Metals," *J. Mat.*, **3**, 537-566 (1967).

[3] Herrera-Franco, P. J. and Valadex-González, A., "Mechanical Properties of Continuous Natural Fibre-reinforced Polymer Composites," *Composites Part A: Applied Science and Manufacturing.* **35**, 339-345 (2004).

[4] Abot, J. L., Yasmin, A., Jacobsen, A. J. and I. M. Daniel, "In-plane Mechanical, Thermal and Viscoelastic Properties of a Satin Fabric Carbon/epoxy Composite," *Comp. Sci. and Tech.* **64**, 263-268 (2004).

[5] Zgoul, M and A. D. Crocombe, "Numerical modeling of lap joints bonded with a rate-dependent adhesive." *Int. J. Adhesion and Adhesives*, **24**, 355-366 (2004).

[6] Wu, G. and A. D. Crocombe, "Simplified Finite Element Modeling of Structural Adhesive Joints,: *Computers & Structures*, **61**, 385-391 (1996).

[7] Yan, C. and Mai, Y. W. "Effects of substrate materials on fracture toughness measurement in adhesive joints." *Int. J. Mech. Sci.* **43,** 2091-2102 (2001).

[8] “Standard Test Method for Shear Properties of Composite Materials by the V-notched Beam Method.” *ASTM Standard D 5379-98, Amer. Soc. Test. and Mat.,* Philadelphia (1998).

[9] Hawong, J., Shin, D., and Baek, U. “Validation of pure shear test device using finite element method and experimental methods.” *Eng. Frac. Mech.*, **71**, 233-243 (2004).

[10] Sullivan, J. L., Kao, B. G., and Van Oene, H., “Shear Properties and a Stress Analysis Obtained from Vinyl-ester Iosipescu Specimens,” *Exp. Mech.,* **24**, 223-232 (1984).

[11] Grabovac, I. and Morris, C. E. M. “The Application of the Iosipescu Shear Test to Structural Adhesives.” *J. App. Poly. Sci.*, **43**, 2033-2042 (1991)

[12] Adams, D. F. and Lewis, E. Q., “Further Development of the Iosipescu Shear Test Method,” *Exp. Mech.*, **27**, 113-119 (1987).

[13] Mechanical Test Fixtures for Testing All Types of Materials. 2005. 7 July 2005 <http:// www.wyomingtestfixtures.com/Products/a1.html>.

[14] Boresi, Arthur P. and Richard J. Schmidt. *Advanced Mechanics of Materials.* 6th ed. New York: John Wiley & Sons, 2003.

[15] Shigley, J. E. and Charles R. Mischke. *Mechanical Engineering Design*. 6th ed. New York: McGraw Hill, 2001.

Chapter 4: In Situ Adhesive Tests

4.1 INTRODUCTION

The *in situ* adhesive performance of the LESA adhesive was determined through bonded adhesive tests and the results from these tests were used to provide a comparison to the bulk adhesive tests described in the previous chapter. The primary test chosen for this characterization involved a napkin-ring geometry that was loaded in tension to create a nominally uniform normal stress distribution, or was alternately loaded in torsion to create a nominally uniform shear stress distribution. The napkin-ring specimen had been standardized by the American Society for Testing and Materials for inducing a shear-stress state, but has recently (2003) been withdrawn as a standard [1]. The napkin-ring geometry seems ideal for this type of testing due to the continuous bondline which does not introduce stress concentrations at sharp corners or bond terminations. Currently, the reason for withdrawal is not known, however there is no other ASTM standard with the potential for determining the *in situ* constitutive properties of structural adhesives loaded both in normal and shear. The data produced from the napkin-ring tests suggests that the LESA adhesive shows sensitivity to the hydrostatic stress. Hydrostatic stress sensitivity has been seen in many structural adhesive systems and currently many new material models used for finite element analysis are utilizing a von Mises failure criterion modified to include hydrostatic stress sensitivity [2,3,4]. All of the test data, from both bulk and *in situ* adhesive tests, were compiled into normal and shear stress-strain plots and the results provide interesting insight into the differences between bulk and *in situ* adhesive performance, this comparison will be presented in Chapter 5. This chapter discusses the details of the fabrication, instrumentation, testing procedure, as well as the results of these test geometries. Following the presentation of both the tension and torsion results is a discussion of results and observations.

4.2 SPECIMEN PREPARATION

The specimens made for the *in situ* testing required significantly more setup than the bulk adhesive specimens. As in the bulk adhesive tests, a pneumatic adhesive dispenser, model PPA-300A manufactured by Cox North America (Haslett, Michigan) was used with a static mixer tube to mix and dispense the adhesive. The static mixer tubes were model MC-08-24 (24

elements in an 8 inch tube) from MIXPAC Systems AG (Switzerland). Again, this method is both accepted and very effective, especially when used to dispense adhesive on a small surface such as with the napkin-ring geometry. For these *in situ* tests, the substrates had to be chemically treated to ensure high quality bonds.

Preliminary testing (the data is not presented) using 6061-T6 aluminum showed some variability in failure surfaces and mode of failures. Therefore to provide better and more consistent adhesion, the aluminum substrates were treated with a P2 etch. This surface treatment was originally introduced by Russell and Garnis as a chromium-free treatment with simple waste disposal procedures that provided similar performance to the popular Forest Products Laboratory (FPL) etch [5]. The P2 etch technique is also an American Society for Testing and Materials procedure for surface treatment of metals, specifically aluminum [6]. The P2 etch is carried out in an acidic Fe(III) solution which leaves a stable and uniform columnar aluminum oxide finish that provides an excellent surface for bonding. The process for treating the aluminum substrates used for *in situ* adhesive characterization was performed as follows:

1. Aluminum substrates were scrubbed with a 3M (St. Paul's, Minnesota) Scotchbrite® Heavy Duty abrasive pad and liquid dishsoap degreaser to remove machining oil and mill scale.
2. A deionized water rinse prepared the substrates for the next step.
3. The substrates were immersed for 2-3 minutes in a 5% (by weight) NaOH solution, which was preheated to 50°C.
4. The substrates were again rinsed with deionized water.
5. The substrates were then immersed in a 50% (by volume) HNO_3 solution at room temperature for 2-3 minutes
6. The substrates were again rinsed with deionized water.
7. The last chemical treatment involved immersing the substrates for 8 minutes in the P2 solution (505.2g $Fe_2(SO_4)_3 \cdot 4H2O$ and 740g H_2SO_4 dissolved in 4L of deionized water), which was preheated to 65°C.
8. Substrates were then once again rinsed in deionized water and allowed to drip dry.
9. Substrates were dried in an oven at 60°C for at least 1 hour to ensure that all the water evaporated from the substrates.
10. The substrates were then ready for bonding.

After the specimens were surface treated, specially designed fixtures and procedures, discussed in detail below, were used to bond the specimens for *in situ* adhesive testing. After bonding and prior to testing, as with the bulk adhesive specimens, the bonded joints were allowed to cure for 24 hours at room temperature and then placed in an oven at 40°C for four days to ensure a complete cure, as suggested by the adhesive manufacturer. As mentioned, the fixtures and procedures will be described in detail in the corresponding sections below.

4.3 ASTM E-229 NAPKIN-RING TESTS

This section will begin by describing the napkin-ring geometry and specimen fabrication procedure. Following this discussion the specimen loading, instrumentation, and analysis is discussed. Lastly, the results from the napkin-ring tests will be presented and discussed. The geometry used for these tests was based on the ASTM standard E-229 and adapted for use in an Instron 5800 Tension-Torsion test frame [1]. The specimens were machined out of annular aluminum 101.6 mm and 88.9 mm in outer and inner diameter, respectively. A portion of the specimen was turned down to an outer diameter of 95.3 mm diameter to create a reduced cross-section, referred to as the ring, that is ideal for both normal and shear testing as it kept the breaking loads in an appropriate range for the load cells installed in the Instron test frame. The ASTM standard specimen has a moderately larger diameter, with the outer and inner ring diameters of 122 mm and 111.8 mm, respectively. The width of this ring was very important to the shear stress distribution from a torsional load, since simple torsion theory would suggest that the shear stress increases linearly as the radius increases. The shear stress, τ, as determined by simple mechanics of linear elastic, homogeneous, and isotropic materials is defined by:

$$\tau = \frac{Tr}{J} \tag{4.1}$$

where T is the applied torque, r is the radius from the center of the tube, and J is the polar area moment of inertia. The shear stress increases proportionally to the increase in radius, therefore, the ring width was reduced to minimize the shear stress gradient. However, as the ring width decreases, the applied load or torque required to fail the specimens also decreases, which directly affects the signal to noise ratio of the test frame's large load cells. Since these were two competing mechanisms, the test geometry used a ring width of 3.2 mm, which Equation 4.1 predicts a 7.2% variation in shear stress across the bondline, while keeping the failure loads well above of the load cell noise level. This shear variation was well under the variation present in

the previous ASTM standard of 9.1%. The final bond area of the napkin-ring specimen was 918 mm^2. The specimens were also machined with four reamed fixturing holes and several transducer mounting holes. The fixturing holes were used for alignment during specimen construction as well as loading in the test frame. These holes were machined with an angular spacing of 90°. A schematic of the geometry showing the pertinent dimensions and a picture of an actual specimen showing the fixturing and transducer mounting holes is displayed in Figure 4.1. The resulting part from the described machining results in the construction of half of a napkin-ring specimen. These specimens, alignment tools, and sensor instrumentation were designed and fabricated by John Hennage. Additional details on this geometry and further testing will appear in his dissertation entitled "Characterization and Analysis of Adhesives for Joint Design," which will be published upon completion of his research.

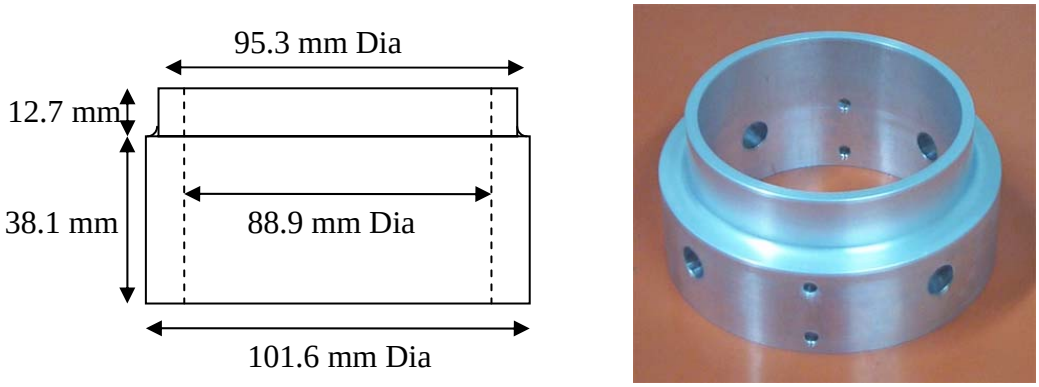

Figure 4.1: Schematic and picture of half of a napkin-ring specimen

Constructing the full napkin-ring specimen involved bonding two rings, as described in the section above. The most important aspect of bonding these two rings together was ensuring that the centerlines were aligned to ensure centric loading. The stress state experienced by the bond is drastically affected by an eccentric load, which results in a bending stress applied where a uniform axial stress is desired. In order to ensure concentricity of the two halves, alignment blocks and spacers were built that were identical to the fixtures used for loading in the actual test frame. By varying the height of the alignment spacers the adhesive bondline thickness could be controlled. Both the alignment blocks and spacers are shown in Figure 4.2 . For the testing performed in this research, an adhesive bondline thickness of 1 mm was used. Another issue relevant to bonded test specimens was examined by Adams et. al. in their study of axisymmetric butt joints loaded in tension and torsion, which resemble the napkin-ring specimens used in this

study [7]. Adams et. al. explored the effect of adhesive spew on the test results and found that there was a stress concentration resulting from the spew. In order to address this issue, the napkin-ring specimens were constructed such that the spew was directed to the interior of the annulus but did not bridge the interior sides. To accomplish this, a stainless steel feeler gauge was held around the outside edge of the specimens and a high-density polyethylene puck was placed inside the specimen during fabrication to catch the spew. Figure 4.3 shows half of a specimen with feeler gauge and the high-density polyethylene puck ready for adhesive to be dispensed, while Figure 4.4 is a schematic showing where the spew was directed to reduce the effects seen by Adams et. al. Once the specimen was set up as shown in Figure 4.3, adhesive was dispensed along the ring. To ensure that a uniform amount of adhesive was dispensed, a turntable running at 12 revolutions per minute was used to spin one adherend while adhesive was dispensed. Specimens were then assembled and allowed to cure at room temperature for 24 hours. After this initial cure time of 24 hours, the pins connecting the alignment blocks were removed and all of the fixturing, alignment blocks and spacers as well as the high-density polyethylene pucks, were removed from the partially cured specimen. The cure was then completed as mentioned above by placing the specimens into an oven set at 40°C for four days. Figure 4.5 shows a specimen that had been fully cured and was ready to be tested.

Figure 4.2: The alignment blocks and spacers controlled adhesive thickness and alignment.

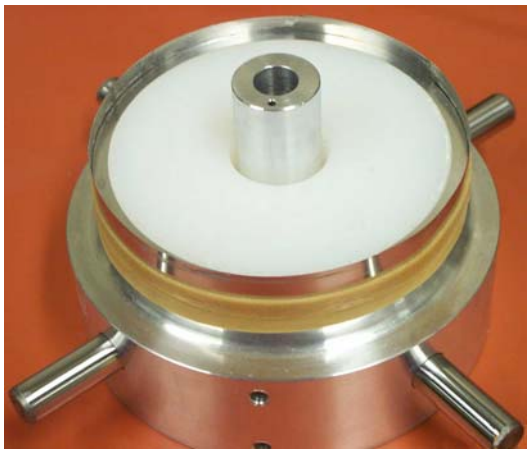

Figure 4.3: Picture of half of a napkin-ring specimen ready for adhesive to be dispensed.

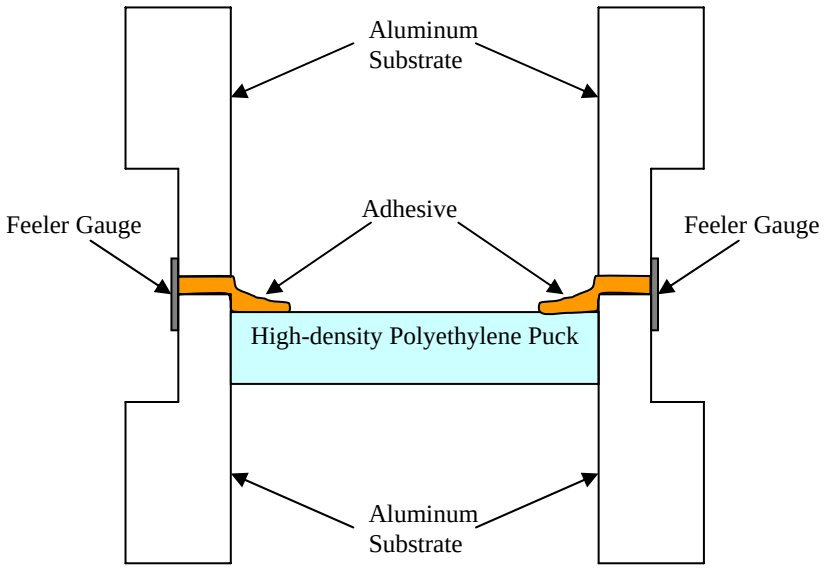

Figure 4.4: Schematic of specimen halves during cure showing where the spew was directed.

Figure 4.5: Fully cured specimen ready to be tested.

To test these napkin-ring specimens, an Instron 8503 load frame with the capability of running pure tension, pure torsion, or a combination of the two loadings was used. This allowed for the same specimen geometry to be tested under varying amounts of normal and shear loading without a change in equipment. The load frame was run under displacement control, at a crosshead displacement rate of 0.3 mm/min, and angular control, at an angular rate of 0.42 degrees/min, for normal and shear loading, respectively. These displacement rates were chosen by John Hennage during preliminary testing in order to match the strain rates from the bulk adhesive tests performed under the testing for this thesis. The axial strain was measured by a custom made transducer that utilized a Capacitec (Ayer, Massachusetts) model HPB-75 sensor aligned in the center of the specimen. All of the complex signal conditioning required for capacitive transducers was performed by a Capacitec 3101-5P unit. Additionally a Capacitec micron-resolution calibrator was used to calibrate the capacitive transducer. The shear strain was measured by a MTS (Eden Prairie, Minnesota) extensometer, model 632.11B.23, attached to the outside napkin-ring specimen using custom-made mounts which straddled the bondline. Calibration of the shear transducer proved to be more troublesome than the axial capacitive sensor. The extensometer was also calibrated using the Capacitec calibrator, however when the extensometer was mounted onto the custom-made mounts, the output was significantly larger than predicted by simple mechanics of materials calculations. Currently, the source of this problem has not been isolated but the difference was reproducible. In order to correct for this

consistent difference, the extensometer output was calibrated to the output from an Iosipescu shear strain gage, with the ±45° grids, that was bonded onto an aluminum blank specimen. The normal and shear strain transducers are shown in Figures 4.6 and 4.7, respectively. The loads and torques were measured by the test frames tensile and torsional load cells, respectively. Both the load and strain data were read into a desktop computer through an IOtech (Cleveland, Ohio) PersonalDAQ model 55 data acquisition system utilizing a four-times oversampling rate for data averaging.

Figure 4.6: A Capacitec model HPB-75 was used to measure the axial deformations

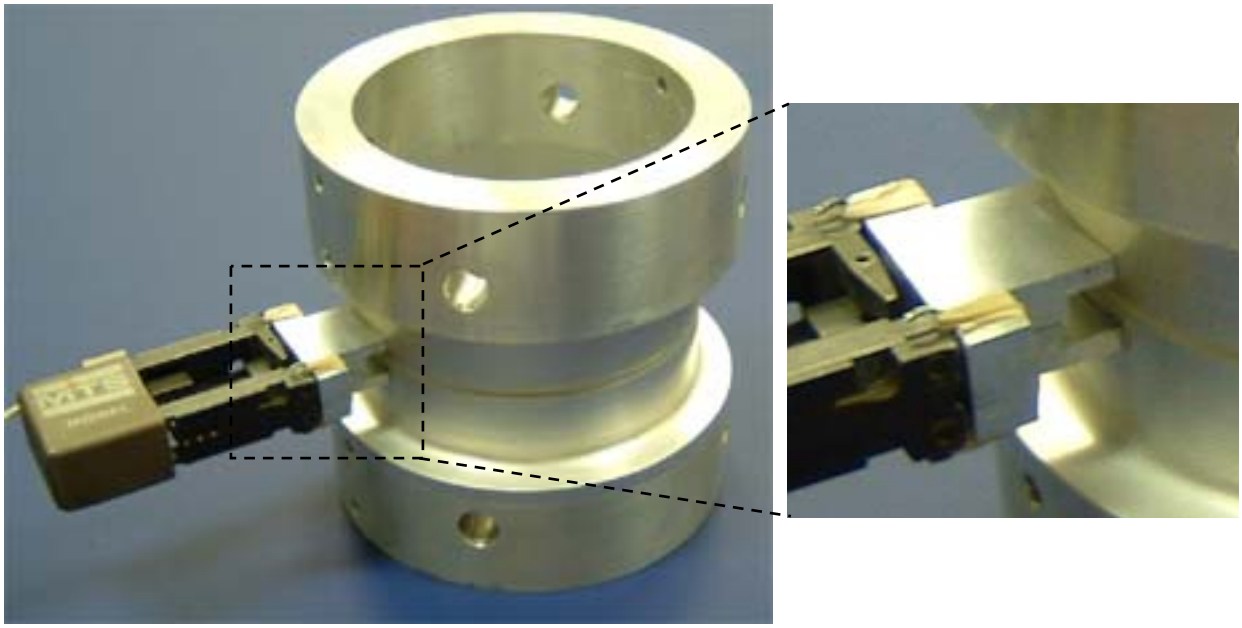

Figure 4.7: A MTS extensometer was used to measure the shear deformations.

Unlike the fairly simple analysis presented in the bulk adhesive testing chapter, the *in situ* adhesive performance proved to be much more difficult to analyze. This section will begin with

analyzing the tensile data, and then move on to the shear analysis. The interactions at the aluminum-adhesive interface create a nonuniform stress field in the adhesive, and as a result, an average engineering stress was used for analysis. The average normal stress, σ_{ave}, seen in the axial direction by the adhesive is identical to the bulk adhesive case, and is determined simply from:

$$\sigma_{ave} = \frac{P}{A} \tag{4.2}$$

where P is the applied tensile load, and A is the bond cross-sectional area. The applied axial force was assumed to be uniform over the specimen, and thus the stress could be calculated with Equation 4.2. In order to minimize the error from the uniform distribution assumption, the Instron test frame grips were aligned before testing and verified by using two identical extensometers (MTS model 632.11B.23) spaced 90° apart on the circumference of a blank specimen (solid aluminum specimen with no bondline). The axial deflections of the adhesive in the specimen had to be corrected for some of the deflection that occurred in the aluminum between the extensometer attachment points.

The axial strains were measured by the custom-made axial transducer, which contacted the specimen 6 mm above and below the center of the bondline. This transducer measured the aluminum and adhesive deflections between these contact points. In order to remove the aluminum adherends' contribution to the total displacement signal, multiple calibrations with the blank aluminum specimen were performed to produce a relationship between aluminum displacement and tensile load. The data collected during the tensile tests of bonded joints was then corrected by subtracting out the appropriate amount of aluminum deflection from the overall deflection, thus leaving only the adhesive deflection. Only then could the nominal axial strain, ε_{axial}, be calculated from the normal strain equation:

$$\varepsilon_{axial} = \frac{\delta_{adhesive}}{t} \tag{4.3}$$

where $\delta_{adhesive}$ is the adhesive deflection and t is the adhesive bondline thickness. The lateral contraction of the adhesive bondline was not measured, and measuring the contraction would require a great deal of effort. A Poisson effect and necking, as seen in bulk tensile dogbone tests, was not seen visually and would have been altered by the constraint introduced by the aluminum substrates. Unlike the bulk adhesive tensile dogbone test, the adhesive in the napkin-ring test

was not under a plane-stress state. Since the adhesive bond was not under true uniaxial stress, determination of the modulus of elasticity is not straightforward; however an apparent modulus was determined using the same relation and analysis shown in the bulk adhesive tests. The apparent modulus of the bonded joint, E_{ap}, was defined from the following equation:

$$E_{ap} = \frac{\sigma_{ave}}{\varepsilon_{axial}} \tag{4.4}$$

These analysis procedures were used to determine the constitutive properties of the LESA adhesive in the *in situ* tension tests. Just as in the bulk adhesive tests, 10 replicated tests were performed at each test condition to add statistical relevance to the data set. As mentioned previously, some preliminary testing indicated that the P2 surface treatment was required to ensure proper substrate adhesion, the failure modes of the tested specimens showed a cohesive failure of the adhesive. Any bond failure in the *in situ* specimens that showed any visual evidence of adhesive failure (aluminum/adhesive interface) as opposed to cohesive failure (bulk adhesive in bondline) was also discarded from this analysis. Approximately 25-30% of the specimens tested were eliminated from this analysis due to adhesive bondline failure. The loads and deflections were converted into average stresses and strains, which were then plotted as shown in Figure 4.8. The new yield criterion described in the previous chapter was once again used to determine the yield point. After the yield point was identified, several important design properties were measured: yield stress, yield strain, ultimate stress, and ultimate strain. The yield stress and strain was determined to be 19.1 MPa with a standard deviation of 2.8 MPa and 0.85% with a standard deviation of 0.07%, respectively. The ultimate stress and strain was determined to be 22.2 MPa with a standard deviation of 2.4 MPa and 2.16% with a standard deviation of 0.53%, respectively. The apparent modulus of elasticity was determined using the same original criterion of the initial linear portion of the stress-strain curve, between 5 and 50% of the yield stress, which is plotted in Figure 4.9. The modulus of elasticity was determined to be 2.15 GPa with a standard deviation of 280 MPa. All of these properties are summarized and tabulated in Table 4.1. The significant increase in data scatter between the bulk and *in situ* tensile test is both a result of a more complex stress state as well as inaccuracies of attempting to measure such small deflections.

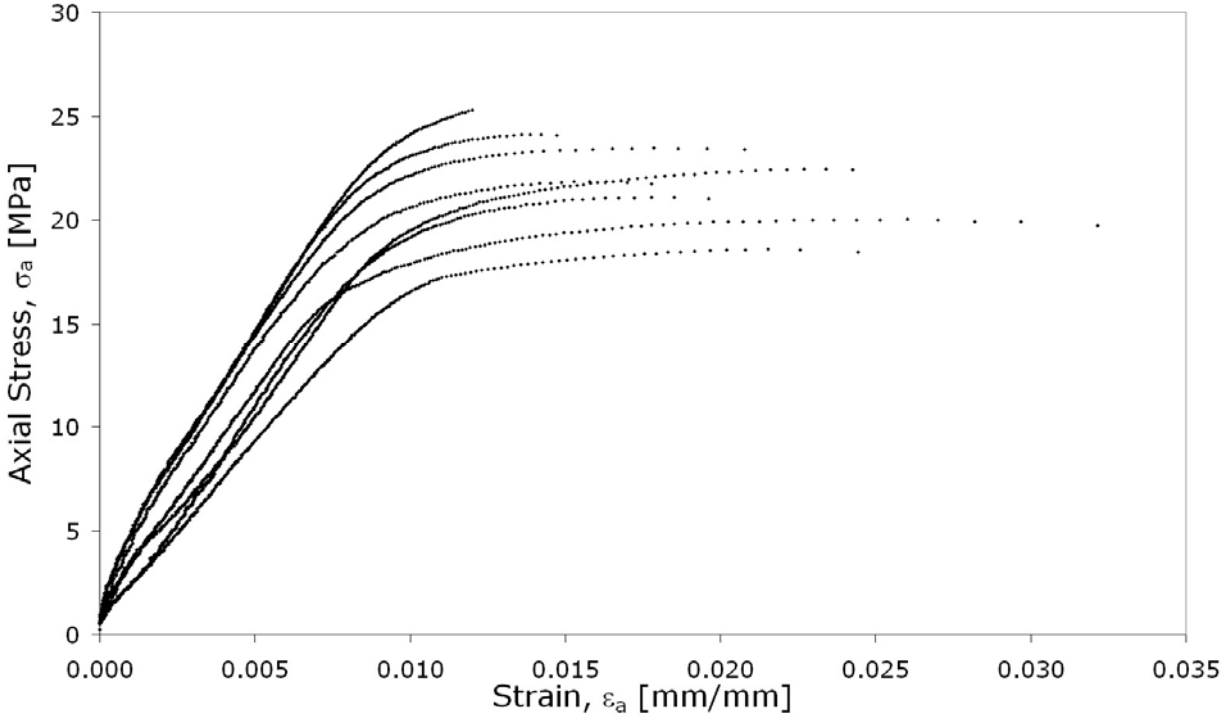

Figure 4.8: Stress-strain plots from the napkin-ring tension tests.

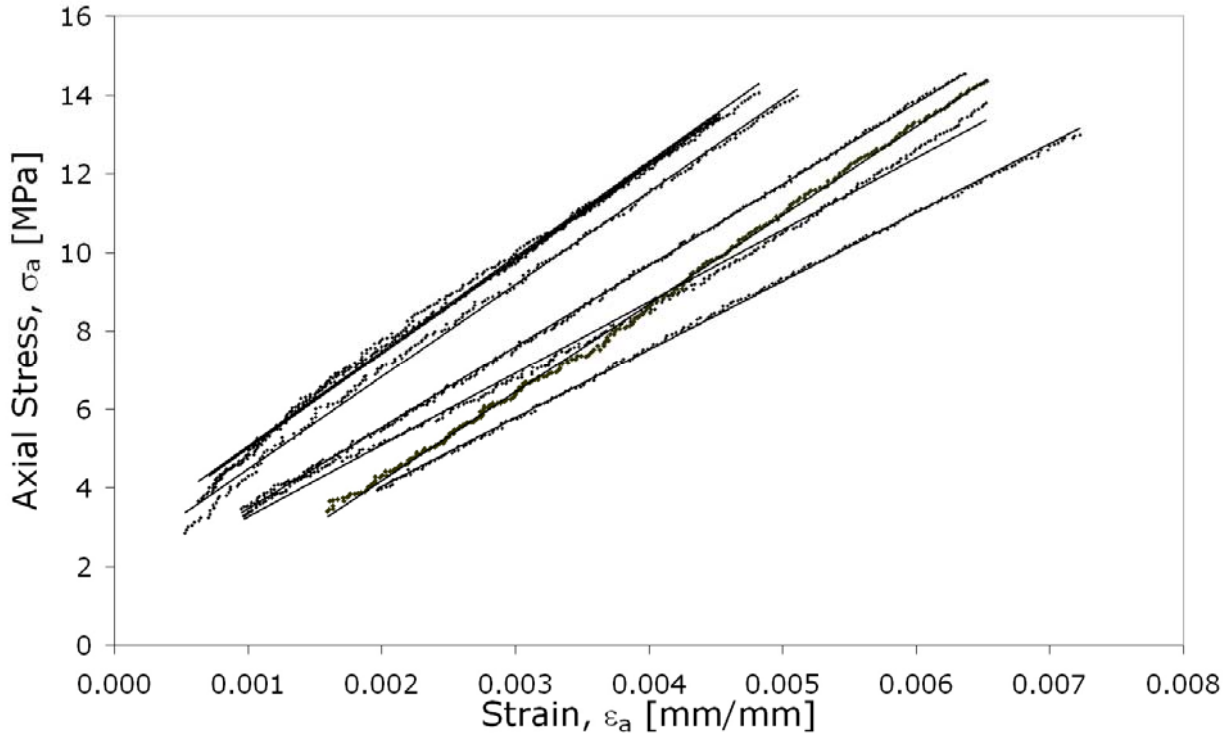

Figure 4.9: Initial linear portion of the stress-strain plots from napkin-ring tension tests.

Table 4.1: Napkin-ring Tensile LESA Properties

LESA *In Situ* Adhesive Properties		
	Average	Standard Deviation
Effective Modulus [MPa]	2150	280
Yield Stress [MPa]	19.1	2.8
Yield Strain [%]	0.85	0.07
Ultimate Stress [MPa]	22.2	2.4
Ultimate Strain [%]	2.16	0.53

Likewise for the shear tests, the analysis followed the same progression. An average engineering shear stress was used for this analysis. This average shear stress, τ_{ave}, from a torsional load can be calculated from Equation 4.1, and the average shear stress is calculated as follows:

$$\tau_{ave} = \frac{T\left(\frac{r_o + r_i}{2}\right)}{\frac{1}{2}\pi\left(r_o^4 - r_i^4\right)} \tag{4.5}$$

where T is the applied torque, r_o is the outer radius of the ring, and r_i is the inner radius of the ring.

In order to measure the adhesive deflection, the custom-made mounts for the shear strain transducer were bonded to the outside of the napkin-ring specimen such that the mount equally straddled the bondline, as shown in Figure 4.7. The shear strain was determined using the same basic procedure of correcting the total deflection by subtracting the aluminum contribution of the displacement signal from this total deflection. Therefore, with only the adhesive shear deflection remaining from the correction, the shear strain, γ, was determined as follows:

$$\gamma = \frac{\Delta_{adhesive}}{t} \tag{4.6}$$

where $\Delta_{adhesive}$ is the shear deflection and t is the adhesive bondline thickness. As mentioned above, the napkin-ring loading in shear does not produce a perfectly uniform shear stress state due to the ring thickness. However, using the average shear stress, the effective modulus of rigidity, G_{eff}, can be determined from the shear stress and shear strain as follows:

$$G_{eff} = \frac{\tau_{ave}}{\gamma} \tag{4.7}$$

These analysis procedures were used to determine the constitutive properties of the LESA adhesive in the *in situ* torsion tests. As with the tension tests, 10 replicated torsion tests were performed at each test condition to add statistical relevance to the data set. As with the tension specimens the failure modes of the torsion specimens produced cohesive failures. However unlike the tension specimens, which had a fairly uniform adhesive thickness on both halves of the tested specimens, the torsion specimens had both a section of a majority of the original adhesive thickness and another section which had only a thin layer remaining. This result is expected as the shear stress will force the failure to move toward one of the interfaces. The torques and deflections were converted into average stresses and strains, which was then plotted as shown in Figure 4.10. From these tests the following properties were determined: yield point, yield shear stress, yield shear strain, and ultimate shear stress. The yield stress and strain was determined to be 18.6 MPa with a standard deviation of 0.6 MPa and 3% with a standard deviation of 0.3%, respectively. Due to the large-scale deformations and plastic flow that occurred during these torsion tests, the shear strain at break could not be determined. The ultimate stress was measured to be 22.3 MPa with a standard deviation of 2.4 MPa. The apparent modulus of rigidity was determined using the same original criterion of the initial linear portion of the stress-strain curve, between 5 and 50% of the yield stress, which is plotted in Figure 4.11. The modulus of rigidity was determined to be 753 MPa with a standard deviation of 72 MPa. All of these properties are summarized and tabulated in Table 4.2. Unlike the tension tests, the torsion tests did not show as much data scatter, possibly due to the increased ductility in shear versus the lack of ductility in tension.

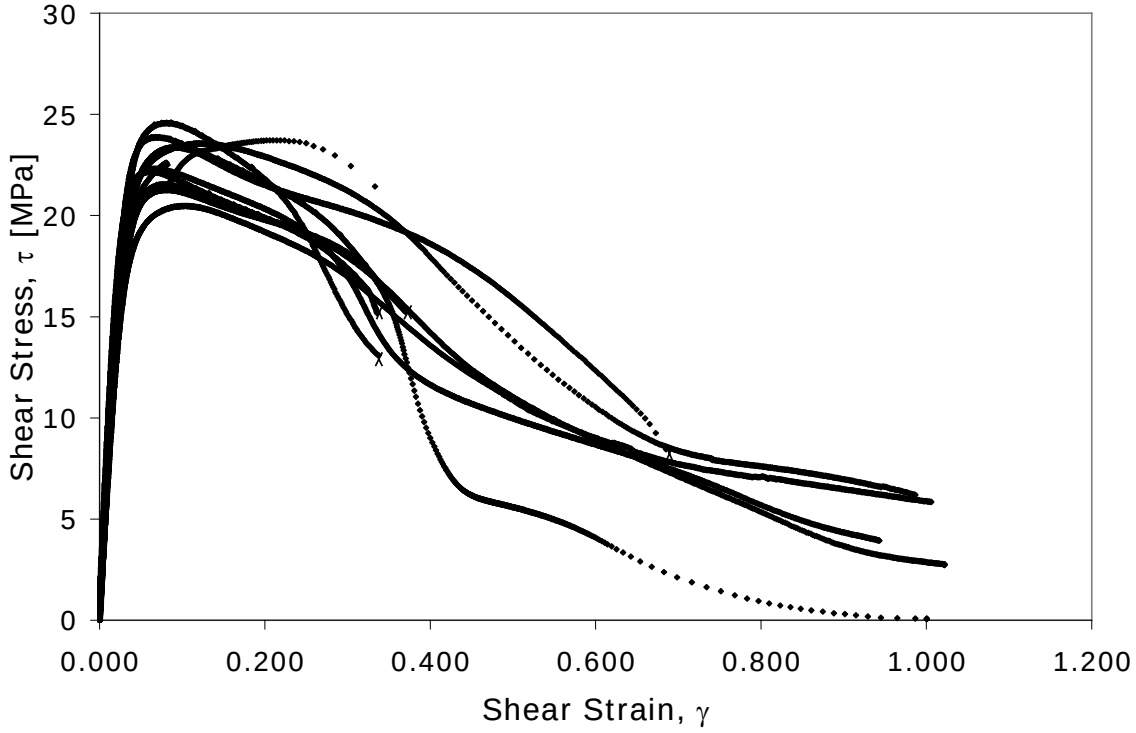

Figure 4.10: Stress-strain plots from the napkin-ring torsion tests.

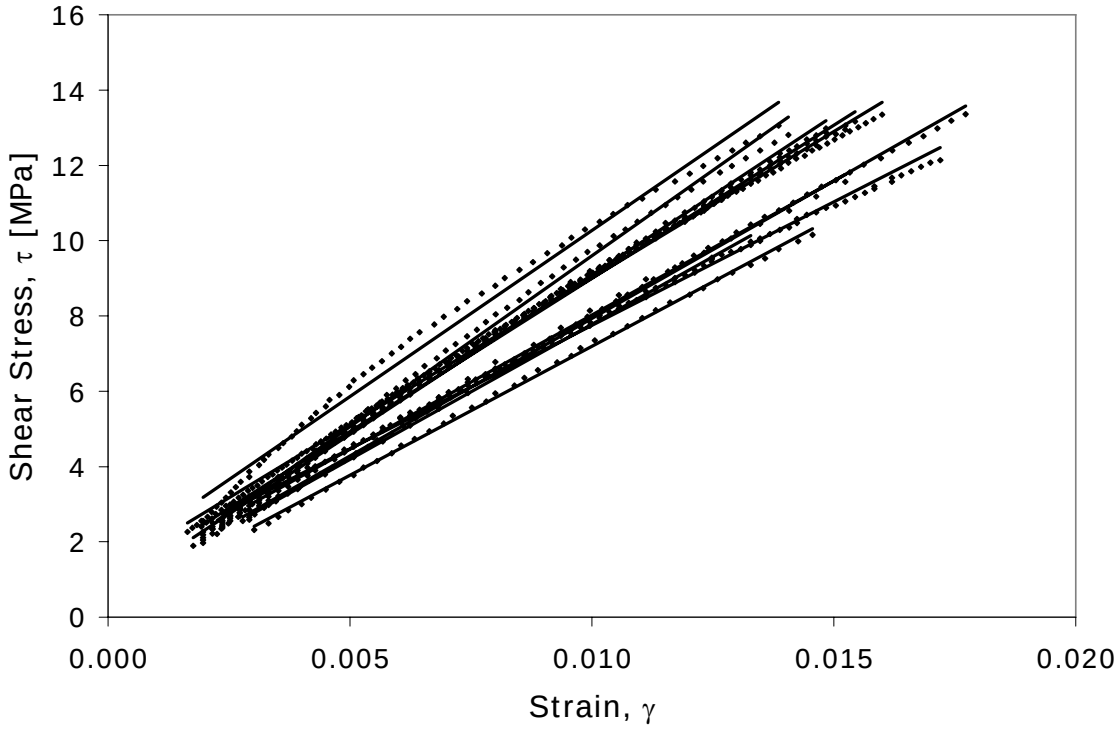

Figure 4.11: Initial linear portion of the stress-strain plots from the napkin-ring torsion tests.

Table 4.2: Napkin-Ring Torsion LESA Properties

LESA *In Situ* Adhesive Properties		
	Average	Standard Deviation
Shear Modulus [MPa]	753	72
Yield Shear Stress [MPa]	18.6	0.6
Yield Shear Strain [%]	3.0	0.3
Ultimate Shear Stress [MPa]	22.3	0.9

4.4 COMPARISON OF *IN SITU* NORMAL AND SHEAR TESTS

Similar to the comparison made between the bulk adhesive shear and normal tests, the properties measured in the *in situ* tests can be compared. The first of these comparisons was to examine the similarities of the tension and torsion results to build some confidence that the loading on the specimen was as planned. To accomplish this, the effective modulus of elasticity was compared to the effective modulus of rigidity using Hooke's law. Equation 3.13 from the previous chapter will relate these two properties via the Poisson's ratio and the equation is reproduced below:

$$G = \frac{E}{2(1+\nu)} \tag{4.8}$$

In order to perform a comparison of these two test results, Equation 3.13 was used with the effective modulus of elasticity from the tension tests and Poisson's ratio from the direct measurement of the bulk adhesive to calculate a predicted effective modulus of rigidity that was then compared to the torsion test results. Uncertainty and error propagation were used in this calculation and the predicted effective modulus of rigidity was 775 ± 101 MPa. The actual measured value of the effective modulus of rigidity from the torsion tests was 753 ± 72 MPa. These two results can be compared statistically by utilizing the unpaired Student's t-test [7].
The t-statistic can be calculated from the following equation:

$$t = \frac{\bar{X}_1 - \bar{X}_2}{\sqrt{\frac{s_{X_1}^2 + s_{X_2}^2}{n}}} \tag{4.9}$$

where n is the number of samples, $\bar{X}_1$ and $\bar{X}_2$ are the average values, and $s_{x_1}^2$ and $s_{x_2}^2$ are the estimated error variance for X_1 and X_2 of the effective modulus from the tension and torsion tests respectively. Based on this analysis at a 99% confidence level, there is no statically significant difference between the effective modulus values in the tension and torsion tests. It should be noted that the effective modulus of elasticity measured from the tension tests would have some

Poisson's ratio contraction influence while the directly measured effective modulus of rigidity from torsion data would not have any Poisson contraction. With this noted and this simplistic analysis, the adhesive seems to have preformed similarly in both stress states in its linear region.

Outside of the linear region, there was a large difference in the ductility between the tension and torsion, the torsional specimens showed large scale deformation, the tension specimens exhibited yield and breaking strain values of .085% and 2.16%, respectively. The large difference could be explained by the presence of voids in the tension-torsion specimens, where the tension loading would be more sensitive to these flaws. Similar behavior was seen in the bulk adhesive specimens, where the failure mode went from brittle fracture to plastic deformation and yielding when the specimen quality was increased and internal flaws minimized.

The total elimination of voids in the *in situ* specimens was not possible; however, using the fixturing described at the beginning of this chapter, voids were minimized. Figure 4.14 shows a picture of one of the failed napkin-ring specimens when loaded in tension, from visual inspection it is estimated that bondlines had approximately a 10-20% loss in cross-sectional area due to voids. As with the bulk adhesive tests, the LESA adhesive showed a much larger capability of dissipating energy as well as a decreased sensitivity to flaws when loaded in shear.

Figure 4.12: Picture of a failed napkin-ring specimen with voids.

While the adhesive showed similarities in the linear region, one of the biggest differences between the tension and torsion results was the yield stresses. The yield stresses for tension and torsion were 19.1 MPa and 18.6 MPa, respectively, implying that the adhesive can carry almost

as much stress in shear as in normal loading. This is contradictory to traditional stress-based failure criteria, such as the maximum shear stress or maximum distortional energy criteria, which predict that shear stress should only be a little more than half the normal stress if under uniaxial loading and possibly even less than half under multi-axial loading. Due to the fact that the shear yield strength of the both the bulk and *in situ* adhesive are similar, 19.1 and 18.6 MPa, respectively, and there was almost a 35% decrease in normal yield strength from the bulk to the *in situ* adhesive, 29.6 MPa to 19.1 MPa. To further examine this, a failure analysis based on the yield criterion was performed on the multi-axial stress state in the *in situ* tension tests.

For this analysis, four different failure stress criteria used for this analysis included the following: Maximum Principal Stress, Maximum Shear Stress, Maximum Distortional Energy (von Mises stress), and the Raghava (modified von Mises stress). These failure criteria were examined at two different analysis points, shown in Figure 4.15, since these points had different distributions of hydrostatic and deviatoric stresses. This analysis assumed perfectly rigid adherends, which allow for the estimation of the nominal stress state and helped to understand the driving failure mechanisms of the tension specimen and provide insight into the reduced load carrying capacity. Only the nominal stress was considered for comparisons and the assumption was made that the stresses were uniform throughout the adhesive layer. Additionally the napkin-ring geometry was examined with the assumption that the aluminum adherends would perform as perfectly rigid substrates due to the fact that the substrate modulus of elasticity was over 33 times greater than the modulus of the LESA adhesive.

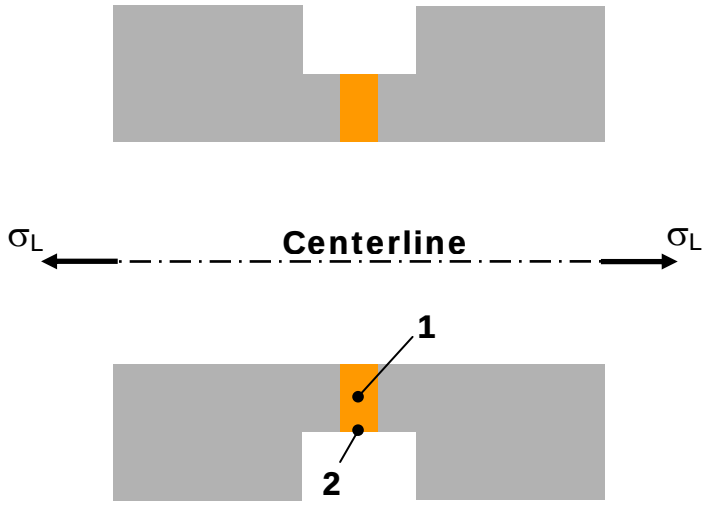

Figure 4.13: Representation of the different points where the stress state estimated.

Failure Analysis – Point 1

The first point to be examined was the point where the overall stress state was the greatest, the center of the bondline. In order to estimate the stress state, the tangential and radial strains were considered negligible as the bondline thickness was assumed to be small compared to the bondline width (Bondline width / thickness ratio = 3.3). Following this simplification and the previous assumptions, Hooke's law could be written out as follows [8]:

$$\begin{aligned}
\varepsilon_L &= \frac{\sigma_L}{E_a} - \frac{\nu_a \sigma_R}{E_a} - \frac{\nu_a \sigma_T}{E_a} \\
\varepsilon_R &= \frac{\sigma_R}{E_a} - \frac{\nu_a \sigma_L}{E_a} - \frac{\nu_a \sigma_T}{E_a} = 0 \rightarrow \sigma_R = \nu\left(\sigma_L + \sigma_T\right) \\
\varepsilon_T &= \frac{\sigma_T}{E_a} - \frac{\nu_a \sigma_R}{E_a} - \frac{\nu_a \sigma_L}{E_a} = 0 \rightarrow \sigma_T = \nu\left(\sigma_L + \sigma_R\right)
\end{aligned} \tag{4.10}$$

where σ, ε, ν, and E are the stress, strain, Poisson's ratio, and Young's modulus, respectively. The subscripts L, R, and T represent the longitudinal, radial, and tangential components, respectively. Since σ_L was the applied axial stress, the other stress components can be determined as a function of this applied stress and calculated using the Poisson's ratio determined from the bulk specimen testing, 0.387.

$$\begin{aligned}
\sigma_T &= \left(\frac{\nu + \nu^2}{1 - \nu^2}\right)\sigma_L \rightarrow 0.631\sigma_L \\
\sigma_R &= \left(\frac{\nu + \nu^2}{1 - \nu^2}\right)\sigma_L \rightarrow 0.631\sigma_L
\end{aligned} \tag{4.11}$$

With these stresses, which happen to also be the principal stresses, it was possible to both determine the hydrostatic stresses and the deviatoric stress that make up this triaxial stress state and perform the failure stress analyses previously mentioned.

The hydrostatic stress, $\sigma_{hydrostatic}$, is the stresses that would cause an element to only undergo volumetric changes and is defined by the following equation:

$$\sigma_{hydrostatic} = \frac{1}{3}\left[\sigma_1 + \sigma_2 + \sigma_3\right] \rightarrow \frac{1}{3}\left[\sigma_L + 0.631\sigma_L + 0.631\sigma_L\right] = 0.754\sigma_L \tag{4.12}$$

The counterpart of the hydrostatic stress is the deviatoric stress, $\sigma_{deviatoric}$, which is defined as the stresses which would cause an element to undergo shape changes and is defined by the following equation:

$$\sigma_{deviatoric} = \frac{1}{3}\left[\left(\sigma_1 - \sigma_2\right)^2 + \left(\sigma_2 - \sigma_3\right)^2 + \left(\sigma_3 - \sigma_1\right)^2\right]^{1/2} \rightarrow 0.1739\sigma_L \tag{4.13}$$

Quantifying these two stresses, hydrostatic and deviatoric, is important when performing the failure analysis, since two of the four (maximums shear stress, and maximum distortional energy) only incorporate the deviatoric portion in their predictions.

Starting with the simplest analysis method, the maximum principal stress criteria states that yield occurs when the maximum principal stress exceeds the uniaxial tensile yield strength [9]:

$$\bar{S}_{MPS} = \max(\sigma_1, \sigma_2, \sigma_3) \rightarrow \sigma_L \tag{4.14}$$

The maximum shear stress analysis predicts that yielding begins whenever the maximum shear stress becomes greater than the maximum shear stress in a tension-test specimen at yield, which can be defined as half of the uniaxial tensile yield strength [8]. This is defined by the following equations:

$$\bar{S}_{MSS} = 2\tau_{\max} = \max\left(|\sigma_1 - \sigma_2|, |\sigma_2 - \sigma_3|, |\sigma_3 - \sigma_1|\right) = |\sigma_L - 0.631\sigma_L| \rightarrow 0.369\sigma_L \tag{4.15}$$

The third failure analysis used was the maximum distortional energy criteria, which predicts that yield occurs when the distortion energy reaches the same energy required for yield in uniaxial tension. The Maximum Distortional Energy is defined mathematically as follows [8]:

$$\bar{S}_{MDE} = \left[\frac{(\sigma_1 - \sigma_2)^2 + (\sigma_2 - \sigma_3)^2 + (\sigma_3 - \sigma_1)^2}{2}\right]^{1/2} = \left[\frac{(.369\sigma_L)^2 + (-.369\sigma_L)^2}{2}\right]^{1/2} \rightarrow 0.369\sigma_L \tag{4.16}$$

The Raghava failure analysis builds on the effective stress used in the Maximum Distortional Energy analysis and incorporates the hydrostatic stress portion to form what is known as a modified von Mises stress [10]. The Raghava analysis predicts failure as shown below:

$$\bar{S}_{Raghava} = \frac{\left\{J_1(S-1) + \left[J_1^2(S-1)^2 + 12J_{2D}S\right]^{1/2}\right\}}{2S} \tag{4.17}$$

Where J_1 and J_{2D} are defined by:

$$J_1 = \sigma_1 + \sigma_2 + \sigma_3 = \sigma_L + .631\sigma_L + .631\sigma_L \rightarrow 2.26\sigma_L$$

$$J_{2D} = \frac{\left[(\sigma_1 - \sigma_2)^2 + (\sigma_2 - \sigma_3)^2 + (\sigma_3 - \sigma_1)^2\right]}{6} = \frac{\left[(.369\sigma_L)^2 + (-.369\sigma_L)^2\right]}{6} \rightarrow .0454\sigma_L^2 \tag{4.18}$$

The term, *S*, in Equation 4.15 is a ratio of the compressive and tensile yield strength of the material. Determining the value of the *S* parameter can be accomplished by utilizing tensile data (bulk adhesive dogbone tests) and pure shear loading data (Iosipescu shear tests) gathered from the previously performed bulk adhesive tests [11]. Using the Raghava yield criterion for a pure shear loading condition and manipulating for the S parameter yields the following result:

$$S = \frac{3\tau_y^2}{\sigma_y^2} \rightarrow \frac{3(19.1)^2}{(29.6)^2} \rightarrow 1.25 \qquad (4.19)$$

where τ_y is the shear yield stress and σ_y is the tensile yield stress. Using this information and simplifying Equation 4.15 with the terms in Equation 4.16, one can calculate the failure stress as predicted by the Raghava analysis as follows:

$$\bar{S}_{Raghava} = \frac{\left\{2.26\sigma_L(.25) + \left[(2.26\sigma_L)^2(.25)^2 + 12\left(.0454\sigma_L{}^2\right)(1.25)\right]^{1/2}\right\}}{2(1.25)} \rightarrow 0.626\sigma_L \quad (4.20)$$

As a comparison, these four failure theories were used with the yield strength, as determined from the uniaxial bulk adhesive ($\sigma_{yield} = 29.6$ MPa), to predict the nominal failure stress of the napkin-ring specimens at yield. Table 4-3 provides a summary of this analysis at Point 1. From this one can see that all of the four analyses over predict the yield stress when compared to the measured nominal yield stress from the napkin-ring tests. At Point 1, a stress element is under a large amount of hydrostatic stress and the two failure criterion which do not account for the hydrostatic stress significantly over predict the failure stress, by over 300%. The Raghava criterion which does incorporate still over predicts the nominal yield stress by over 100%. Before performing a further examination of potential differences that analysis will be repeated at Point 2, the outside edge of the ring.

Table 4.3: Predicted Axial Stress at Failure @ Point 1

		Point 1			
		In terms of σ_L	Predicted Nominal Stress at Yield [MPa]	Measured Nominal Stress at Yield [MPa]	Percent Difference
Principal Stresses	σ_1	σ_L			
	σ_2	$0.631\sigma_L$			
	σ_3	$0.631\sigma_L$			
Hydrostatic Stress, $\sigma_{hydrostatic}$		$0.754\sigma_L$			
Deviatoric Stress, $\sigma_{deviatoric}$		$0.1739\sigma_L$			
Maximum Principal Stress		$S_{MPS} = \sigma_L$	29.6	19.1	-55%
Maximum Shear Stress		$S_{MSS} = 0.369\sigma_L$	80.2		-320%
Maximum Distortion Energy		$S_{MDE} = 0.369\sigma_L$	80.2		-320%
Raghava		$S_{Raghava} = 0.626\sigma_L$	43.8		-129%

Failure Analysis – Point 2

The second point to be examined was the point where the deviatoric stress state was the greatest, the outside edge of the bondline. For this analysis the same assumptions were made

(bondline thickness << bondline width), and now since the stress element is at the free edge the radial stress component is zero. Using Hooke's law (Equation 4.10) and solving for the principal stresses in terms of σ_L reveals the following state:

$$\begin{aligned}\sigma_1 &= \sigma_L \\ \sigma_2 &= 0.513\sigma_L \\ \sigma_3 &= 0\end{aligned} \tag{4.21}$$

With the principal stresses calculated, one could then determine the hydrostatic and deviatoric stresses for the Point 2 analysis. These were calculated from Equations 4.12 and 4.13 as shown below. When compared to Point 1, Point 2 has approximately a 1:1 ratio of hydrostatic to deviatoric stress whereas Point 1 had approximately a 4.3:1 ratio.

$$\begin{aligned}\sigma_{hydrostatic} &= \frac{1}{3}\left[\sigma_1+\sigma_2+\sigma_3\right] \rightarrow \frac{1}{3}\left[\sigma_L+0.531\sigma_L\right] = 0.504\sigma_L \\ \sigma_{deviatoric} &= \frac{1}{3}\left[\left(\sigma_1-\sigma_2\right)^2+\left(\sigma_2-\sigma_3\right)^2+\left(\sigma_3-\sigma_1\right)^2\right]^{1/2} \rightarrow 0.408\sigma_L\end{aligned} \tag{4.22}$$

Repeating the same calculations for determining the yield criterions from Point 1 (Equations 4.14 – 4.20), the criterions corresponding to Point 2 were determined to be as shown below:

$$\bar{S}_{MPS} = \max(\sigma_1,\sigma_2,\sigma_3) \rightarrow \sigma_L$$

$$\bar{S}_{MSS} = 2\tau_{\max} = \max\left(\left|\sigma_1-\sigma_2\right|,\left|\sigma_2-\sigma_3\right|,\left|\sigma_3-\sigma_1\right|\right) = \left|\sigma_L-0.513\sigma_L\right| \rightarrow 0.487\sigma_L$$

$$\bar{S}_{MDE} = \left[\frac{\left(\sigma_1-\sigma_2\right)^2+\left(\sigma_2-\sigma_3\right)^2+\left(\sigma_3-\sigma_1\right)^2}{2}\right]^{1/2} = \left[\frac{\left(.487\sigma_L\right)^2+\left(.513\sigma_L\right)^2+\left(\sigma_L\right)^2}{2}\right]^{1/2} \rightarrow 0.513\sigma_L \tag{4.23}$$

$$\bar{S}_{Raghava} = \frac{\left\{J_1\left(S-1\right)+\left[J_1{}^2\left(S-1\right)^2+12J_{2D}S\right]^{1/2}\right\}}{2S} \rightarrow 0.943\sigma_L$$

Once again, these four failure theories were used with the yield strength, as determined from the uniaxial bulk adhesive ($\sigma_{yield} = 29.6$ MPa), to predict the nominal failure stress of the napkin-ring specimens at yield. Table 4-4 provides a summary of this analysis at Point 2. As before, all of the four analyses over predict the yield stress when compared to the measured nominal yield stress from the napkin-ring tests however as the deviatoric component of the stress state is greater, the percent differences are not quite as large.

Table 4.4: Predicted Axial Stress at Failure @ Point 2

		Point 2			
		In terms of σ_L	Predicted Nominal Stress at Yield [MPa]	Measured Nominal Stress at Yield [MPa]	Percent Difference
Principal Stresses	σ_1	σ_L			
	σ_2	$0.513\sigma_L$			
	σ_3	0			
Hydrostatic Stress, $\sigma_{hydrostatic}$		$0.504\sigma_L$			
Deviatoric Stress, $\sigma_{deviatoric}$		$0.408\sigma_L$			
Maximum Principal Stress		$S_{MPS} = \sigma_L$	29.6	19.1	-55%
Maximum Shear Stress		$S_{MSS} = 0.497\sigma_L$	59.6		-212%
Maximum Distortion Energy		$S_{MDE} = 0.513\sigma_L$	57.7		-202%
Raghava		$S_{Raghava} = 0.943\sigma_L$	31.4		-64%

Potential Explanations

From examining this analysis, one could quickly jump to the conclusion that traditional failure theories over predict the yield strength of the bonded napkin-ring tension specimens when in actuality there are several items to note before jumping to conclusions. First, this basic analysis does not factor in any stress singularities at the bondline edge, these are areas where local yielding occurs. In addition to singularities, this analysis assumes that there is no load eccentricity in the load frame, and while measures were taken to minimize these effects, they still may have had an effect on the testing. Lastly, the impact of adhesive voids was not considered for this analysis. The effect of the voids occurs as both a loss in cross-sectional area and then secondly as a potential for a stress concentration. As mentioned previously, visual estimates of tested specimens determined the voiding to be approximately 10-20% of the cross-sectional area. What can be concluded is that a more complex failure mechanism may be at work here and standard failure theories may need to include modifiers to correct the over-prediction of joint failure stress. Many researchers have found that unlike metals, polymers and adhesives are susceptible to the hydrostatic stress state and as such require failure criteria which include a modifier for the hydrostatic stress in their prediction [10,11]. It is believed that the LESA adhesive is also susceptible to hydrostatic stress buildup causing the adhesive joint to fail prematurely.

4.5 CONCLUSIONS

In conclusion, the results from the *in situ* testing provided some very interesting details and insights into the adhesive behavior. The adhesive properties measured during these tests are

summarized in Table 4.5. When comparing all of the adhesive properties of the LESA adhesive in an *in situ* state, a common theme is seen. The adhesive performance in the linear region was comparable between the tension and torsion loading and this was verified by the predicting the effective modulus of rigidity from the measured effective modulus of elasticity. However, as the adhesive was stressed into the nonlinear region in tension, adhesive performance seemed to deviate from the expected behavior and a new failure mechanism began to take place. For the tension tests, both the sensitivity to flaws and the multi-axial stress state and hydrostatic stress sensitivity seemed to contribute to reduction in strength. Overall these tests provided many useful results, and these findings along with the bulk adhesive tests will be compared in the next chapter to examine the bulk and *in situ* adhesive performance of LESA adhesive.

Table 4.4: *In Situ* Adhesive Properties

LESA *In Situ* Adhesive Properties		
	Average	Standard Deviation
Young's Modulus [MPa]	2150	280
Yield Stress [MPa]	19.1	2.8
Yield Strain [%]	0.85	0.07
Ultimate Stress [MPa]	22.2	2.4
Ultimate Strain [%]	2.16	0.53
Shear Modulus [MPa]	753	72
Yield Shear Stress [MPa]	18.6	0.6
Yield Shear Strain [%]	3.0	0.3
Ultimate Shear Stress [MPa]	22.3	0.9

4.6 REFERENCES

[1] "Standard Test Method for Shear Strength and Shear Modulus of Structural Adhesives" *ASTM Standard E 229-97, Amer. Soc. Test. and Mat.,* Philadelphia (1997).

[2] Dean, G., Crocker, L., Read. B, and L. Wright., "Prediction of deformation and failure of rubber-toughened adhesive joints." *Int. J. Adhesion Adhesives.* **24**, 295-306 (2004).

[3] Zgoul, M. and A. D. Crocombe. "Numerical modeling of lap joints bonded with a rate-dependent adhesive." *Int. J. Adhesion Adhesives.* **24**, 355-366 (2004).

[4] Duncan, B. and G. Dean. " Measurements and models for design with modern adhesives." *Int. J. Adhesion Adhesives.* **23**, 141-49 (2003).

[5] Russell, W.J., and Garnis, E.A., "A Chromate-Free Low Toxicity Method of Preparing Aluminum Surfaces for Adhesive Bonding," *SAMPE J*, **17**, 19-23 (1981).

[6] "Standard Guide for Preparation of Metal Surfaces for Adhesive Bonding" *ASTM Standard D 2651-01, Amer. Soc. Test. and Mat.,* Philadelphia (2001).

[7] Vining, G. Geoffrey. *Statistical Methods for Engineers.* California: Duxbury Press, 1998.

[8] Adams, R D. Coppendale, J. and N. A. Peppiatt, "Stress Analysis of Axisymmetric Butt Joints Loaded in Torsion and Tension." *J. Strain Anal.,* **13**, 1-10)(1978).

[9] Shigley, J. E. and Larry D. Mitchell. *Mechanical Engineering Design*. 4th ed. New York: McGraw Hill, 1993.

[10] Raghava, R.S. and Cadell, R.M., "The Macroscopic Yield Behavior of Polymers," *J. Mater. Sci.,* **8**, 225-232 (1973).

[11] Zgoul, M. and Crocombe, A. D., "Numerical Modelling of Lap Joints Bonded with a Rate-dependent Adhesive," *Int. J. Adhesion and Adhesives,* **24**, 355-266 (2004).

Chapter 5: Bulk & In Situ Adhesive Comparison

This chapter is written in a format for publication in the *Journal of Adhesion* with the title "Bulk and *in situ* comparison of a two-part acrylic structural adhesive". It repeats some material provided in prior chapters.

5.1 INTRODUCTION

Adhesives, with many structural or semi-structural applications, may have become common place; however, designing with these adhesives is not as straightforward as traditional fastening methods. For structural and semi-structural adhesive applications, the prediction of adhesive bond failure is very important. In order to predict failure, extensive characterization of the specific structural adhesive is required to form an accurate determination of adhesive performance. Adhesive strength-based characterization and mathematical material modeling for finite element analysis have the capabilities to predict adhesive performance, but these analyses require adhesive characterization through a variety of standardized tests, with a currently preferred method of combining bulk tensile properties with bonded shear joint results[1,2]. Such a combination of bulk normal properties with *in situ* shear properties is convenient; however, this combination must be validated. Researchers[3,4,5] have noted potential mechanical property differences of bulk and *in situ* adhesive test specimens for quite some time. As a result of these potential differences, several specific studies have been performed to examine and determine the mechanisms that would cause differences in bulk versus *in situ* adhesive performance[6,7,8,9,10,11,12,13,14,15]. The majority of these studies concluded that there is substantial agreement between measured linear elastic mechanical properties and Young's and shear moduli, however, nonlinear design properties such as tensile and shear strengths and tensile and shear ultimate strains frequently showed deviation from the bulk adhesive. Researchers have taken two different sides in explaining this difference, with some claiming that experimental problems have created fictitious differences and others arguing that there are actual differences in adhesive performance. Proponents of experimental problems causing the differences commonly cite poor bonded specimen quality (voiding and/or incomplete curing), inaccuracies of measuring the very small bondline deformations, and non-uniform stresses induced during testing. The purpose of this paper is to present a study of the bulk and *in situ* properties of a structural adhesive while

attempting to minimize the reported experimental problems. By reducing these experimental issues one can make a more accurate appraisal of the bulk and *in situ* adhesive performance and examine mechanisms for any differences observed.

5.2 EXPERIMENTAL DETAILS

With concerns over experimental problems causing performance differences, the selection of the appropriate test geometries was critical. For bulk adhesive characterization, the standard dogbone tensile and the Iosipescu shear tests, were chosen for normal and shear loading, respectively. The dogbone tensile test has long been used for characterization of polymers and has been standardized by the American Society for Testing and Materials[16] (ASTM), while the Iosipescu shear specimen, first introduced in the 1960s[17], has been used with much success in the composites field[18,19] as an ASTM standard[20]. These tests were chosen for their relatively uniform stress states and because the specimens for the both tests could be made from uniform thickness adhesive patties. For the *in situ* adhesive tests, a napkin-ring geometry that was loaded in tension or torsion was chosen. Torsional loading of this specimen had been standardized by ASTM for shear characterization, but the method has recently (2003) been withdrawn as a standard[21] for unknown reasons. The napkin-ring geometry seems ideal for this type of strength testing due to the continuous bondline which does not introduce stress concentrations at sharp corners and bond terminations. Currently, the reason for withdrawal is not known, however there is no other ASTM standard with the potential for determining the *in situ* constitutive properties of structural adhesives loaded both in normal and shear. Again these tests were chosen for their fairly uniform stress states and the dual use of the napkin-ring geometry in both tension and torsion loading.

The adhesive chosen for this study was formulated by Dow Chemical Company and it is an experimental two-part acrylic room temperature cure with a 1:1 mix ratio designed for low energy substrates. For the remainder of this article the adhesive will be referred to as low energy substrate adhesive, or LESA for short. Since the LESA adhesive is a two-part acrylic system, a pneumatic adhesive dispenser was used with a static mixer tube to mix and dispense the adhesive. The pneumatic adhesive dispenser coupled with the static mixers is an effective and widely accepted method of dispensing two-part adhesive systems. Although this adhesive was a room temperature cure system, all specimens were left at room temperature for 24 hours and then

elevated to 40°C for 4 days in order to ensure complete curing of both the bulk and bonded adhesive. This addressed the specific concern of incomplete curing cited in some of the previous bulk and *in situ* comparisons.

Bulk Adhesive Specimens

Initial tensile tests were performed on specimens cast in individual molds, but the significant shrinkage observed as LESA cures induced rough surfaces that exhibited extensive microcracking. These specimens resulted in relatively brittle failures at strain levels of only 1 %. The effect of this shrinkage was only observed at the outside edges of the original specimens and subsequently, both tensile and Iosipescu test specimens were machined from large cast patties (2.85 mm thick) made by sandwiching the liquid adhesive between 0.051 mm thick stainless steel foil sheets supported by two 6.35 mm thick aluminum plates. After the patties were cast they were machined into rectangular strips, 165 mm x 19 mm, and then machined into ASTM D-638 Type 1 specimens using a Tensilkut® machine (Maryville, Tennessee). The Tensilkut® machine utilized a stainless steel jig and a high speed router to create the necked area of the specimen, as shown in the schematic in Figure 5.1.

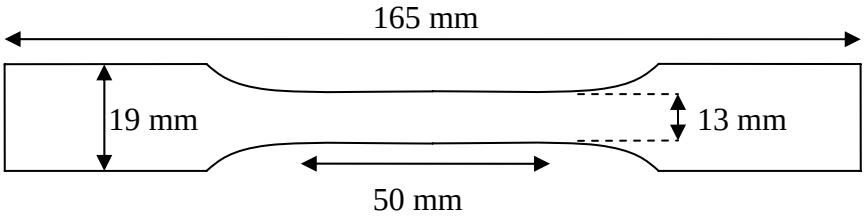

Figure 5.1 Schematic of ASTM D-638 Type I tensile specimen

Manufacturing the Iosipescu shear specimens was similar; the same patties used for the tensile tests, with a 2.85 mm nominal thickness, were cut into 76 mm by 20 mm strips. Notches were machined into the specimens using a double angle cutter with a custom tip radius of 1.3 mm. The notch depth, notch angle, and notch radius have been explored by several researchers and the chosen geometry follows the suggested geometry for isotropic materials[22,23,24]. After machining, these specimens conformed to the standard ASTM D-5379 specimens. Figure 5.2 shows a schematic of the finished Iosipescu specimen.

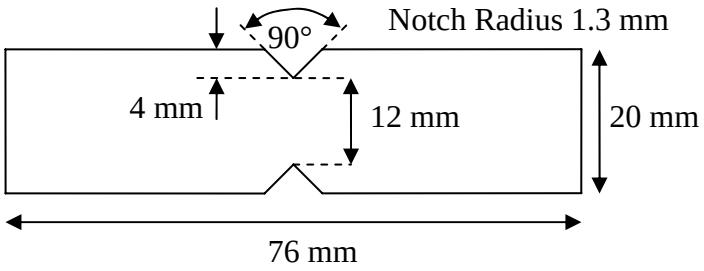

Figure 5.2 Schematic of ASTM D-5379 Iosipescu shear specimen

Both of these specimens were tested in an Instron 4505 (Canton, Massachusetts) running under displacement control at 1 mm/min with an Instron 5-kN load cell for both geometries. Tensile dogbone specimens were tested in wedge grips and instrumented with either biaxial or axial extensometers for strain measurements. Iosipescu specimens were tested in a Wyoming Test fixtures (Larame, Wyoming) modified Iosipescu shear fixture and instrumented with special Iosipescu shear strain gages (Gage Number: N2P-08-C032A-500/SP61), manufactured by Micro-Measurements Group (Raleigh, North Carolina). All signal conditioning and bridge completion were performed in a Micro-Measurements Group 2310 Signal Conditioning Amplifier in a half bridge configuration.

In Situ Adhesive Specimens

The geometry used for these tests was based on the ASTM standard E-229 and adapted for use in an Instron 8503 Tension-Torsion test frame. The specimens were machined out of annular aluminum 101.6 mm and 88.9 mm outer and inner diameter respectively. A portion of the specimen was turned down to an outer diameter of 95.3 mm to create a bonding surface with a reduced cross-section, referred to as the land. This configuration is advantageous for both normal and shear testing because comparisons are possible with the same specimen configuration. The ASTM standard specimen has a moderately larger diameter, with the outer and inner ring diameters of 122 mm and 111.8 mm, respectively. The width of this land was very important to the shear stress distribution from a torsional load, and had to be minimized while keeping the applied failure load in the range of the test-frame load cell. The test geometry used a land width of 3.2 mm, which has approximately a 7.2% variation in shear stress across the bondline yet keeping the failure loads well above of the load cell noise level. This shear variation was well under the variation present in the previous ASTM standard. The final bond area of the napkin-ring specimen was 918 mm^2. The cylindrical adherends were also machined

with four reamed fixturing holes and several transducer mounting holes. The fixturing holes were used for alignment during specimen construction as well as loading in the test frame. These holes were machined with an angular spacing of 90°. A schematic of one adherend showing the pertinent dimensions and a picture showing the fixturing and transducer mounting holes is displayed in Figure 5.3.

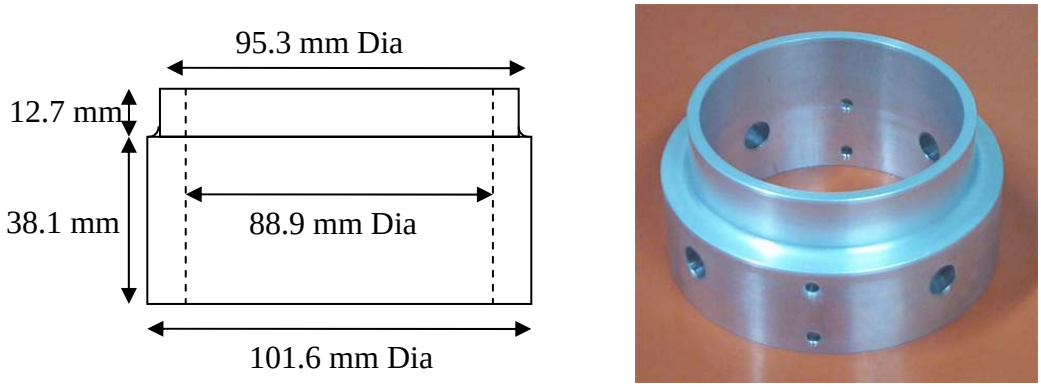

Figure 5.3 Schematic and picture of one napkin-ring adherend.

After machining, the substrates were chemically treated to ensure high quality bonds and result in cohesive failures within the adhesive layer. Preliminary testing (data is not presented) indicated that the best and most consistent adhesion to aluminum substrates involved a P2 etch. The P2 etch technique is also an American Society for Testing and Materials procedure for surface treatment of metals, specifically aluminum[25]. The P2 etch is carried out in an acidic Fe(III) solution which leaves a stable and uniform columnar aluminum oxide finish that provides an excellent surface for bonding. After the substrates were surface treated, specifically designed fixtures and procedures were used to construct the bonded specimens with uniform bond thicknesses for *in situ* adhesive testing.

Constructing the full napkin-ring specimen involved bonding two of the rings described above. With the goal of fabricating high quality specimens, special fixtures were made to ensure concentricity, uniform bond thicknesses, and minimal adhesive spew. Previous research has shown these factors can drastically affect the adhesive performance of napkin-ring specimens[26]. Figure 5.4 shows a schematic of the napkin-ring geometry with a stainless steel feeler gage and high-density polyethylene puck which are used to control spew and then are subsequently

removed after the specimens have cured. Figure 5.4 also shows a finished napkin-ring specimen ready for testing.

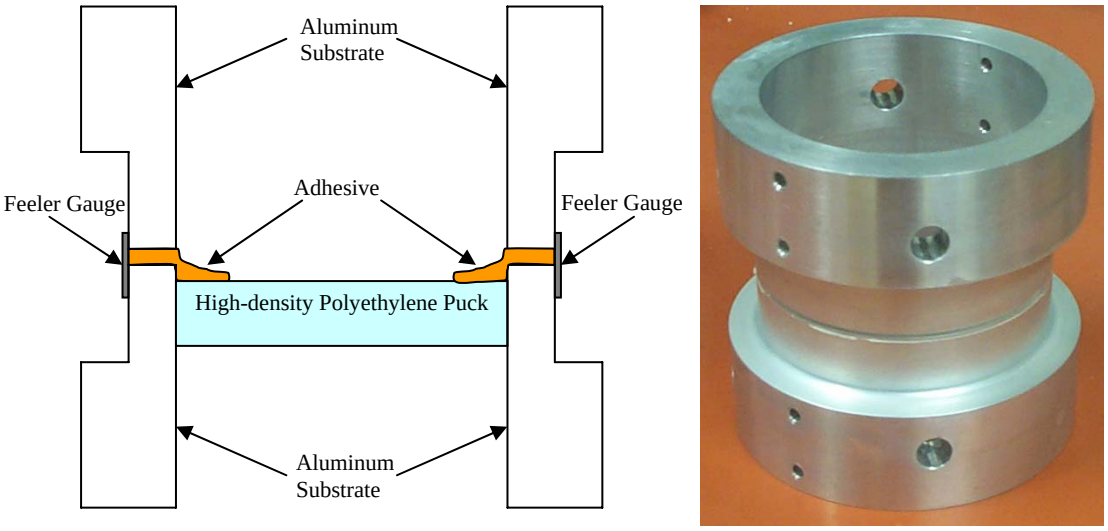

Figure 5.4 Bonded napkin-ring specimens ready for testing

The napkin-ring specimens were tested in an Instron 8503 tension-torsion test frame, and were run under displacement control at a crosshead rate of 0.3 mm/min for the tensile loading and under angular control at an angular rate of 0.42 degrees/min. These rates were chosen from preliminary testing to provide a similar strain rate in both conditions. Axial strain within the adhesive was estimated from axial displacements measured at the centerline of the specimens using a high sensitivity custom-made transducer. This transducer utilized a capacitive sensor, Capacitec (Ayer, Massachusetts) model HPB-75, capable of measuring the small displacements in the adhesive bondline. The shear strain was measured by a MTS (Eden Prairie, Minnesota) extensometer, model 632.11B.23, that was attached to the outside napkin-ring specimen using custom-made mounts. Both of these strain measurements were corrected for the substrate deformations by running identical tests on a blank napkin-ring specimen and subtracting the aluminum displacements from the measured overall displacements.

5.3 RESULTS AND DISCUSSION

A summary of the experimental data for bulk and *in situ* testing is shown in Table 5.1 and the stress-strain curves for both the normal and shear are found in Figures 5.5 and 5.6, respectively. Each test was replicated ten times to provide some statistical significance to the adhesive properties and the standard deviations are included in the data summaries. Both of the

bulk adhesive tests showed pronounced yielding and significant plastic deformation , while only the torsion tests showed significant yielding and deformation. Some of the *in situ* tension tests showed small amounts of ductility, but significantly less than was seen in the corresponding bulk adhesive tests. Another important observation was that after some specimen fabrication refinement, the bulk adhesive tests involved specimens that appeared to be void free, however this was not achievable in the bonded adhesive joints. Much effort was put into constructing the highest quality specimens; however it was not possible to eliminate all of the voids in the *in situ* tests. In order to minimize the effect of the voids any test which showed a failure that was dominated by a void was discarded from the analysis. Additionally bond failures in the *in situ* specimens that showed any visual evidence of adhesive failure (aluminum/adhesive interface) as opposed to cohesive failure (bulk adhesive in bondline) was also discarded from this analysis. By eliminating those test specimens that contained significant flaws (voids & interfacial failure), it became possible to directly compare the *in situ* specimens to the bulk adhesive tests.

Table 5.1 Bulk and *In Situ* Adhesive Properties from Testing

LESA Bulk Adhesive Properties		
	Average	Standard Deviation
Young's Modulus [GPa]	2.290	0.110
Poisson's Ratio	0.387	0.003
Yield Strength [MPa]	29.6	1.8
Yield Strain [%]	1.64	0.16
Ultimate Stress [MPa]	32.6	1.8
Breaking Stress [MPa]	30.8	2.1
Strain at Break [%]	4.94	0.53
Shear Modulus [MPa]	773	86
Yield Shear Strength [MPa]	19.1	1.5
Yield Shear Strain [%]	2.9	0.2
Ultimate Shear Streength [MPa]	25.2	1.6

LESA *In Situ* Adhesive Properties		
	Average	Standard Deviation
Effective Young's Modulus [GPa]	2.150	0.280
Average Stress at Yield [MPa]	19.1	2.8
Yield Strain [%]	0.85	0.07
Average Stress at Peak Load [MPa]	22.2	2.4
Strain at Break [%]	2.16	0.53
Shear Modulus [MPa]	753	72
Average Shear Stress at Yield [MPa]	18.6	0.6
Yield Shear Strain [%]	3.0	0.3
Average Stress at Peak Load [MPa]	22.3	0.9

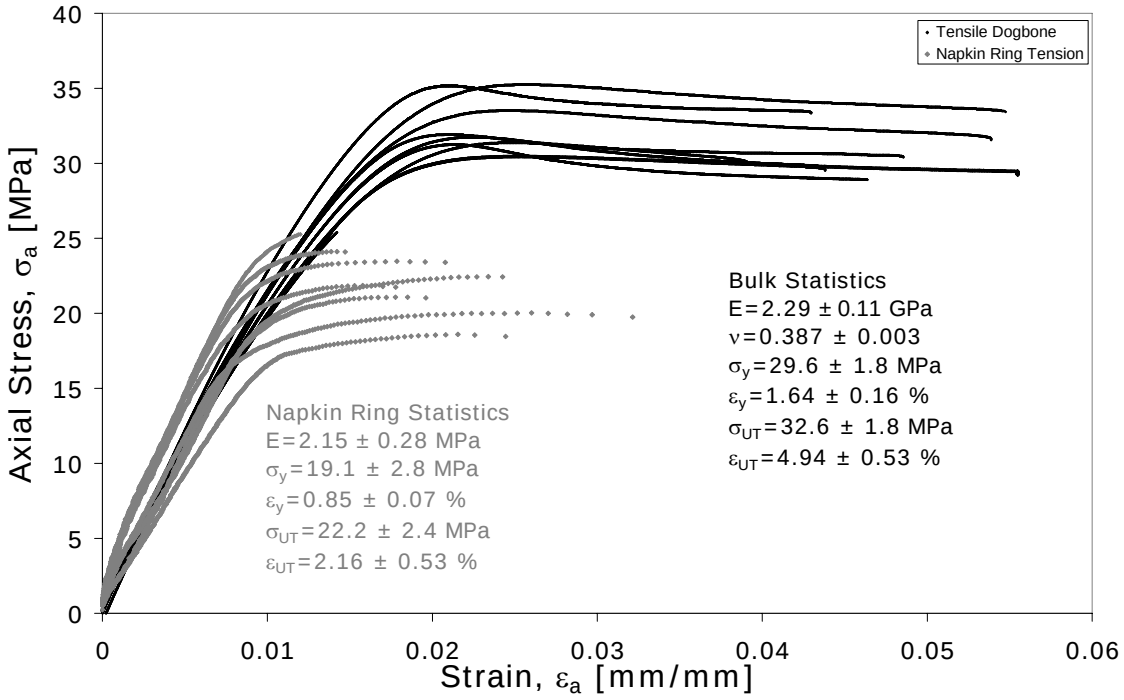

Figure 5.5 Comparison of bulk and *in situ* stress-strain curves.

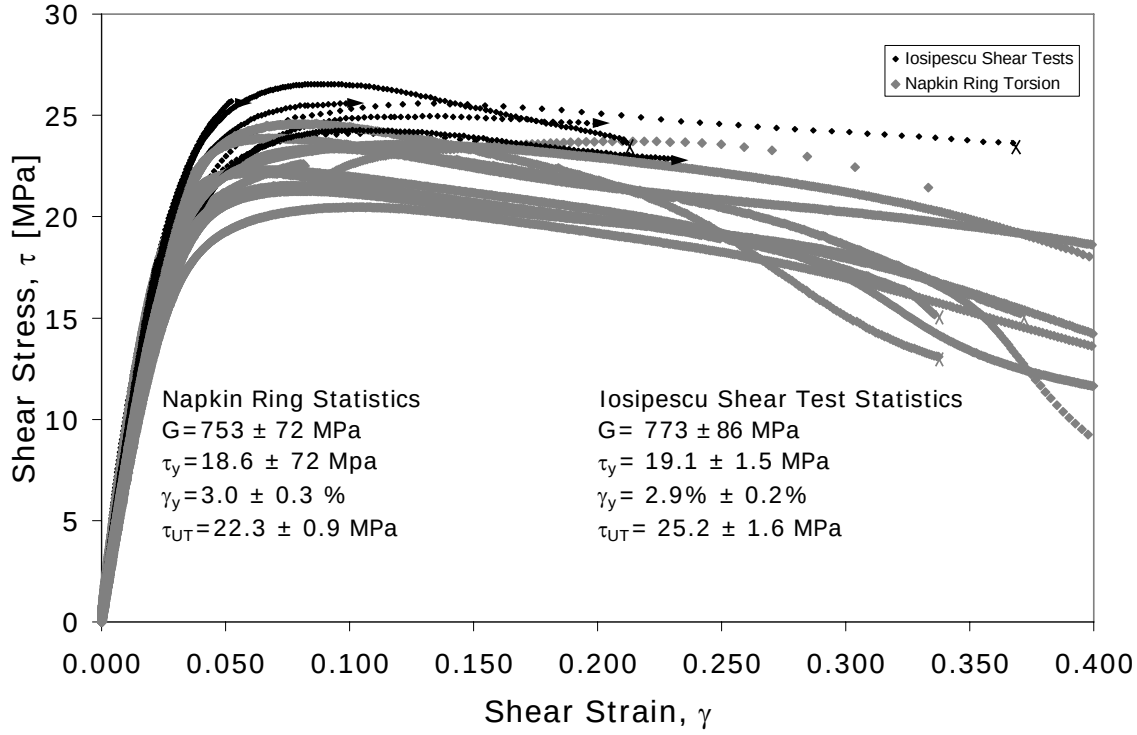

Figure 5.6 Comparison of bulk and *in situ* shear stress-strain curves.

From stress-strain plot, Figures 5.5 and 5.6, one can see that the adhesive performed similarly in the initial portion of the loading curve, specifically in the linear region. Additionally both the bulk and *in situ* shear test followed closely together in nonlinear region. In general, the bulk adhesive specimens showed less data scatter than the *in situ* tests, however this is expected due to the increased complexity of the bonded specimens and the accuracy of strain measurements within the thin bondlines. In order to better quantify the differences and similarities between the bulk and *in situ*, Table 5.2 summarizes both the properties as well as providing a numerical comparison of each property.

Table 5.2 Comparison of Bulk and *In Situ* Adhesive Performance

Adhesive Property	Bulk Adhesive	*In Situ* Adhesive	Percent Difference
Young's Modulus [MPa]	2290	2150	6.3
Yield Stress [MPa]	29.6	19.1	43.1
Yield Strain [%]	1.64	0.85	63.5
Ultimate Stress [MPa]	32.6	22.2	38.0
Ultimate Strain [%]	4.94	2.16	78.3
Shear Modulus [MPa]	773	753	2.6
Yield Shear Stress [MPa]	19.1	18.6	2.7
Yield Shear Strain [%]	2.9	3.0	-3.4
Ultimate Shear Stress [MPa]	25.2	22.3	12.2

A review of Table 5.2 shows adhesive performance in the linear region to be similar for the bulk and *in situ* test results. This is in keeping with the majority of the scientific community's findings. Both the moduli of rigidity and elasticity proved to be within a few percent of one another, 2.6% and 6.3%, respectively. In shear, the adhesive performed very similar in bulk and bonded states, with the only deviation greater than 10% being the average shear stress at break. From the results, one could accurately predict the adhesive performance, both linear and nonlinear, in shear with the Iosipescu shear tests, without the need for fabricating intricate *in situ* shear specimens. However, the same cannot be said for the normal loading scenario. Interestingly, it seems like one can use bulk shear properties and linear tensile properties to predict *in situ* behavior in shear, however there is a significant decrease in yield stress in tensile loading for bonded specimens over the bulk adhesive, yield strengths showed a 43.1% difference while yield strains showed a 63.5% difference.

There are two different possible phenomena that could be responsible for this difference in adhesive strength. The first is characteristic of many researchers' initial concerns of tests results suggesting different bulk and *in situ* adhesive performance. As mentioned above, the bonded napkin-ring specimens were not completely void free, and preliminary testing of the bulk

adhesive showed a high sensitivity to flaws. When the initial bulk adhesive specimens were tested, a brittle failure mode was observed; however after the specimen fabrication process was refined, the failure mode changed to a more gross plastic deformation with necking. An attempt was made to minimize the experimental impact of these voids, and as such specimens which showed failure related to a flaw were discarded. If specimen flaws were indeed responsible for the differences, then what was seen was a high sensitivity to flaws in a normal loading scenario, but almost no effect when the specimens were loaded in shear. It is the author's belief however that while specimen flaws may have played a small role in the adhesive performance difference, the flaws alone were not the driving mechanism. The other possible phenomenon could be sensitivity to a hydrostatic stress state that results due to the constraint added by the aluminum substrates. This hydrostatic stress states develops as the stiffer adherends inhibit the Poisson contraction of the adhesive. Several researchers have found that a triaxial stress state encourages polymer mobility and expands the free volume, which would result in increased ductility[27,28,29,30]. However more recently several researchers who specialize in finite element analysis material models and joint failure predictions have begun to include hydrostatic sensitivity terms to their materials models[31,32,33]. It is believed that the LESA adhesive falls into this category where hydrostatic stresses have a negative performance effect since the failure mode of these tension tests was not completely brittle and some ductility was seen. This is supported by the stress-strain plot in Figure 6 where the *in situ* tests load on a similar slope however reach a maximum elastic stress and begin plastically deforming at a stress level approximately 35% less then the bulk adhesive.

5.4 CONCLUSIONS

In this study, a two-part room temperature cure acrylic adhesive was compared in both the bulk and *in situ* forms and the adhesive performance was compared. This comparison included stress-strain behavior both in the linear and nonlinear regions. Much care was taken in addressing previous researchers' concerns of poor specimen quality (voiding and/or incomplete curing), inaccuracies in measurement systems for bondline deformations, and non-uniform stress states induced during testing. The experimental test plan that resulted from these concerns included the selection a standard tensile test and Iosipescu shear tests for the bulk adhesive and an ASTM E-229 style napkin-ring geometry loaded in either tension or torsion for the *in situ*

adhesive tests. The napkin-ring specimens were instrumented with high resolution custom transducers and corrected for substrate deformations to capturing the adhesive bondline displacements. Execution of the test plan allowed for several observations of the LESA adhesive which are summarized below:

1. Bulk shear adhesive tests provided a simple and accurate method for predicting *in situ* shear adhesive performance throughout both the linear and nonlinear region.
2. The modulus of elasticity in the bulk adhesive tests was similar to the effective modulus of elasticity measured in the *in situ* tests.
3. Prediction of normal yield strengths and plastic deformation of the *in situ* adhesive was not possible using traditional failure criterion based on the bulk adhesive results, however these analyzes did not consider any void effects, stress singularities, or loading eccentricities that may have occurred in testing. .
4. The LESA adhesive showed a high sensitivity to voiding and surface flaws when loaded in a normal scenario, however through careful specimen fabrication techniques, these flaws were minimized. The LESA adhesive showed very little sensitivity to these voids and flaws when loaded in shear.

Acknowledgements

The author would like to thank the Dow Automotive Corporation and the Center for Adhesive and Sealant Science (CASS) for supporting this research.

5.5 REFERENCES

[1] Dean, G., Crocker, L., Read. B, and L. Wright., "Prediction of deformation and failure of rubber-toughened adhesive joints." *Int. J. Adhesion Adhesives.* **24**, 295-306 (2004).

[2] Zgoul, M. and A. D. Crocombe. "Numerical modeling of lap joints bonded with a rate-dependent adhesive." *Int. J. Adhesion Adhesives.* **24**, 355-366 (2004).

[3] Gardon, J., "Variables and Interpretation of Some Destructive Cohesion and Adhesion Tests," in *Treatise on Adhesion and Adhesives*, Vol. 1, (Dekker, New York, 1966), Chap 8, pp. 269-324.

[4] Tanner, W., "Manufacturing Processes with Adhesive Bonding." *Appl. Polymer Symposia.* **19**, 1-21 (1972).

[5] Miller, G., "Adhesion and the Glassy State," in *Treatise on Adhesion and Adhesives*, Vol. 3, (Dekker, New York, 1973), Chap 3, pp. 123-159.
[6] Bascom, W. D., Cottington, R. L., Jones, R. L., and Peyser, P. J., "The Fracture of Epoxy- and Elastomer-Modified Epoxy Polymers in Bulk and as Adhesives." *Appl Polym Sci*,**19**, 2545-2562 (1975).
[7] Adams, R. and Coppendale, J., "The Elastic Moduli of Structural Adhesives," in *Adhesion*, Vol. 1, (Applied Science Publishers, London, UK, 1977), pp. 1-17.
[8] Sancaktar, E. and Brinson, H., "The Viscoelastic Shear Behavior of a Structural Adhesive," in *Adhesion and Adsorption of Polymers*, Vol. 12A, (Plenum Press, New York, 1980), pp. 279-299.
[9] Dwight, D., Sancaktar, E. and Brinson, H., "Failure Characterization of a Structural Adhesive," in *Adhesion and Adsorption of Polymers*, Vol. 12A (Plenum Press, New York, 1980), pp. 141-163.
[10] Brinson, H. F., "The Viscoelastic Constitutive Modeling of Adhesives." *Composites*, **13**, 377-382 (1982).
[11] Gali, S., Dolev, G., and Ishai, O., "An Effective Stress/Strain Concept in the Mechanical Characterization of Structural Adhesive Bonding." *Int. J. Adhesion and Adhesives*, **1**, 135-140 (1981).
[12] Dolev, G., and Ishai, O., "Mechanical Characterization of Adhesive Layer in-situ and as bulk material." *J. Adhesion*, **12**, 283-294 (1982).
[13] Jeandrau, J. P., "Intrinsic Mechanical Characterization of Structural Adhesives." *Int. J. Adhesion and Adhesives*, **6**, 229-231 (1986).
[14] Lilleheden, L., "Mechanical Properties of Adhesives in situ and in bulk." *Int. J. Adhesion and Adhesives*, **14**, 31-37 (1994).
[15] Spigel, B. and Roy, S., "Comparison of the Adhesive Shear Modulus in Bulk and Bonded States." *J. Adhesion*, **47**, 151-163 (1994).
[16] "Standard Test Method for Tensile Properties of Plastics" *ASTM Standard D 638-01, Amer. Soc. Test. and Mat.,* Philadelphia (2001).
[17] Iosipescu, N., "New Accurate Method for Single Shear Testing of Metals," *J. Mat.*, **3**, 537-566 (1967).

[18] Herrera-Franco, P. J. and Valadex-González, A., "Mechanical Properties of Continuous Natural Fibre-reinforced Polymer Composites," *Composites Part A: Applied Science and Manufacturing.* **35**, 339-345 (2004).

[19] Abot, J. L., Yasmin, A., Jacobsen, A. J. and I. M. Daniel, "In-plane Mechanical, Thermal and Viscoelastic Properties of a Satin Fabric Carbon/epoxy Composite," *Comp. Sci. and Tech.* **64**, 263-268 (2004).

[20] "Standard Test Method for Shear Properties of Composite Materials by the V-notched Beam Method." *ASTM Standard D 5379-98, Amer. Soc. Test. and Mat.,* Philadelphia (1998).

[21] "Standard Test Method for Shear Strength and Shear Modulus of Structural Adhesives" *ASTM Standard E 229-97, Amer. Soc. Test. and Mat.,* Philadelphia (1997).

[22] Hawong, J., Shin, D., and Baek, U. "Validation of pure shear test device using finite element method and experimental methods." *Eng. Frac. Mech.,* **71**, 233-243 (2004).

[23] Sullivan, J. L., Kao, B. G., and Van Oene, H., "Shear Properties and a Stress Analysis Obtained from Vinyl-ester Iosipescu Specimens," *Exp. Mech.,* **24**, 223-232 (1984).

[24] Grabovac, I. and Morris, C. E. M. "The Application of the Iosipescu Shear Test to Structural Adhesives." *J. App. Poly. Sci.,* **43**, 2033-2042 (1991)

[25] "Standard Guide for Preparation of Metal Surfaces for Adhesive Bonding" *ASTM Standard D 2651-01, Amer. Soc. Test. and Mat.,* Philadelphia (2001).

[26] Adams, R D. Coppendale, J. and N. A. Peppiatt, "Stress Analysis of Axisymmetric Butt Joints Loaded in torsion and tension.**"** *J. Strain Anal.*, **13**, 1-10)(1978).

[27] Gardon, J., "Variables and Interpretation of Some Destructive Cohesion and Adhesion Tests," in *Treatise on Adhesion and Adhesives*, Vol. 1, (Dekker, New York, 1966), Chap 8, pp. 269-324.

[28] Miller, G., "Adhesion and the Glassy State," in *Treatise on Adhesion and Adhesives*, Vol. 3, (Dekker, New York, 1973), Chap 3, pp. 123-159.

[29] Chai, H., "Deformation and Failure of Adhesive Bonds Under Shear Loading." *J. Mater. Sci.*, **28**, 4944-4956 (1993).

[30] Chai, H., "On the Correlation Between the Mode I Failure of Adhesive Joints and Laminated Composites," *Engng. Fract. Mech.,* **24**, 413-431 (1986).

[31] Dean, G., Crocker, L., Read. B, and L. Wright., "Prediction of deformation and failure of rubber-toughened adhesive joints." *Int. J. Adhesion Adhesives.* **24**, 295-306 (2004).

[32] Zgoul, M. and A. D. Crocombe. “Numerical modeling of lap joints bonded with a rate-dependent adhesive.” *Int. J. Adhesion Adhesives.* **24**, 355-366 (2004).
[33] Duncan, B. and G. Dean. “ Measurements and models for design with modern adhesives.” *Int. J. Adhesion Adhesives.* **23**, 141-49 (2003).

Chapter 6: Summary & Conclusions

6.1 ACCOMPLISHMENTS AND OBSERVATIONS

This thesis presents a study of both bulk and *in situ* stress-strain behavior, including linear and nonlinear regions, under both shear and normal loading for a two-part acrylic adhesive. Included in this thesis is the documentation of test geometry selection, specimen fabrication methods, specimen instrumentation, presentation of the results, as well as a discussion of potential driving mechanisms for discrepancies between bulk and *in situ* adhesive behavior. The bulk adhesive characterization was performed using standard dogbone tensile and Iosipescu shear tests, while the *in situ* testing was performed on an ASTM E-229-inspired napkin-ring geometry loaded in either tension or torsion. In order to address concerns raised in previous research, much care was taken to ensure high specimen quality, uniform stress states during testing, and use of high resolution measurements of adhesive deformation. Overall the successful completion of the testing regimen was a substantial accomplishment.

While addressing the concerns from previous research in this field, there were several major advancements in the fabrication of both the test fixtures and test specimens. A method of fabricating bulk adhesive specimens was developed by sandwiching the liquid adhesive between removable stainless steel foils supported by aluminum plates. After the adhesive was partially cured, the foil could be easily removed, leaving a smooth surface which was free of voids. These large cast patties were then cut into strips to be machined into tensile or Iosipescu shear specimens. Another accomplishment was the successful use of the Iosipescu shear specimen for measuring the shear properties of an isotropic adhesive. Traditionally, this test has primarily been used in composites research with only a few researchers attempting application on bulk adhesive specimens. Based on the successful test results generated in this study, this methodology could be used for simple characterization of adhesive shear properties that appear to correlate well with *in situ* shear behavior of bonded joints, at least for the LESA system studied herein. Another major accomplishment was the fabrication of an entirely new testing setup which utilized the napkin-ring geometry. The credit for this work is shared with a doctoral student, John Hennage. By working side-by-side, we were able to construct many of the specimen fabrication procedures and custom transducer mounts which were used to support the

efforts in this thesis. Based upon the data collected and the many hours spent working with the machine and setup, clearly the test geometry and instrumentation can be considered a success.

The research performed by this thesis also provided many interesting observations which will help future researchers and designers utilize structural adhesives. Results from these tests suggest that bulk shear adhesive tests provide an accurate and simpler method of predicting *in situ* shear adhesive performance in both the linear and nonlinear region. Results from the bulk testing were also able to predict the effective moduli of rigidity and elasticity in the bonded state. However, the *in situ* adhesive performance of specimens loaded in tension fell short of the prediction from the bulk adhesive performance. A closer analysis of the results suggested potential mechanisms for this difference, however a definitive cause was not identified. This basic analysis does not factor in any void effects, stress singularities, or loading eccentricities that may have occurred in testing. What can be concluded is that a more complex failure mechanism may be at work and standard failure theories may need to include modifiers to correct the over-prediction of joint failure stress in tensile loading. The *in situ* shear strength and nonlinear adhesive performance was less affected by these voids, suggesting that the sensitivity these voids was due to the stress concentration effects since both these and the corner stress singulaties would not have an effect under the torsional loading.

As a reminder, the motivation for the research performed during this thesis stemmed from the preliminary stress-strain data collected by the adhesive manufacturer and the large difference between a standard dogbone tensile test and a thick-adherend shear test. After the completion of this research, one can conclude that the differences can most likely be attributed to small flaws in the bulk adhesive specimens which precipitated premature failure. There may have been some flaws/voids in the thick-adherend specimen; however, the LESA adhesive showed a much reduced sensitivity to flaws and voids in shear as opposed to normal loading. A critical aspect to adhesive testing is ensuring specimen quality and Dr. Tom Ward captured it best when lecturing on adhesive testing, you spend you time in the following manner: “80% making, and 20% breaking.”

6.2 AREAS FOR IMPROVEMENT

Although there were many accomplishments and observations that stemmed from this research, it can definitely be said that research sometimes asks more questions than it answers.

The largest area of improvement for this research would be to expand the *in situ* testing to utilize the capabilities of the tension-torsion test frame. In this research the tension-torsion test frame was used in only pure tension or pure torsion, however a lot of insight could be gained by including combined loading in both tension and torsion. This would provide data to further challenge the various failure theories to predict the on-set of yield under various *in situ* scenarios. Exploration of this loading scenario could shed light on the hydrostatic sensitivity observed with the LESA adhesive. However it was not possible to include these tests in this project due to the remaining development of the displacement transducers during two-dimensional motion. Additional work is being performed on these topics and more in John Hennage's dissertation entitled "Characterization and Analysis of Adhesives for Joint Design."

Another area of improvement would be the investigation of bond thickness effects, since a large amount of research has been performed on this subject and the effect on adhesive performance. The variation of bondline thicknesses would again provide a better understanding of the hydrostatic stress sensitivity as well as supporting the previous research in this field. Additionally, a larger sample set should be used in order to increase the statistical significance of these findings.

6.3 FUTURE WORK

Each one of the improvements suggested above should be addressed in future work, several of which are worth an entire Masters' thesis. On a much larger scope, this research only concentrated on a single structural adhesive, but a thorough survey of the different types of structural adhesives would be valuable to the research community. Using the testing setup laid out in this thesis as a baseline, additional studies focusing on other types of structural adhesives could be performed to create general guidelines for the characterization of these certain types of adhesives through a suggested series of tests. It would also be very interesting to further examine the effects of stress concentration factors (voids, singularities, etc.) and the actual stress distributions across the bondline and relate these to the nominal applied stress. Such a large project would most likely fall into the realm of a dissertation; however, such a study would reduce both time and cost for characterizing the *in situ* adhesive performance and allow the proper design properties to be supplied to the finite element analyses or mechanical design. Clearly there is merit in such a study.

Attacking the issue of adhesive characterization from a different angle, this study focused on a strength-based adhesive characterization in both the bulk and *in situ* adhesive. It would be interesting to perform a study which parallels this thesis, one that focuses on a fracture-based approach using the identical adhesive. The observations and results from such a fracture-based study would further the understanding of bulk and *in situ* adhesive performance. Such a study would be an excellent Masters' thesis for an upcoming graduate student interested in material characterization and fracture-based design properties. By performing additional work such as that suggested here, one would be able to better understand the intricacies of both bulk and *in situ* adhesive performance.

Appendix A: Bulk Adhesive Specimen Refinement

As with all research, the quality of the results is only as good as the quality of the test specimens. As described in the chapters above, the preliminary bulk adhesive testing showed very inconsistent test results, and as such it became necessary to ensure that the specimens were both fully cured and did not contain any voids or surface flaws. A large amount of the surface flaws and voids were eliminating by changing from individual casts to larger blocks/patties as described in Chapter 3, this Appendix presents some of the test results during the fine tuning of the specimen fabrication process utilizing the larger casts. Figure A.1 displays the effect on specimen performance as a result of different aging times before testing. After this effect was seen, the post-curing process was developed to ensure a total cure of the LESA adhesive. Figure A.2 contains the results that confirmed the 4 days at 40°C was sufficient to complete the cure. After the post-cure process was determined, there was a final iteration in the specimen fabrication process, the usage of the stainless steel foil. Before the use of the foil, the adhesive patty had to be removed from between the aluminum plates before completing the post-cure and occasionally the patty warped as it continued to cure. Figure A.3 shows the results of specimens made using the aluminum plates both with and without stainless steel foil as well as specimens which were heated after the curing process to removing the warping. As a clarification, the test results shown in Figures A.1 & A.2 are with a different generation of the LESA adhesive than the results presented in this thesis chapters and in Figure A.3.

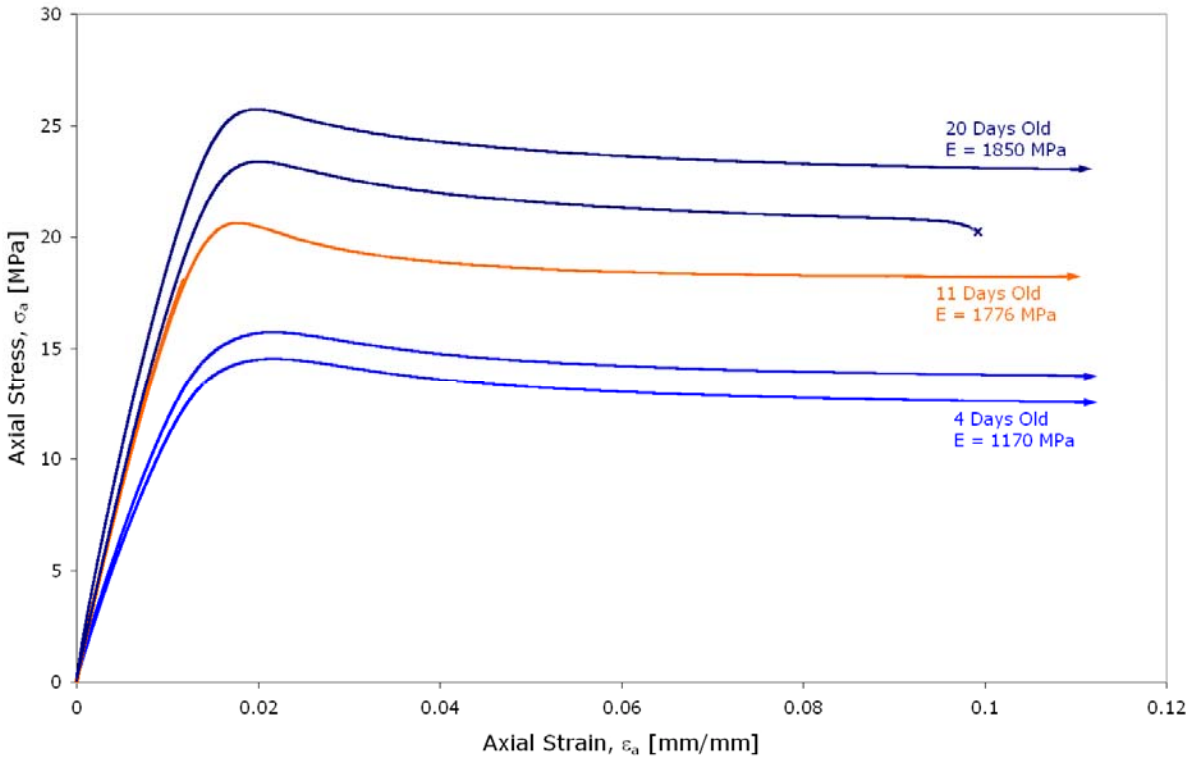

Figure A.1: Aging Time Effects in Tensile Tests Specimens

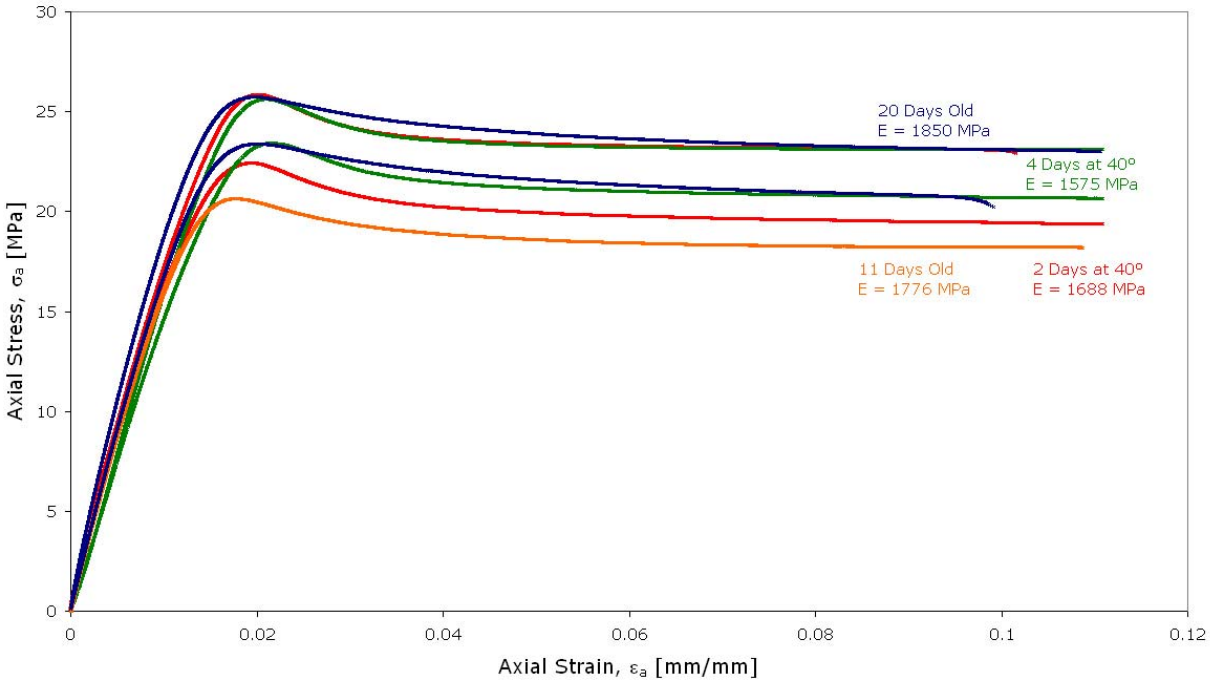

Figure A.2: Aging Time Effects and Post-Curing Heating in Tensile Tests Specimens

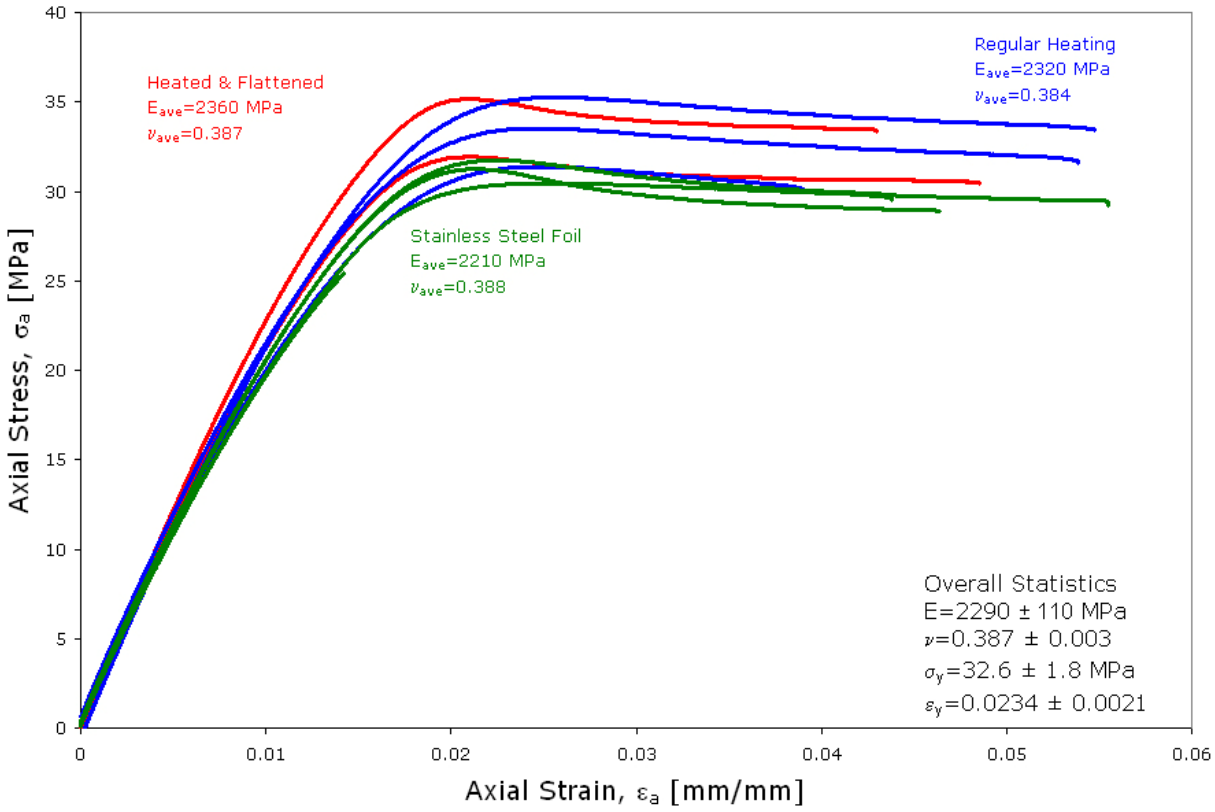

Figure A.3: Tensile Test Results from Different Fabrication Methods

Appendix B: Yield Definition

B.1 INTRODUCTION

When determining the constitutive properties from the various testing one of the more difficult properties to measure was the yield point. According to the ASTM standard, the yield point is defined as the first instance where the strain increased without a corresponding increase in stress for materials that exhibit a zero slope region. However using this definition for the yield point seemed dangerous, as the *in situ* adhesive tension tests experience very little plasticity after yield. Additionally for other geometries, using this method would have designs which could experience in excess of 10% yield under normal operation without failing, which is unacceptable for most structural design.

Another common method for determining the yield point is the offset method and an attempt was made using a 0.2% strain offset. This worked well for a couple of the test geometries; however, applying this method to all geometries, proved to be overly conservative at times and non-conservative at others. In an attempt to define a yield point which is consistent in all geometries, a new method was formed by monitoring an instantaneous slope of the stress-strain curve using a multipoint average. The concept was to monitor the amount of damage occurring and when a predetermined amount occurred, yield was declared. Measuring the damage was performed by monitoring the instantaneous slope of the stress-strain curve and yield was determined when the instantaneous average dropped below 50% of the original modulus of elasticity determined from the initial linear portion. Figure B.1 shows a stress-strain plot from a tensile dogbone specimen that had been loaded and unloaded in a 5 MPa increments to help confirm the use of this new method. From this plot, one can see that in between the unloading of the 6^{th} curve and the loading of the 7^{th} cycle significant plastic damage was done. Using the slope change method described above, the yield point was defined at the top of the 6^{th} loading cycle, right before the loading cycle that experience the plastic damage.

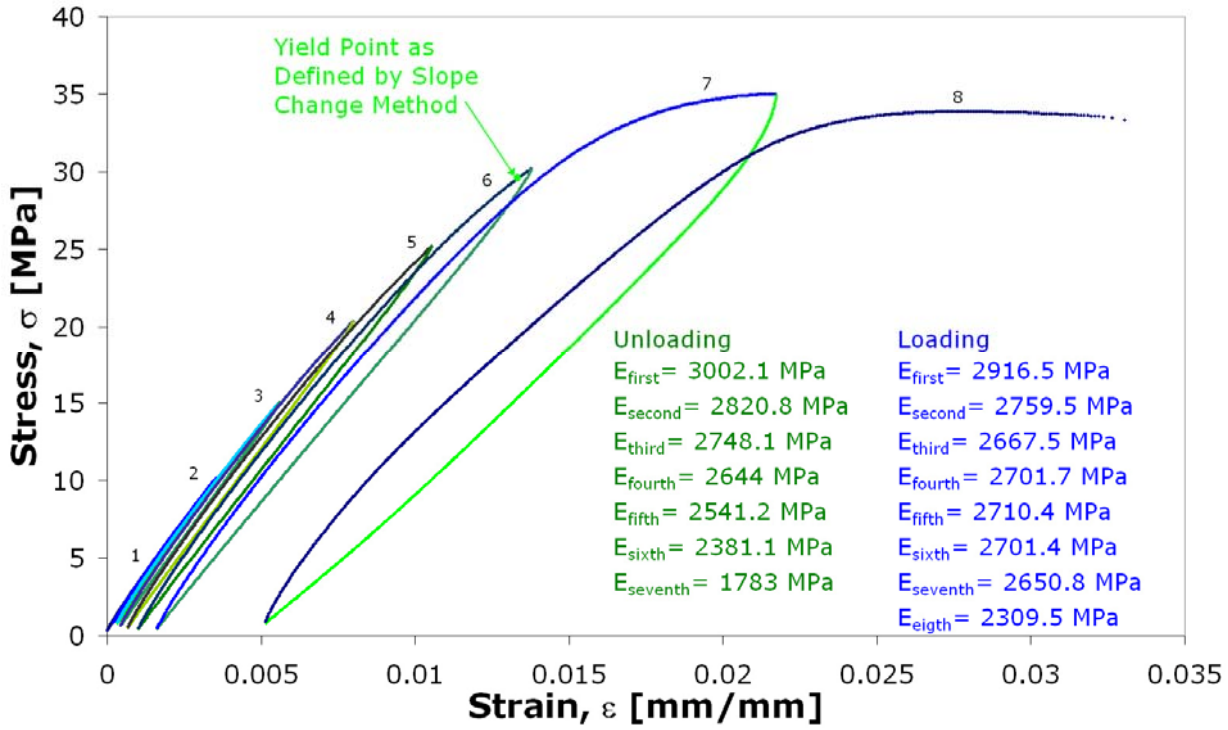

Figure B.1: Loading and Unloading of a Tensile Dogbone Specimen

A comparison of the new slope change method and the offset method for all of the different test geometries in this research was performed. Figure B.2 shows the yield point as determined by the two different methods for the normal loading configuration of the bulk adhesive specimens. In this test geometry the offset method was slightly more conservative and had a lower standard deviation in yield properties than the slope change method. Figure B.3 displays the yield points as measured from the shear loading configuration of the bulk adhesive specimen. In this configuration, the offset method was once again more conservative, almost too much so, however in this instance the standard deviation was much greater than the the slope change method. Figure B.4 shows the comparison for the *in situ* adhesive in the normal loading configuration. Here the offset method was too non-conservative, specifically in the large amount of yield strain. While the scatter was significantly large in this test geometry for all constitutive properties, there was no noticeable difference between the standard deviations of the yield properties from the offset and slope change methods. Lastly, Figure B.5 provides a comparison of the yield point definition from the *in situ* adhesive loaded in a shear configuration. As with the bulk adhesive tests, in this configuration the offset method was once again conservative, almost overly conservative. There was no substantial difference between the standard deviations

of yield properties between the two methods. Table B.1 summarizes the yield properties for both of the methods as well as quantifies the percent difference between the two methods. From this analysis, the new slope change method was selected in order to make full use of the adhesive's strength while still providing a conservative and consistent approach for all test geometries.

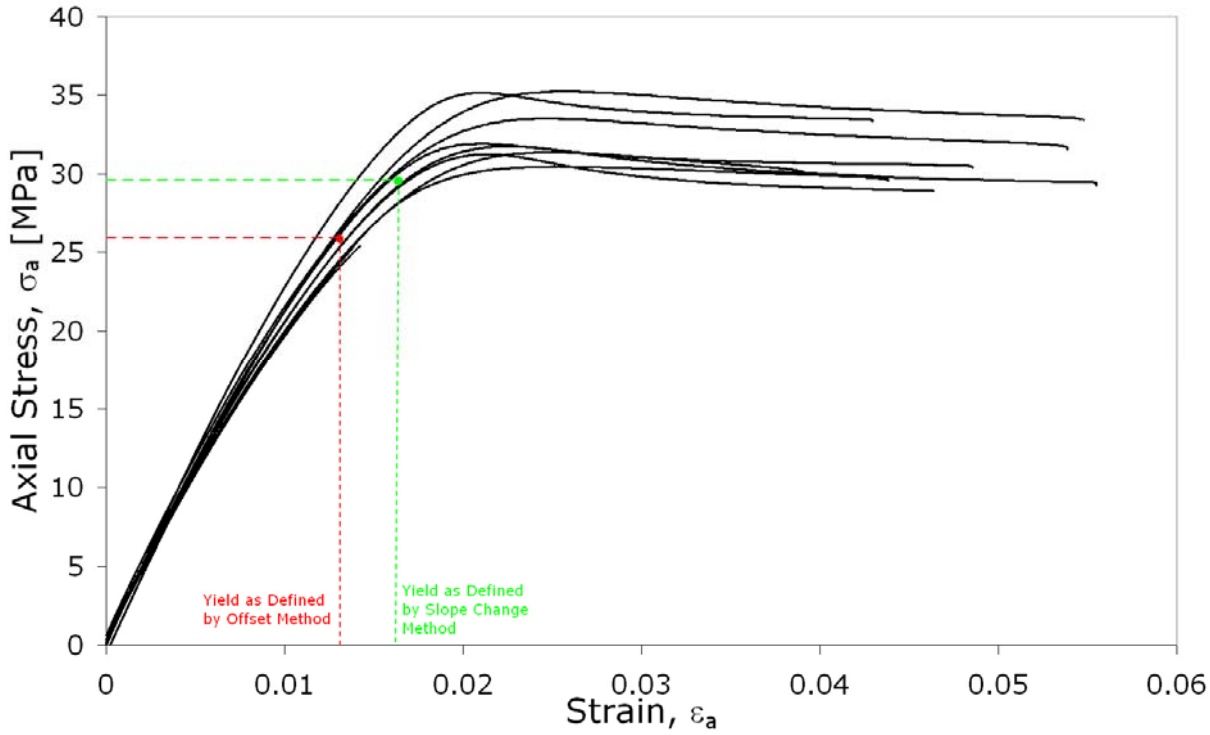

Figure B.2: Yield Point Comparison for the Bulk Adhesive – Normal Configuration

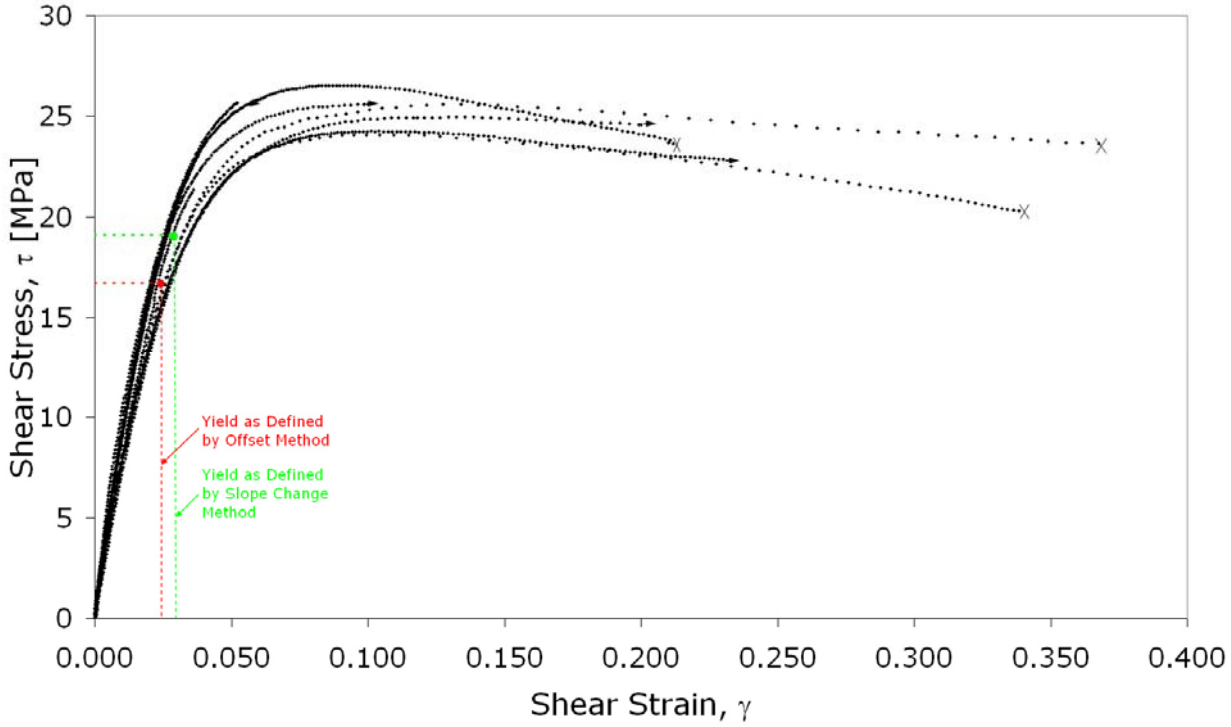

Figure B.3: Yield Point Comparison for the Bulk Adhesive – Shear Configuration

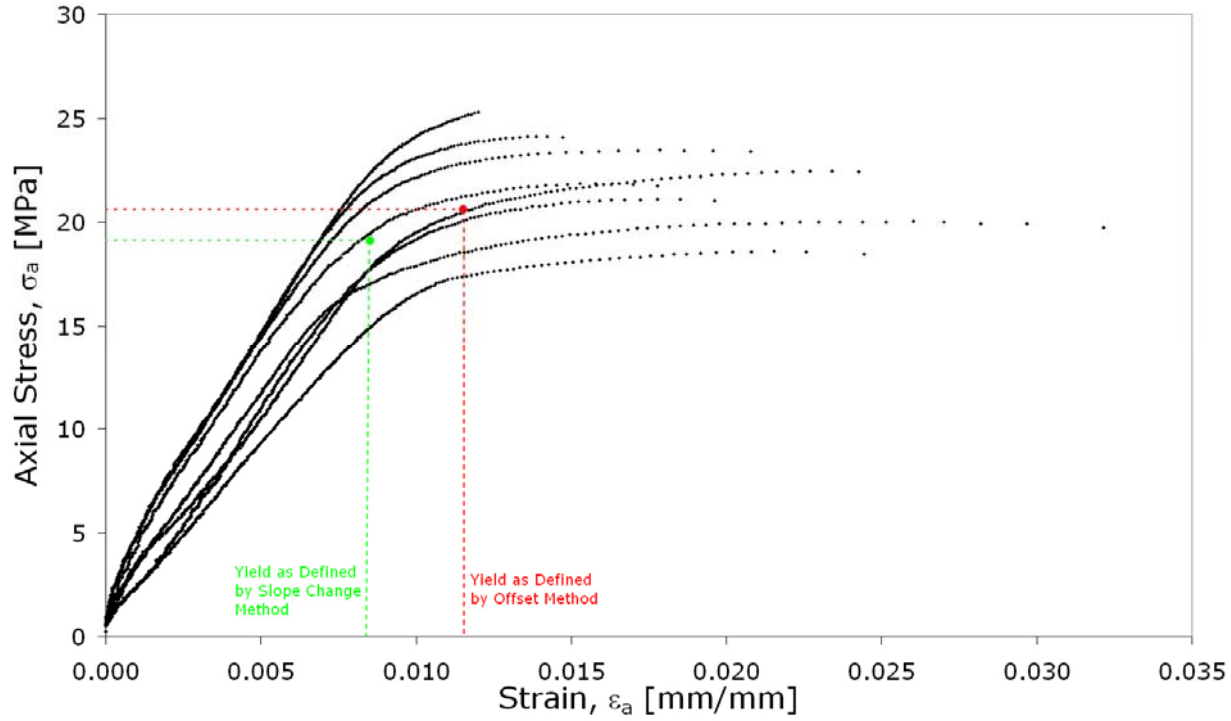

Figure B.4: Yield Point Comparison for the *In Situ* Adhesive – Normal Configuration

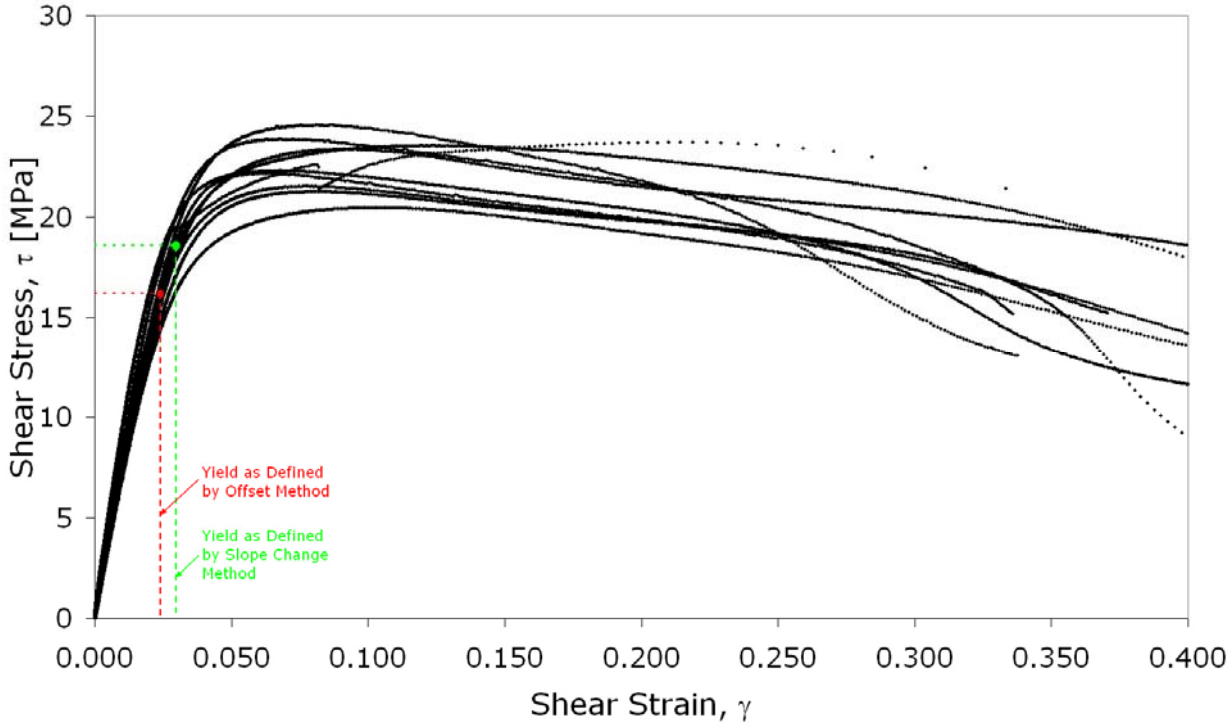

Figure B.5: Yield Point Comparison for the *In Situ* Adhesive – Shear Configuration

Table B.1: Comparison of Yield Properties from the Offset & Slope-Change Methods

LESA Bulk Adhesive Properties					
	Offset Method		Slope-Change Method		Percent Difference
	Average	Standard Deviation	Average	Standard Deviation	
Yield Stress [MPa]	25.9	1.6	29.6	1.8	-14%
Yield Strain [%]	1.3	0.04	1.64	0.16	-24%
Yield Shear Stress [MPa]	16.7	4.4	19.1	1.5	-14%
Yield Shear Strain [%]	2.4	0.8	2.9	0.2	-21%

LESA In Situ Adhesive Properties					
	Offset Method		Slope-Change Method		Percent Difference
	Average	Standard Deviation	Average	Standard Deviation	
Yield Stress [MPa]	20.6	2.3	19.1	2.8	7%
Yield Strain [%]	1.2	0.1	0.85	0.07	27%
Yield Shear Stress [MPa]	16.2	0.5	18.6	0.6	-15%
Yield Shear Strain [%]	2.4	0.2	3	0.3	-25%

Appendix C: "Uncracked" Crack Lap Shear

C.1 INTRODUCTION

In an attempt to begin to bridge the gap between strength-based and fracture-mechanics based-analysis, a modified cracked-lap-shear specimen was used. Before describing the modification, the standard cracked lap shear specimen is briefly introduced. This test geometry is used as a predominately Mode II (shear) fracture specimen and Figure C.1 shows a schematic of the standard cracked lap shear specimen where the specimen is introduced with a load, P and typically has a pre-initiated sharp crack tip in the adhesive. As the bottom strap is loaded the adhesive transfers energy to the top lap.

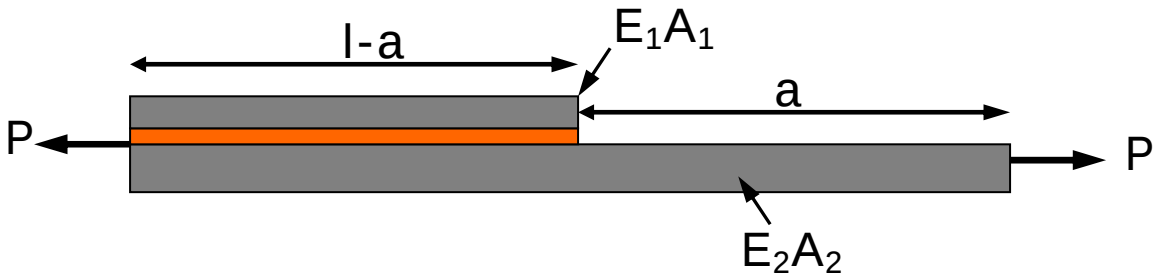

Figure C.1: Schematic of an "Uncracked" Crack Lap Shear Specimen

Using linear elastic fracture mechanics analysis, one can determine the fracture energy given a loading condition for this test. The fracture energy, $\mathcal{G}$, is defined to be:

$$\mathcal{G} = \frac{1}{2} P^2 \frac{\partial C}{\partial A} \tag{C.1}$$

where P is the load, C is the compliance, and A is the bond area. The compliance of this geometry is determined by:

$$C = \frac{\ell - a}{E_{lap} A_{lap} + E_{strap} A_{strap}} + \frac{a}{E_{strap} A_{strap}} \tag{C.2}$$

where E is the modulus of elasticity for the corresponding substrate. After taking the partial derivative, simplifying it, and inputting it into Equation C.1, one can conclude that the fracture energy, $\mathcal{G}$, is:

$$\mathcal{G} = \frac{P^2 A_{lap}}{2wA_{strap}(E_{strap} A_{strap} + E_{lap} A_{lap})} \tag{C.3}$$

where *w* is the bond width. By changing the substrate dimensions one can vary the strain energy release rate.

In this testing the cracked lap shear specimen was left uncracked and the local shear strain at the location of crack initiation was measured visually. The substrates used for these tests utilized a 6.35 mm thick strap of 7075 aluminum and a 4.76 mm thick lap of 6061 aluminum. As with the other *in-situ* testing, these substrates were P-2 etched to ensure proper adhesion to the substrate. The 0.0813 mm adhesive bondline was set using spherical glass beads embedded in the adhesive outside of the testing area. In order to provide a consistent reference for the visual strain measurements, these specimens were first machined to a smooth finish and then blued with machinist's dye. After this the specimen was fed underneath, at approximately 254 millimeters per minute, a large diameter fly cutter, spinning at approximately 1000 rpm, was used to scribe the surface of the specimen. Figure C.2 is a picture of the area of interest on a specimen ready for testing. The result of this process produced a series of scribes evenly spaced with a resolution of approximately 4 lines per millimeter.

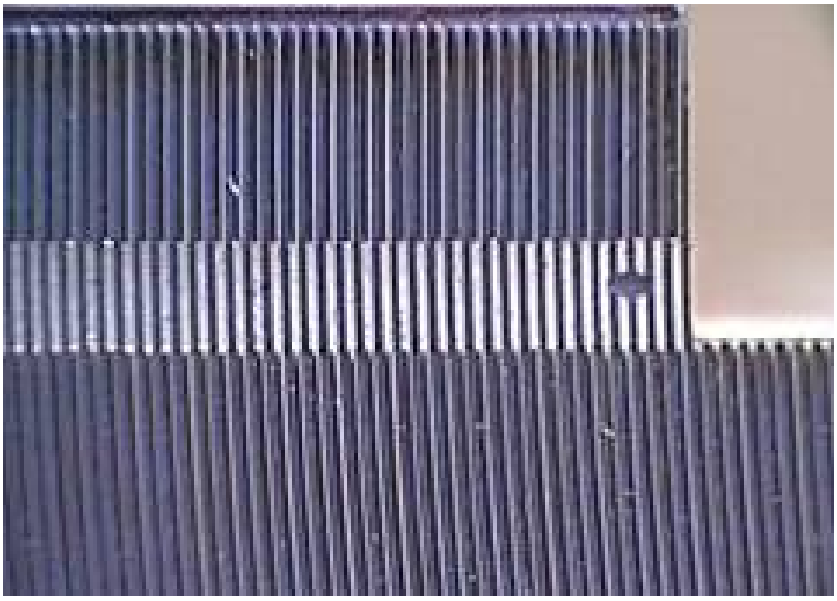

Figure C.2: Finished "Uncracked" Crack Lap Shear Specimen

C.2 TESTING RESULTS

All of the testing of these modified cracked lap shear tests were performed on a large Tinius Olsen machine due to the large amounts of loads required to initiate a crack. A video

recorder was used to capture the local shear strain at the instant of crack initiation. During the testing, two different types of failure were witnessed: an interfacial failure between the adhesive and the strap and a cohesive failure which began in the bulk adhesive and traveled down the bondline. The local shear strain at crack initiation for the interfacial and cohesive failures was γ_{ci}=32% and γ_{ci}=53%, respectively. Along side of the laboratory testing, Vinay Goyal, a doctoral student working with Dr. Eric Johnson, was developing a decohesion finite element model which incorporated both strength and fracture properties. What proved to be interesting was while working with the decohesion models if the interfacial element strength was less than cohesive element strength a result similar to the interfacial failure was seen, shown in Figure C.3. When the interfacial element strength was greater than the cohesive element strength the crack began in the bulk adhesive and then migrated to the strap interface, displayed in Figure C.4. Lastly, during one of the preliminary tests while refining the test specimen, there was a void inside the area of interest. During this test cracks initiated both from the strap/lap interface and the void and they began propagating. The finite element analysis model was able to replicate these results by creating a void in the model, and cracks propagated from both areas as shown in Figure C.5.

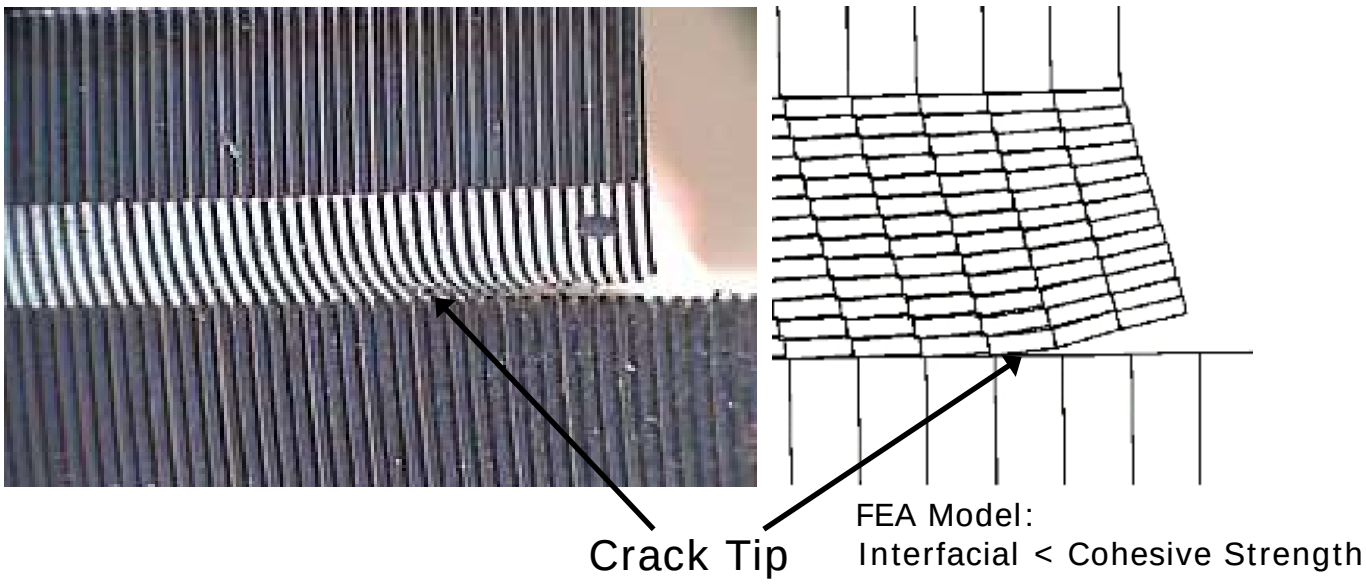

Figure C.3: “Uncracked” Cracked Lap Shear Specimens with Interfacial Failure

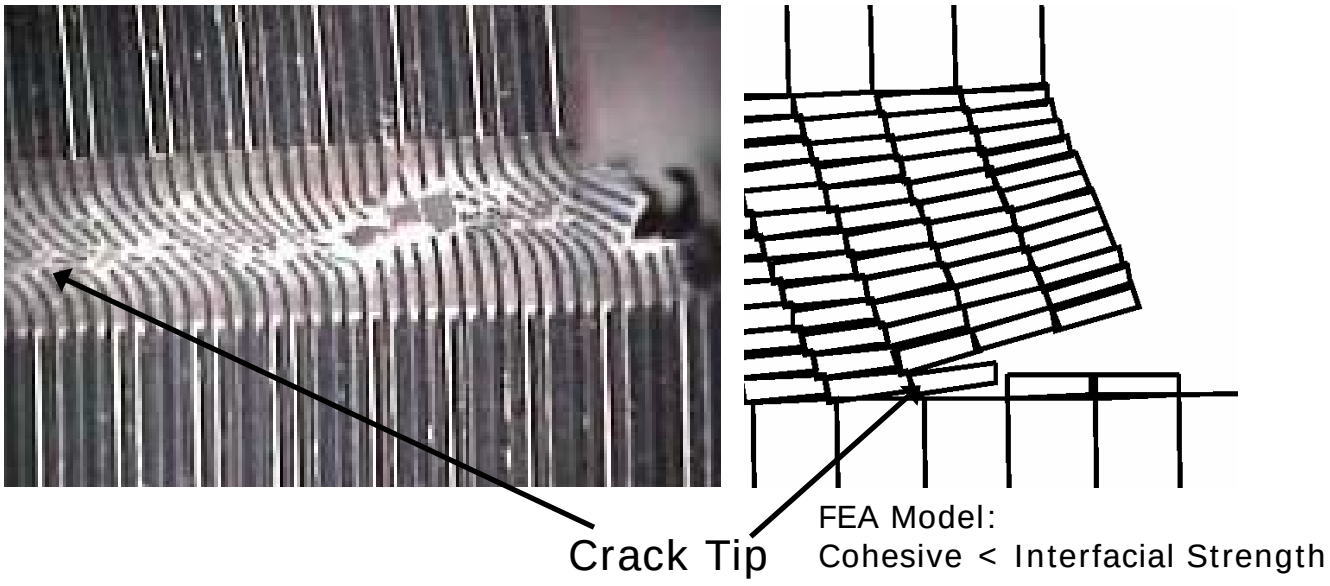

Figure C.4: “Uncracked” Cracked Lap Shear Specimens with Cohesive Failure

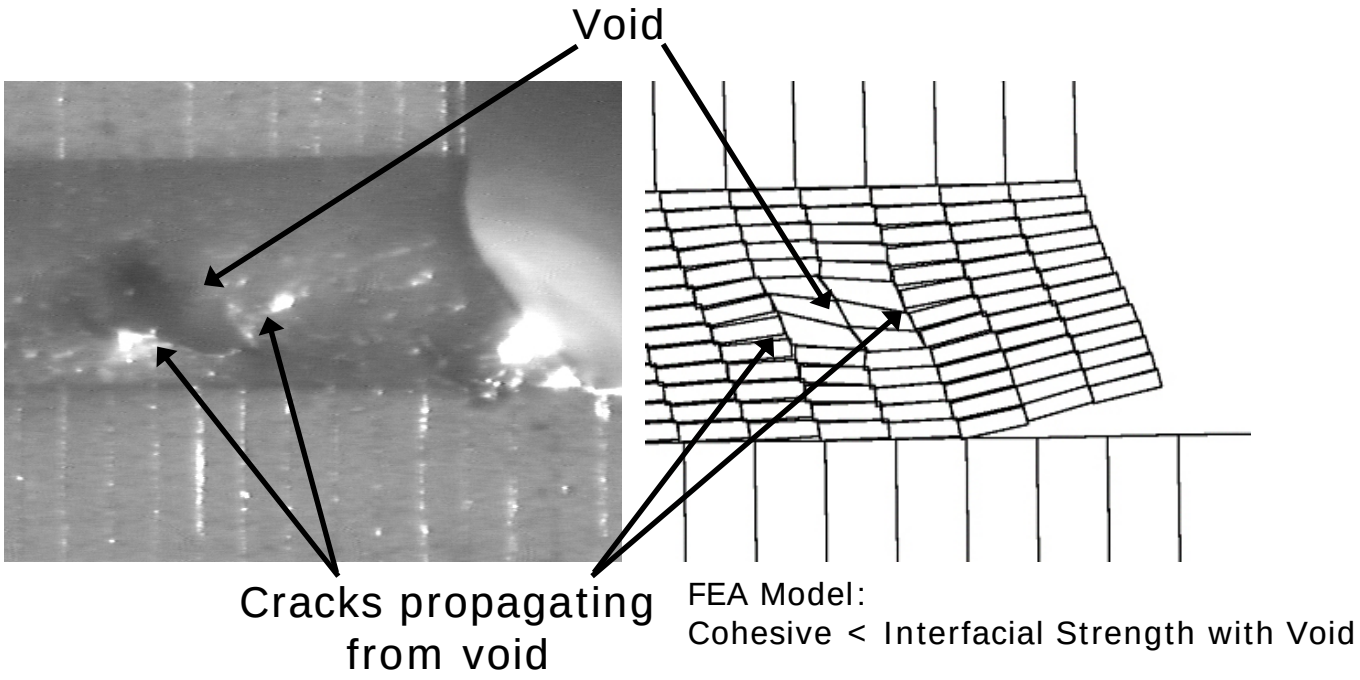

Figure C.5: “Uncracked” Cracked Lap Shear Specimens with a Void

In conclusion, these tests helped to establish a basis for the uncracked crack lap shear specimen. Even from the very limited test set there was good correlation between the results and the predictions from a decohesion finite element analysis model. This testing developed a process for fabricating high quality specimens and a fully exercised test matrix could provide

some very interesting results that may help bridge the gap between strength-based and fracture-based analyses.

JOSHUA W. GROHS

Mailing Address:
52 Boxthorn Rd
Abingdon, MD 21075

Office: (410) 471-6904
Home: (443) 512-3385
Email: josh@grohs.us

EDUCATION

Master of Science in Mechanical Engineering, Virginia Polytechnic Institute & State University, Blacksburg, VA. GPA: 3.91/4.0. Master's Thesis: *Comparing In Situ and Bulk Constitutive Properties of a Structural Adhesive*. August 2007

Bachelor of Science in Mechanical Engineering, Virginia Polytechnic Institute & State University, Blacksburg, VA. GPA: 3.84/4.0. May 2003

CORPORATE EXPERIENCE

Northrop Grumman Electronic Systems – May 2003 – Present

- Lead system architect (proposal phase) and Integrated Product Team Lead (program execution) for a wireless mesh network based video surveillance system designed for the Neighborhood Watch Iraq Program
- System architect and Mechanical/Electrical Lead on remote border surveillance system, a self-powered deployable net-centric sensor tower.
- Lead engineer on environmental hardening / next generation development of USPS Biological Detection System
- Aided in system architecture and wrote proposal for a nationally deployed sensor (Radar, EO/IR, DF/SIGINT, UGS) network and C4ISR package in the Qatar National Security Shield project.
- Integrated various security system sensors (biometrics, turnstiles, CCTV, magnetometer, baggage & personnel x-ray, document authentication) in Dot.net based Command & Control GUI
- Fabricated test setup and wrote LabVIEW code for Automated Aerosol Release Mechanism for bioaerosol testing
- Performed and supported bioaerosol testing of Biological Detection System at Edgewood Chemical and Biological Center in Aberdeen, MD
- Experience with mechanical packaging of various sensors and components

NASA Langley Summer Internship – May 1998 & Summer 2000

- Converted System Identification Toolbox from Matlab into Scilab language
- Constructed Online user guide and homepage for Dr. Juang's Toolbox
- Applied full and partial factorial design of experiments to wind tunnel testing procedures.
- Presented project to panel of engineers at conclusion of internship

RESEARCH EXPERIENCE

Graduate Research Assistant – January 2003 – May 2004

- Develop adhesive design methodology
- Perform tests to characterize adhesives
- Exploring differences between bulk and in-situ adhesive properties

National Science Foundation Summer Undergraduate Research Program – Summer 2002

- Awarded Sharpe Award for Research presentation
- Presenting findings at Adhesion Society Meeting in February 2003
- Documented findings "Contrasting In-situ and Bulk Constitutive Properties of Adhesives." Grohs J. W., NSF SURP Report, 2002.

Research Project Tester for Dr. David Dillard – January 2000 – January 2003

- Design test fixtures in AutoCAD
- Perform tests and data analysis
- Give presentations and write quarterly reports
- Documented findings "Strength Testing for Pressure Sensitive Adhesives." Grohs J. W., CASS Undergraduate Report, 2001

National Science Foundation Summer Undergraduate Research Program – Summer 2001

- Performed Creep Rupture Tests on Pressure Sensitive Adhesives
- Presented at Research Symposium
- Documented findings "Creep Rupture of Semi-Structural Pressure Sensitive Adhesives." Grohs J. W., NSF SURP Report, 2001

HONORS & AWARDS

Awarded numerous patent disclosure awards at Northrop Grumman
Awarded numerous performance awards at Northrop Grumman
Honors Program Selectee at Virginia Tech
Henry H. Arnold Educational Grant recipient
Air Force Communications Education Association Scholarship recipient
Thomas W. Drewry Scholarship recipient
Bailey Family Foundation Scholarship recipient
Hamilton M Mabie Scholarship recipient
Edward H Cahill Memorial Scholarship recipient
S. Dewey Roberson Scholarship recipient
VT Engineering Graduate Fellowship Recipient Center for Adhesive and Sealant Science (CASS) Scholarship recipient
Active member with Center for Adhesive and Sealant Science
Tau Beta Pi Engineering Honors Fraternity Selectee
Attended 2001 GE/VT Leadership Conference
Member of the Society for Automotive Engineers